Modeling and Analysis of Amorphous *Si* /Crystalline *Si* Heterojunction Photovoltaic Cells

by

Farzad Khalvati

A thesis
presented to the University of Waterloo
in fulfillment of the
thesis requirement for the degree of
Master of Applied Science
in
Electrical & Computer Engineering

Waterloo, Ontario, Canada, 2003

I hereby declare that I am the sole author of this thesis.

I authorize the University of Waterloo to lend this thesis to other institutions or individuals for the purpose of scholarly research

Farzad Khalvati

I further authorize the University of Waterloo to reproduce this thesis by photocopying or by other means, in total or in part, at the request of other institutions or individuals for the purpose of scholarly research.

Farzad Khalvati

Acknowledgements

I would like to thank sincerely a few people who played an important role in accomplishing this research. Specifically I would like to thank Mahdi Farrokh Baroughi for his invaluable help in lab and discussions through out my research. This research wouldn't have been possible without his help. For lab work, I must also thank Dr. Jeyakumar for his valuable helps.

I would also like to thank Peyman Servati for his time and patience in answering my questions.

My special thanks go to Professor Arokia Nathan and Professor Andrei Sazonov for their time in refereeing this work.

Finally, I would like to extend my sincerest thanks to my supervisor, Professor Siva Sivoththaman who gave me a chance to pursue my studies at graduate level.

Abstract

Amorphous/crystalline silicon (a-Si/c-Si) heterojunctions are of particular importance in photovoltaic (PV) energy conversion since they provide a cost-effective way for solar cell manufacturing. The low temperature (low-T) nature of the process allows the use of defective, low quality (and hence low cost) silicon substrates, which can be improved by low temperature passivation techniques such as plasma hydrogenation that can be retained if the process temperatures are kept low (<300°C). Further, low-T processes are also attractive for defective crystalline silicon substrates which generally have a tendency to degrade when subjected to multiple high temperature excursions. In this work, we have developed analytical models for $n^{+}ip$ and $p^{+}in$ a-Si/c-Si heterojunction solar cells and used those models for device simulation. The carriers transport and recombination mechanisms in illuminated a-Si/c-Si heterojunction devices have been fully studied and complete equations for I-V have been derived. The $n^{+}ip$ and $p^{+}in$ a-Si/c-Si device structures were simulated for several design features and the internal quantum efficiency and illumination I-V behaviour were analyzed. The specific nature of the heterojunctions and their effects on both $n^{+}ip$ and $p^{+}in$ devices I-V characteristics have been modeled through a number of factors. We have calculated these factors in terms of effective velocities which limit the carrier flow across the heterojunction and depletion region. Substrates with various surface and bulk passivation levels have been considered in our simulations. Thin silicon substrates (<100 μm) in combination with low-T bulk (e.g. plasma hydrogenation) and surface (e.g. plasma silicon nitride deposition) passivation schemes can lead to a cost effective device fabrication process with competitive conversion efficiency. We have also compared our analytical simulations with a numerical simulator (AMPS) that is a very general and versatile computer simulation tool for the analysis of device physics. Our model, on the other hand specifically targets the a-Si/c-Si heterojunction solar cells. When heterojunction solar cell structures (with similar parameters) are simulated by AMPS and our model, the results agree very well. Finally, we have compared our analytical simulation results to experimental results obtained from $n^{+}ip$ a-Si/c-Si heterojunction solar cells fabricated in our laboratory. By comparing the simulated spectral response of the device to the experimental curves we were able to extract a number of device parameters such as doping levels, bulk and surface recombination parameters.

Table of Contents

List of Figures

List of Tables

Foreword

Since the solar cell was invented, the crystalline silicon has been used enormously as a light-absorbing semiconductor in fabricating most of solar cells. It converts the photons with the energy of the bandgap with good efficiency. However, the photons with lower energy are not absorbed and those with higher energy are reduced to gap energy by thermalization of the photogenerated carriers [1].

Presently two types of c-Si are used in producing the solar cell; monocrystalline and multicrystalline. The monocrystalline is produced by slicing wafers from a high-purity single crystal wafer. The second is made by sawing a cast block of silicon first into bars and then wafers. Silicon is an indirect semiconductor and the light absorption is weaker in indirect semiconductor than in a direct semiconductor. This results in high absorption length, so that for a 90% of light absorption, it takes only 1µm of GaAs (a direct semiconductor) versus 100µm of Si [1]. Therefore, the photogenerated carriers in Si have to travel a long way to reach the p-n junction that is so close to the front surface. This means that the minority carriers diffusion length should be at least twice the silicon wafer thickness to have a good amount of light absorption. High carriers diffusion length means that the material should be of very high purity and quality. However, the thicker cell requires more materials to be used in fabricating of a solar cell which causes higher cost.

The reason that silicon has been used enormously in solar cell industry, besides the good efficiency (14% to 17%), is that silicon technology has already been well developed before the invention of the solar cell and therefore high quality materials have been produced for the microelectronic market. However, due to the cost issues associated with solar cells, the industry has already started looking for other materials as replacement for silicon. The requirements for the ideal solar cell are [1]:

- bandgap between 1.1 and 1.7eV
- direct band structure
- consisting of readily available, non-toxic materials
- easy, reproducible deposition technique, suitable for large area production

- good photovoltaic conversion efficiency
- long-term stability

The alternative solar cell structures are: crystalline thin-film silicon, amorphous silicon, amorphous silicon/crystalline silicon heterojunction, copper indium diselenide and cadmium telluride.

Crystalline thin-film silicon

The crystalline thin-film silicon is considered because of the fewer amounts of material used and consequently the lower cost. The thin-layer silicon refers to the silicon layers with the thickness of between 5μm and 50μm. Because of very thin c-Si, an underlying substrate is needed as a mechanical support for the thin c-Si layer. The type of substrate (that can be low quality silicon, glass, ceramic or graphite) determines the maximum temperature allowed for the solar cell processing. Therefore, there can be either high temperature or low temperature process for thin-film c-Si. There are a few points in technology for crystalline thin-film silicon that needs consideration [1]:

- Because of the weak absorbance of the crystalline, the light trapping must be used to achieve the high degree of light internal reflection.
- Regarding the very low thickness of the silicon, the high surface recombination velocity can reduce the cell efficiency very drastically. Therefore, the front and back surfaces should be passivated to avoid it.
- If non-conducting intermediate layers or substrates are used, both the emitter and the base contacts have to be formed on the front side.
- For the solar cell formation, the layers are deposited at different temperatures so the individual layer temperatures as well as the total thermal budget are crucial parameters for a successful manufacturing of c-Si thin solar cells.

Amorphous silicon

Amorphous silicon is an alloy of silicon with hydrogen. Because of the disorder of the atomic structure, it is quite different from the crystalline silicon. The structural disorder also influences the electronic properties of the material in several ways. This makes differences between the c-Si and a-Si structures and therefore the researchers face new concepts in studying the properties of the a-Si such as: band tails, localization and scattering, mid-gap states etc. However, amorphous silicon absorbs solar radiation 40 times more efficiently than does single-crystal silicon, so a film only about 1µm thick can absorb 90% of the usable solar energy. As an important result, the potential cost is significantly low. The low temperature process that is used to produce a-Si is another factor that makes it reasonable to be used in solar cell industry. Although the amorphous silicon benefits the low cost in solar cell fabrication but the low efficiency (8%) obtained so far is a weak point of it.

a-Si/c-Si heterojunctions

Combining the a-Si and c-Si as a heterojunction solar cell gives the opportunity to have a high potential of maintaining the current collection advantages offered by the crystalline silicon, while at the same time, offering a low temperature-processing scheme via the heterojunction formation, thereby avoiding the high thermal budget of p-n homojunction formation. Because of cost-effective PV device fabrication, a-Si/c-Si heterojunction technology has become very attractive in solar cell industry. Because the process that has been used for this fabrication is essentially a low-T process (<250ºC), there is a possibility to use certain moderate quality Silicon substrates (e.g. ribbons) whose bulk carrier lifetime degrades after high-T thermal excursions. Further, the low-T nature of the process allows bulk defect passivation techniques such as plasma hydrogenation to be implemented prior to device fabrication. The advantages of this structure can be summarized as follows [1]:

- high efficiency (>20%)
- very good surface passivation: low surface recombination velocity
- low processing temperature
- reduced cost of cell technology

Copper indium diselenide

This technology that is based on the ternary compound semiconductors $CuInSe_2$, $CuGaSe_2$, $CuInS_2$ and their multinary alloy $Cu(In,Ga)(S,Se)_2$ was extremely promising at first but the complexity of the material complicates thin-film technology implementations. Very high efficiencies (19%) have been reported for laboratory scale devices. This result has been obtained by this material system by empirical optimization of process parameters. However, a further challenge is to make high voltage devices on the basis of the ternary chalcopyrite compounds $CuInS_2$ and $CuGaSe_2$. The efficiency achieved with these wide energy gap materials is still considerably lower than that of the low gap $Cu(In,Ga)Se_2$ [1].

Finally, copper indium diselenide is not yet commercial and significant further research is needed to understand the manufacturing processes.

Cadmium telluride

CdTe is nearly ideal material for thin-film photovoltaics because it combines several advantageous properties. Although the highest efficiency that has been achieved by this material in laboratory is 16% but the commercial module efficiencies hover around 6%. It has an optical bandgap close to the optimum for solar energy conversion. It is also easy to handle in thin-film deposition processes. A problem associated with CdTe is the fact that Cd and Te are toxic materials although the compound is quite stable and harmless. This makes it hard to be accepted by the market [1].

In this work we have taken up the a-Si/c-Si solar cell structure for our research. This structure has a high potential for cost reduction in fabrication since it can use low quality (defective) substrates where high temperature processes cannot be applied. The direction of the research at University of Waterloo is to develop technologies to achieve cost-effectiveness, and not to achieve high efficiencies at any cost.

Outline of Thesis

In chapter 1, we have presented our analytical modeling and simulation results of n^+p homojunction solar cell. We have discussed and simulated the quantum efficiency and the photocurrent of the n^+p homojunction solar cell, producing the quantum efficiency and I-V curves of the cell for different qualities of bulk, front and rear surface of the device.

In chapter 2, we have discussed the structure of heterojunctions in general and particularly have focused on the a-Si/c-Si heterojunction structure. We have calculated the equations of the built in voltage, the widths of space charge region and the amount of dropped voltage over n- and p-side of the device (including the intrinsic a-Si layer) for both n^+ip and p^+in a-Si/c-Si heterojunctions.

In chapter 3, we have covered different carrier transport mechanisms in heterojunctions (including SCLC, MTCE and drift-diffusion and emission) literally and have discussed the transport mechanisms that we have chosen to use in our modeling.

In chapter 4, we have modeled two transport mechanisms (drift-diffusion and emission) as two effective velocities of carriers (interface effective velocity and drift-diffusion effective velocity) which limit the carriers flow through the heterojunction. We have also calculated the effective velocities for the case that an intrinsic layer of amorphous silicon is inserted at the heterojunction. The direct tunneling has also been modeled while modeling the thermionic emission mechanism.

In chapter 5, we have developed an analytical model for n^+ip and p^+in a-Si/c-Si heterojunction solar cells under illumination and also under forward bias. We have calculated the quantum efficiency of the cells as well as the photocurrent and developed the complete I-V curves under forward bias and illumination, considering the lowering factors of current and direct tunneling.

In chapter 6, we have discussed the results that we have obtained by using our analytical model for both n^+ip and p^+in a-Si/c-Si heterojunction solar cells. We have used AMPS software to simulate n^+ip and p^+in heterojunction solar cells and have compared the results with the ones that we have obtained form our model.

In chapter 7, we have used the n^+ip heterojunction cells fabricated in our laboratory to analyze and compare with our analytical model. By adjusting the analytical model to fit with the experimental curve, we were able to extract important parameters for the experimental device.

Chapter 1

Modeling and Analysis of Homojunction Solar Cells

Following the invention of p-n junction in 1949, the concept of the photovoltaics started turning into reality and in 1954, Pearson discovered the crystalline Si solar cell [2]. Solar cell converts the incident solar radiation energy to electrical energy and is the most important long-duration power supply for satellites and space vehicles [3]. Nowadays there is a wide range of applications for solar cells in daily life. They range from calculators and wristwatches to solar powered irrigation systems and grid-connected power lines.

In this chapter, we have modeled an n^+p homojunction solar cell analytically and have created the simulation results. To do so, we have discussed the operation of a homojunction solar cell in more details. We have considered the quantum efficiency and the photocurrent of the homojunction solar cells in section 1.1 and in section 1.2, we have used our model to simulate the n^+p solar cell, producing the quantum efficiency and I-V curves of the cell for different qualities of bulk, front and rear surface of the solar cell.

1.1 Modeling of Homojunction Solar Cells

1.1.1 Solar Spectrum and Absorption Coefficient

Solar Spectrum

The nuclear fusion in sun creates huge amount of radiative energy by a rate of $4 \times 10^{20} J$ per second. This radiative energy that is emitted as electromagnetic radiation in the ultraviolet to infrared and radio spectral regions (0.2 to 3μm) is attenuated by the earth atmosphere upon reaching the earth's surface. This is because of water-vapour absorption in the infrared, ozone absorption in the ultraviolet, and scattering by airborne dust and aerosols.[3] The way in which the atmosphere affects the sunlight is measured by the "air mass" that is defined as follows:

- Air mass: The degree to which the atmosphere affects the sunlight received at the earth surface. It is secant of the angle between the sun and the zenith, and measures the atmospheric path length relative to the minimum path length when the sun is directly overhead.[3]
- Air mass 1.5: (sun at 48°19' to zenith [4]) represents a satisfactory energy-weighted average for terrestrial applications.[3]

Figure 1.1 shows the solar spectrum (power per unit area per unit wavelength) for AM 1.5 that we have used in our modeling. The data for this curve has been taken from [5].

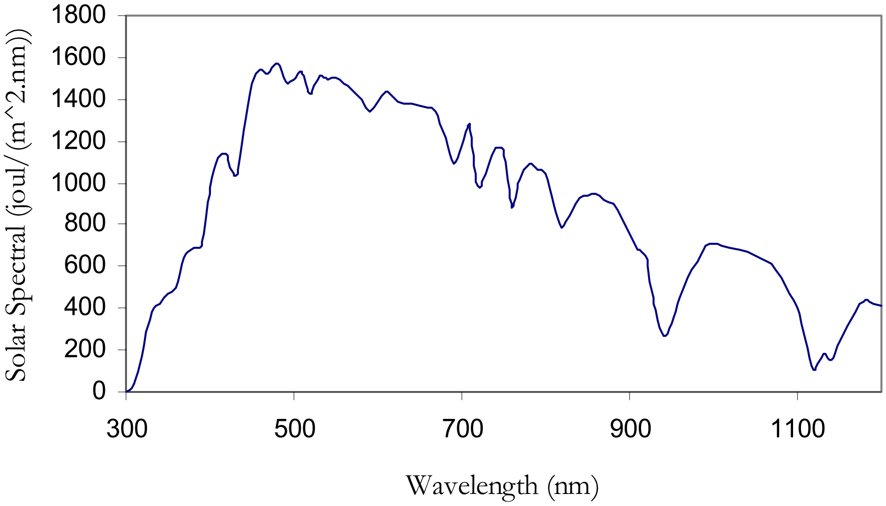

Fig 1.1 Spectral distribution of the AM 1.5 solar spectrum used in our model calculation [5]

Absorption Coefficient

Incident photons with energy more than bandgap energy of the illuminating device, become absorbed (neglecting the reflection) as they travel through the semiconductor, and the light intensity, which is proportional to the number of photons, decays exponentially with distance into the semiconductor. The light intensity, I, at a distance x from the semiconductor surface is given by: [3]

$$I(x) = I_0 \exp(-\alpha x) \tag{1.1}$$

where I_0 is the intensity of the incident radiation and α is the absorption coefficient (unit:$1/cm$) that depends on the photon energy or wavelength. α also depends on material properties [6].

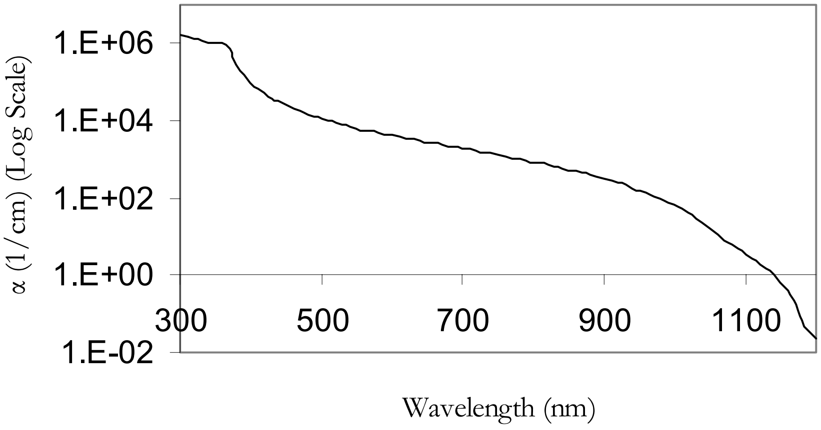

Fig 1.2 Absorption coefficient of *c-Si* used in our modeling [5]

Figure 1.2 shows the absorption coefficient of crystalline silicon that we have used in our modeling [5]. We can see from the figure that the photons with short wavelength are absorbed in very short distance of the cell surface while the long wavelength photons will have to continue traveling along the device until they are absorbed. It is clear that the absorption coefficient has an important role in calculating the quantum efficiency of the solar cell. Therefore, choosing the accurate data will help obtain more accurate simulation results.

1.1.2 Internal Quantum Efficiency: Modeling of the n^+p Solar Cell Structure

When a solar cell is illuminated by sunlight, a photon with energy less than solar cell bandgap does not contribute to the photocurrent of solar cell. However, a photon with energy greater than solar cell bandgap will create an electron-hole pair. The quantum efficiency is defined as the ratio of electron-hole pairs collected with respect to the number of incident photons:

- External quantum efficiency: number of carriers collected per incident photon at each wavelength
- Internal quantum efficiency: number of carriers collected per absorbed photon at each wavelength

By calculating the internal quantum efficiency for a range of wavelengths, one can obtain the total current generated by light (photocurrent) in the whole wavelengths range. The quantum efficiency depends on the device absorption coefficient, carriers lifetime, the surface recombination velocity and the geometry of the device.

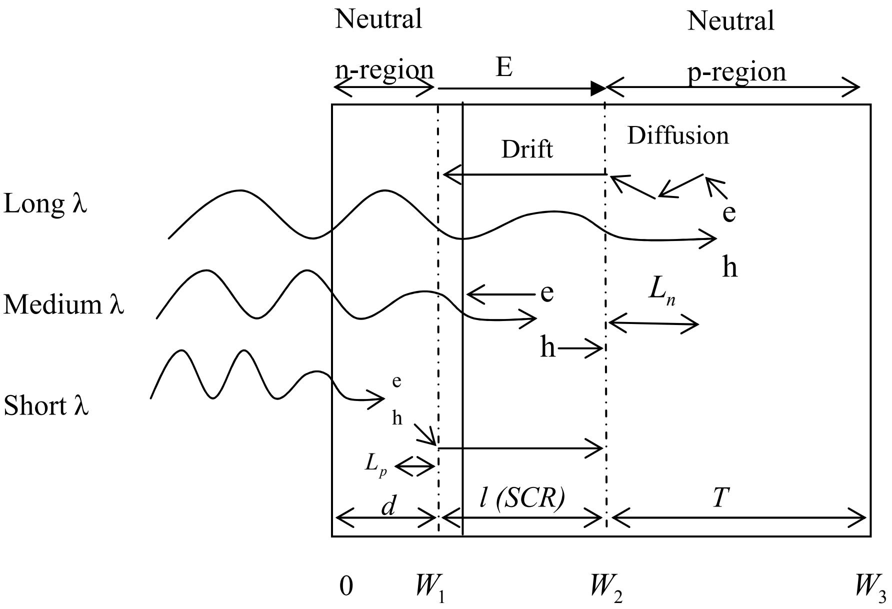

Fig 1.3 Structure of the n^+p homojunction used in our modeling

Figure 1.3 shows a schematic diagram of a typical solar cell. The cell is formed by a very thin and heavily doped n-region (emitter with the thickness of *d*) and a thick and less doped p-region (base with the thickness of *T*). The illumination is through n-region window. The space charge region (SCR with the thickness of l) is expanded primarily into p-side (which is less doped) and there is an electric field (*E*) inside SCR which depletes it from the free carriers (depletion region). L_n and L_p are the diffusion length of the electrons and holes respectively.

The figure shows that the electrons (holes) generated in p-side (n-side) within diffusion length from the edge of SCR, diffuse into SCR and then drift into n-region (p-region). Most of the photons are absorbed within SCR or p-region. This is because the n-region is so thin and heavily doped. The photons absorbed within SCR will generate electron-hole pairs (EHPs). These EHPs will be swept immediately toward the n and p-regions. The electric field inside the SCR (*E*) is responsible for sweeping the electrons and holes toward n and p-regions respectively. Once the electrons (holes) reach n (p)-region, they are collected by recombining with the majority populations. This scenario within the n and p-regions is somehow different. For example, when an EHP is generated in p (n)-region, the holes (electrons) in this region are majority carriers, so they have already been collected by being in p (n)-region. On the other hand, electrons (holes) in p (n)-region are minority carriers. Therefore, they will diffuse toward the p (n)-region and SCR interface, where the population of minority carries are so low. As soon as the electrons (holes) reach this interface, the electric field inside SCR will sweep them to the opposite side, i.e. n (p)-region. This means that the carriers that we should consider in calculation of quantum efficiency are:

- the EHPs generated in SCR
- electrons generated in p-region and diffused to the p-region SCR interface
- holes generated in n-region and diffused to the n-region SCR interface

Space Charge Region Quantum Efficiency

Due to the high electric field in depletion region, all the photo-generated carriers in this region will be collected. This means that we can assume there is no recombination in SCR and whatever is generated will participate in forming the photocurrent of this region.

Using the generation equation (1.1) and assuming that there is only a monochromic incident light to the surface of the device, and also assuming that all the photo-generated carriers are collected in SCR, we can write:

$$J_{SCR} = q\int_{W_1}^{W_2} G(x)dx = q\int_{W_1}^{W_2} \alpha e^{-\alpha x}dx = q[-e^{-\alpha x}]_{W_1}^{W_2} = q[e^{-\alpha d} - e^{-\alpha(d+l)}] \tag{1.2}$$

This means that J_{SCR} will include both hole and electron photo-generated carriers.

p-region Quantum Efficiency

As discussed in previous sections, in p-region (Figure 1.3), the carriers responsible for photocurrent are the minority carriers, i.e. the electrons. Since in p-region there is no electric field, the diffusion current will act as the main stream of carriers and two essential processes will affect this current: Carrier Generation and Recombination.

The generation rate pf EHPs at distance *x* from the semiconductor surface is given by: [3]

$$G_n(x) = F(\lambda)\alpha(\lambda)e^{-\alpha(\lambda)x} \tag{1.3}$$

where *a(λ)* is the absorption coefficient and *F(λ)* is the number of incident photons/ cm^2 /s per unit bandwidth.

In case of doped region (p), the recombination rate of carriers will be the ratio of excess carrier concentration (minority carriers generated by light, $\Delta n(x)$) over the minority carriers lifetime (τ_n): [3]

$$R_n(x) = \frac{\Delta n(x)}{\tau_n} \tag{1.4}$$

We solve the equations for a single photon of monochromic incident light. We start with continuity equation for electrons in p-region and regarding the fact that we consider the device in steady state, time factor will not appear in our equations: [3]

$$0 = \frac{1}{q}\frac{dJ_n(x)}{dx} + G_n(x) - R_n(x) \tag{1.5}$$

According to Figure 1.3, the boundary conditions are:

$$\Delta n(W_2) = 0 \tag{1.6}$$

which means the electrons will be swept by electric field as soon as they reach the SCR border and:

$$D_n \frac{d\Delta n(W_3)}{dx} = -s_n \Delta n(W_3) \tag{1.7}$$

indicating that the recombination rate at the back surface must be equal to the flux of minority carriers flowing into the surface (the recombination rate of minority carriers at the back surface is shown by the surface recombination velocity, s_n)

Due to zero electric field in this region, there will only be diffusion current [3]:

$$J_n = qD_n \frac{dn(x)}{dx} \tag{1.8}$$

where D_n is the carrier diffusion coefficient that is associated with mobility: $D_n = V_T \mu_n$.

We know that:

$$\frac{dn(x)}{dx} = \frac{d\Delta n(x)}{dx} \tag{1.9}$$

By combining the equations 1.3, 1.4, 1.5, 1.8 and 1.9, we will have:

$$\frac{d^2 \Delta n(x)}{dx^2} - \frac{\Delta n(x)}{L_n^2} = -\alpha e^{-\alpha x} \tag{1.10}$$

where L_n is diffusion length of minority carriers (electrons) and is defined by:

$$L_n = \sqrt{D_n \tau_n} \tag{1.11}$$

The general solution to this second order differential equation is:

$$\Delta n(x) = c_1 e^{\frac{x}{L_n}} + c_2 e^{\frac{-x}{L_n}} + \frac{\alpha L_n^2}{D_n (1 - \alpha^2 L_n^2)} e^{-\alpha x} \tag{1.12}$$

We want to calculate the diffusion current at W_2:

$$J_n(W_2) = D_n \frac{dn(x)}{dx} = D_n \frac{d\Delta n(x)}{dx}(x = W_2) \tag{1.13}$$

By substituting equation 1.12 in 1.13 and regarding the boundary conditions (equation 1.6 and 1.7), we reach the following equation for electron photocurrent in p-region, generated by one photon of a monochromic light:

$$J_n(W_2) = q\frac{\alpha L_n e^{-\alpha(d+l)}}{1-\alpha^2 L_n^2}\left[\frac{\frac{s_n\tau_n}{L_n}Cosh(\frac{T}{L_n}) + Sinh(\frac{T}{L_n}) + (\alpha L_n - \frac{s_n\tau_n}{L_n})e^{-\alpha T}}{Cosh(\frac{T}{L_n}) + \frac{s_n\tau_n}{L_n}Sinh(\frac{T}{L_n})} - \alpha L_n\right] \qquad (1.14)$$

It should be noted that the expression $e^{-\alpha(d+l)}$ reflects the fact that the light intensity has been reduced by this factor when it reaches W_2.

We will redo the same procedure to calculate the hole photocurrent generated in n-region.

n-region Quantum Efficiency

In this case the boundary conditions are (Figure 1.3):

$$\Delta p(W_1) = 0 \qquad (1.15)$$

and

$$D_p\frac{d\Delta p(0)}{dx} = s_p\Delta n(0) \qquad (1.16)$$

(s_p indicates the recombination rate of minority carriers at the front surface or the surface recombination velocity)

The current for electrons at W_1 will be:

$$J_p(W_1) = q\frac{\alpha L_p}{1-\alpha^2 L_p^2}\left[\alpha L_p e^{-\alpha d} - \frac{\alpha L_p + \frac{s_p\tau_p}{L_p}[1 - e^{-\alpha d}.Cosh(\frac{d}{L_p})] - e^{-\alpha d}Sinh(\frac{d}{L_p})}{Cosh(\frac{d}{L_p}) + \frac{s_p\tau_p}{L_p}Sinh(\frac{d}{L_p})}\right] \qquad (1.17)$$

1.1.3 I-V Modeling of n^+p Solar Cell

By calculating the internal quantum efficiency of each region in n^+p solar cell of Figure 1.3, we can calculate the photocurrent of the device. The photocurrent that is also called short circuit current is obtained when there is no applied voltage on solar cell. The magnitude of photocurrent, disregarding all the losses in the cell, with AM1.5 radiation, can reach a peak of $44mA/cm^2$ [7].

To calculate the photocurrent, we need to know the photon flux of sunlight. This can be calculated from the energy distribution of sunlight (solar spectrum, Figure 1.4) by dividing the energy content at a given wavelength by the energy of an individual photon [8]. Suppose that we have the data of the flow of the energy (W) per unit area at a given wavelength. The energy of single photon is given by: $E_{ph} = \frac{hC}{\lambda}$ where *C* is the speed of light, *h* the Plank's constant and *λ* the wavelength of light. The number of photons for a given energy of sunlight is obtained by:

$= \frac{W}{E_{ph}} = \frac{\frac{[J]}{[cm^2][cm]}}{\frac{[J][s][cm]/[s]}{cm}} = \frac{1}{[cm^2][cm]}$ which gives the number of photons per unit area at a given wavelength. By integrating these distributions over the wavelength range for which the electron-hole pairs can be generated for a given semiconductor, the photocurrent will be calculated. Since the data used for our work are discrete (numerical), the integral will be replaced by sigma and instead of *dλ* we will put Δ*λ* which for our data is: 0.01 [5].

$J = \sum_{i=1}^{91} n_{ph}(\lambda_i)\Delta\lambda$ where $\lambda_1 = 300nm$ and $\lambda_{91} = 1200nm$.

If we apply a forward bias to the solar cell, dark current will flow through the device in a direction opposite to the photocurrent. This is because of the fact that the direction of electric field in SCR is from n-side to p-side (due to the depletion) while the forward voltage is applied from p-side to the n-side. When the dark current flows through the cell, it compensates the photogenerated current. As we will see later in this chapter, this results in the I-V curve of the device shifting downward by the amount of the photocurrent.

1.2 Simulation of n^+p Homojunction Solar Cell

Now by having the equations (1.2, 1.14 and 1.17) for quantum efficiencies of SCR, p- and n-region, we can draw the total quantum efficiency of the n^+p solar cell shown in Figure 1.3. Figure 1.7 shows the internal quantum efficiency diagrams of an n^+p solar cell for n, p and space charge regions. The sample cell for this simulation has been chosen as the following:

$$N_d = 10^{19}\,cm^{-3} \quad N_a = 10^{16}\,cm^{-3}, \ \mu_n = 1183\frac{cm^2}{V.s} \ \mu_p = 73\frac{cm^2}{V.s}$$

$$L_n = 0.03cm \quad L_p = 500nm, \ s_n = s_p = 1000cm/s$$

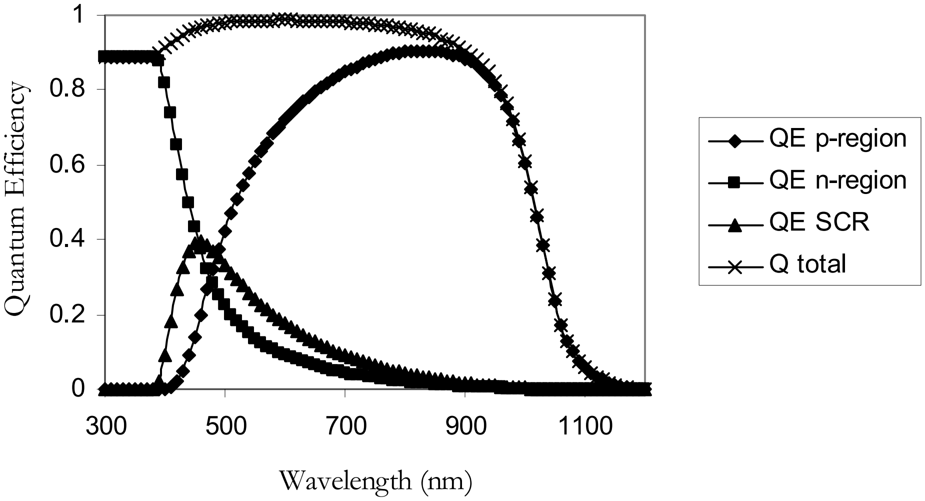

Fig 1.4 n^+p solar cell internal quantum efficiency for n, p and space charge regions

Regarding the size of device that we have chosen, the widths of the regions are:

$$n-region = 250nm \quad p-region = 249.41\mu m \quad SCR = 590nm$$

As discussed earlier, the front and rear surface recombination velocities have important roles in solar cell photocurrent. However, the influence of these parameters on the cell efficiency depends on the diffusion lengths of the carriers. For instance, when the diffusion length of the electrons in p-region (L_n) is comparable to the width of the emitter (p-region), then the back surface velocity (s_n) (which can be changed by passivation techniques) will play a major role in the solar cell photocurrent. The reason is that in this case, the excess minority carriers will reach the back surface of the device before they recombine and therefore, the rate of their recombination in the back surface will definitely influence the number of collected carriers. (Figure 1.5)

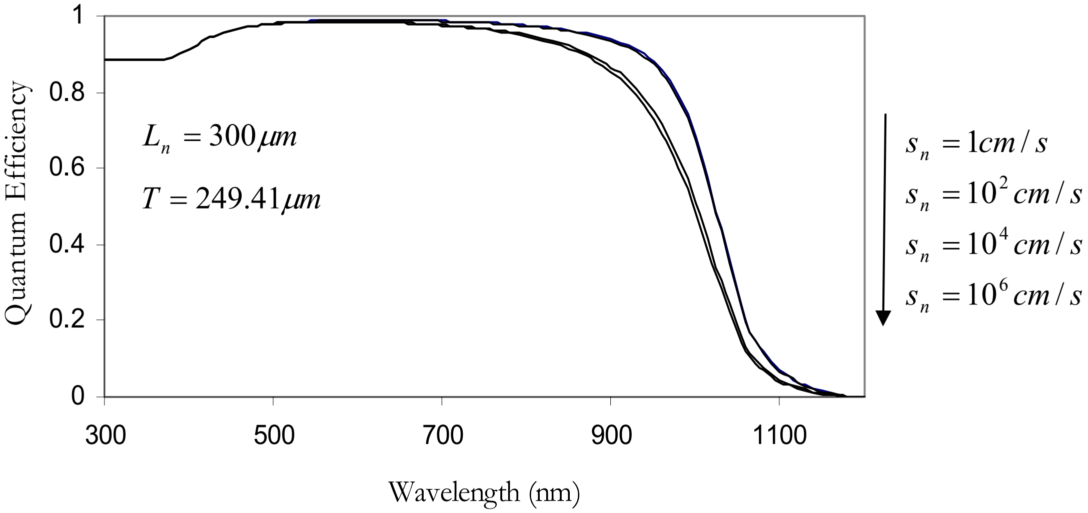

Fig 1.5 n^+p solar cell internal quantum efficiency for different back surface velocities of electrons (for long L_n)

However, if the diffusion length of electrons is much shorter than the emitter width, this means that the electrons will recombine before they reach the back surface and consequently, the back surface recombination velocity cannot affect the electron photogenerated current (Figure 1.6).

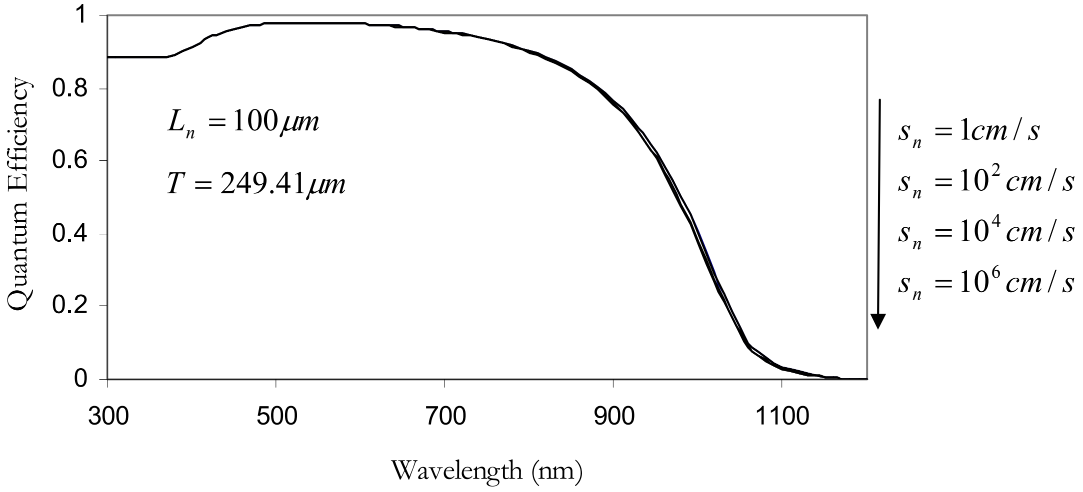

Fig 1.6 n^+p solar cell internal quantum efficiency for different back surface velocities of electrons (for short L_n)

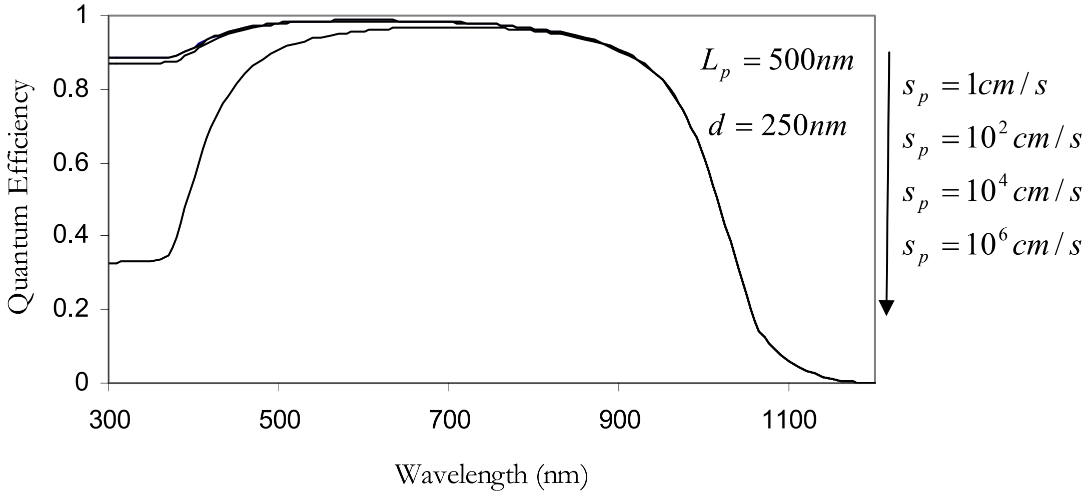

Fig 1.7 n^+p solar cell internal quantum efficiency for different front surface velocities of holes (for long L_p)

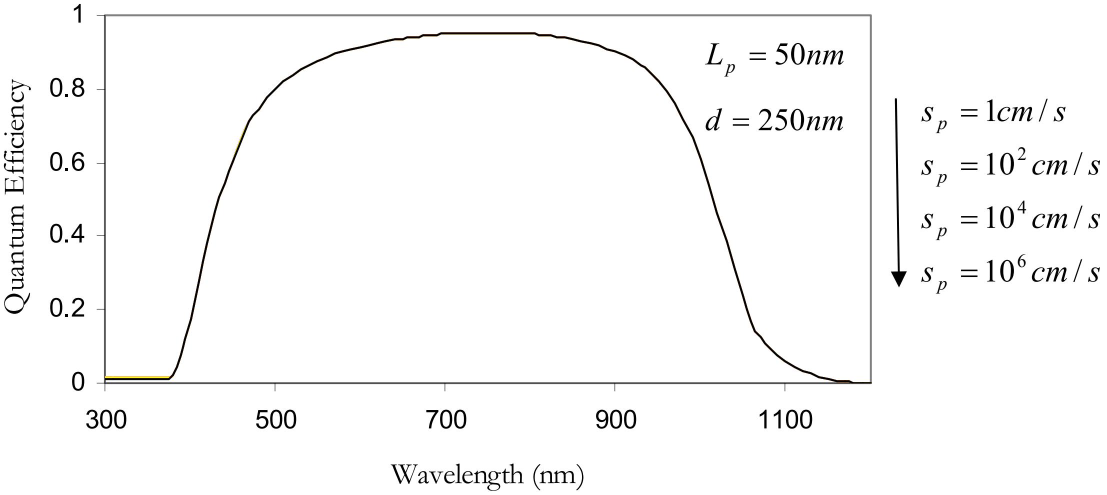

Fig 1.8 n^+p solar cell internal quantum efficiency for different front surface velocities of holes (for short L_p)

Figures 1.7 and 1.8 show the quantum efficiency of the cell for different front surface recombination velocities (s_p) for long and short diffusion length of holes in n-region respectively. As we can see from the figures, for long diffusion lengths, the front recombination velocity can affect the quantum efficiency significantly (Figure 1.7) while in case of short diffusion lengths, the quantum efficiency is almost non-sensitive to the front surface recombination velocity of holes (Figure 1.8).

As we discussed earlier, the diffusion length of minority carriers in the bulk depends on the quality of the device in addition to the doping level. Figure 1.9 shows how this parameter makes the total quantum efficiency of the solar cell to change.

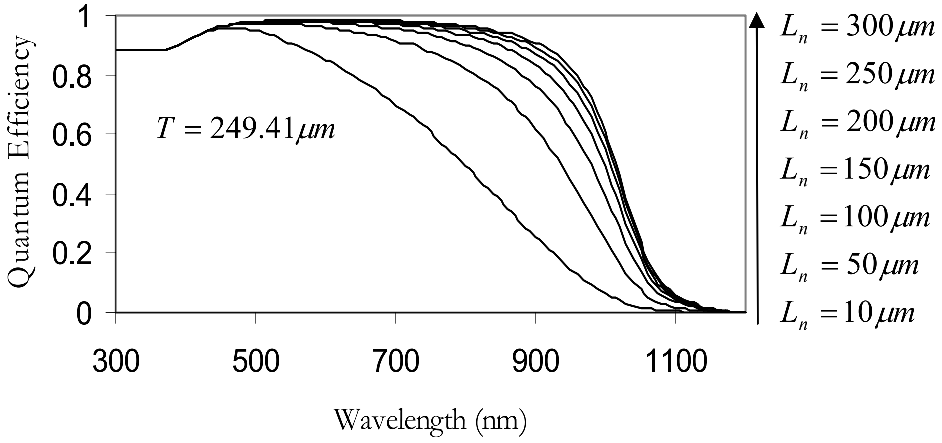

Fig 1.9 n^+p solar cell internal quantum efficiency for different diffusion lengths of bulk

As it is seen from the figure, the higher diffusion length of minority carriers in the bulk, which means the better quality of the device material, will provide higher quantum efficiency.

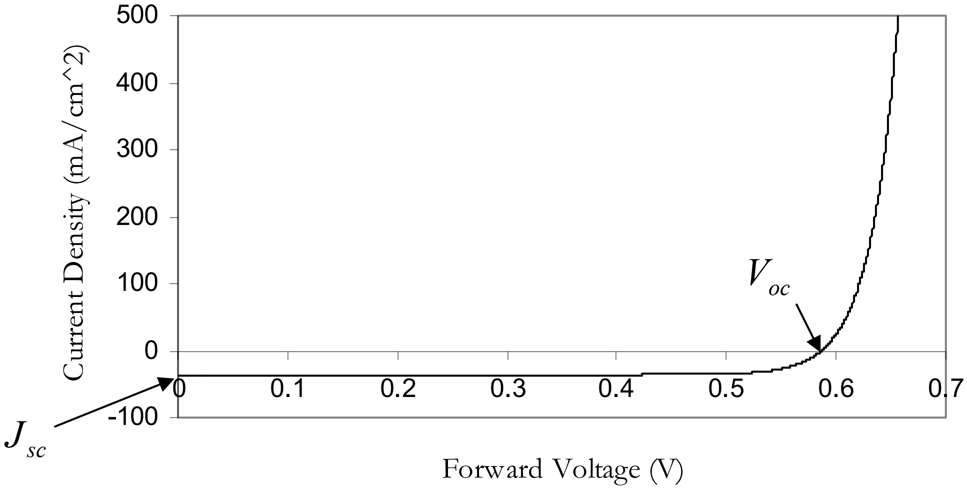

Fig 1.10 I-V diagram of a n^+p solar cell

Using the procedure that we discussed in section 1.1.3, we have calculated and plotted the I-V curve of the n^+p solar cell (with the device parameters indicated in 1.2) shown in Figure 1.10. This figure shows the short circuit current (J_{sc}) and open circuit voltage (V_{oc}) of the solar cell. The short circuit current, as we discussed in section 1.1.3, is obtained when there is no voltage at the cell and the open circuit voltage is obtained when no current is drawn from the solar cell.

For Figure 1.10 have obtained:

$$J_{sc} = 35.88mA \quad V_{oc} = 587.0mV$$

We can calculate the voltage and current of the cell at the optimal operating point (V_m, I_m), and obtain the peak output, $V_m \times I_m$. The ratio of peak output to the variable $I_{sc} \times V_{oc}$ is called the fill factor (FF) of the cell:

$$FF = \frac{V_m I_m}{V_{oc} I_{sc}} \tag{1.18}$$

We can replace I_m and I_{sc} by J_m and J_{sc}, respectively:

$$FF = \frac{V_m J_m}{V_{oc} J_{sc}} = \frac{508.5 \times 34.14}{587.0 \times 35.88} = 82.42\%$$

As we saw earlier, the quality of the bulk region affects the quantum efficiency of the solar cell. Figure 1.11 shows that it affects the I-V curve of the device as well.

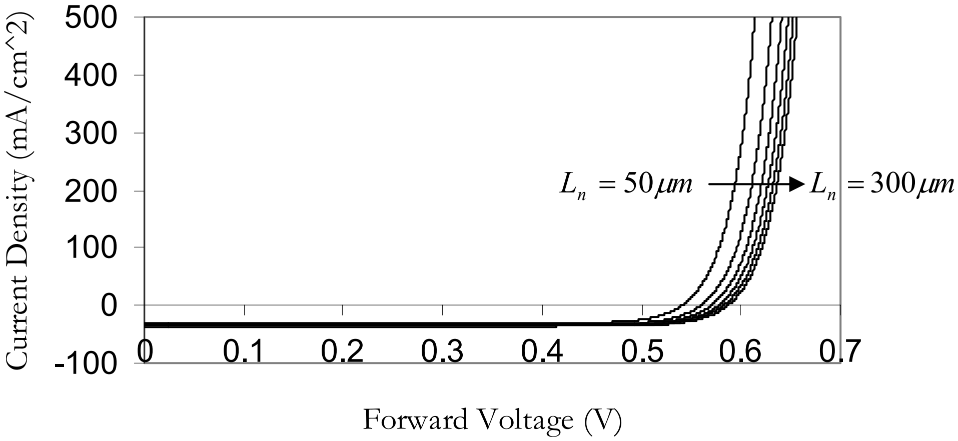

Fig 1.11 I-V diagram of a n^+p solar cell for different bulk diffusion lengths

We see from the Table 1.1 that by increasing the diffusion length of the electrons in the bulk region from $50\mu m$ to $360\mu m$, the short circuit current and open circuit voltage increase from $31.03 mA/cm^2$ and $540.5 mV$ to $35.88 mA/cm^2$ and $587.0 mV$, respectively.

$L_n(cm)$	$J_{sc}(mA/cm^2)$	V_{oc} (mV)	FF
50	31.03	540.5	81.43%
100	33.41	559.5	81.68%
150	34.57	570.5	81.82%
200	35.23	577.5	82.24%
250	35.63	582.5	82.39%
300	35.88	587.0	82.42%

Tab 1.1 J_{sc}, V_{oc} and FF of n^+p solar cell for different L_n

Tables 1.2 and 1.3 show how the short circuit current, open circuit voltage and FF of solar cell change with the changes of the back surface and front surface recombination velocities of the minority carriers.

$s_n(cm/s),[s_p = 10^3]$	$J_{sc}(mA/cm^2)$	V_{oc} (mV)	FF
1	36.53	587.0	82.50%
10^2	36.44	587.0	82.47%
10^4	35.03	586.0	82.46%
10^6	34.78	586.0	82.42%

Tab 1.2 J_{sc}, V_{oc} and FF of n^+p solar cell for different s_n

Table 1.2 shows that the change on rear surface recombination velocity affects the short circuit current and open circuit voltage. It shows that by increasing the s_n, the short circuit current decreases and consequently the open circuit voltage decreases as well. In fact, because the photogenerated carriers in the emitter carry out the major contribution to the photocurrent of the solar cell, any change on this rate will affect the I-V.

$s_p(cm/s)$,$[s_n = 10^3]$	$J_{sc}(mA/cm^2)$	V_{oc} (mV)	FF
0	35.89	587.0	82.42%
10^2	35.89	587.0	82.42%
10^4	35.84	586.5	82.47%
10^6	33.97	585.5	82.41%

Tab 1.3 J_{sc}, V_{oc} and FF of n^+p solar cell for different s_p

Table 1.3 shows the effect of increasing the front surface recombination velocity on the open circuit voltage and short circuit current. As we can see, both V_{oc} and J_{sc} decrease by increasing s_p.

Chapter 2

The *a-Si/c-Si* Heterojunction Structure

In this chapter, we have discussed the structure of heterojunctions in general and particularly have focused on the a-Si/c-Si heterojunction structure. We have calculated the equations of the built in voltage, the widths of space charge region and the amount of dropped voltage over n and p-side of the device. To derive these equations, we have used the Poisson's equation for different parts of the SCR.

In sections 2.1 and 2.2, we have calculated the above-mentioned equations for $n^{+}p$ a-Si/c-Si heterojunction. As we have discussed in section 2.3, in solar cell applications, an ultra thin intrinsic layer of amorphous silicon is introduced through the junction. We have recalculated all the equations for $n^{+}ip$ a-Si/c-Si heterojunction as well as for the $p^{+}in$ a-Si/c-Si heterojunction in sections 2.31 and 2.3.2, respectively.

We have used these equations in modeling and simulation of the a-Si/c-Si heterojunction solar cells in next chapters.

Is a-Si/c-Si a heterojunction?

A heterojunction is a junction between two dissimilar semiconductors with different bandgaps. The junction is called the isotype heterojunction if two devices have the same conductivity and it will be an anisotype heterojunction if the conductivities of two materials constituting the device are different [3]. Although amorphous and crystalline silicon are not completely different semiconductors, the junction between these two is considered as a anisotype heterojunction since the bandgap of amorphous silicon is different from that of the crystalline silicon, in addition to the fact that the conductivity of these two semiconductors differ. It is also approximated that the a-Si/c-Si heterojunction can be considered as an abrupt heterojunction [9].

2.1 n^+p Heterojunction: Energy Band Structure

When we form a heterojunction by putting two materials with different bandgaps beside each other, regarding the difference in electron affinity and bandgap of the devices, two types of heterojunctions band lineup can be formed [10]:

- In first type which includes 80% of heterojunctions, ΔE_C (discontinuity in conduction band) and ΔE_V (discontinuity in valence band) that are derived from the following equations, are both positive:

$$\Delta E_C = E_{C2} - E_{C1} = X_1 - X_2 \tag{2.1}$$

$$\Delta E_V = E_{V1} - E_{V2} = E_{g1} - E_{g2} - \Delta E_C \tag{2.2}$$

where X_1 ,X_2 and E_{g1} ,E_{g2} are the electron affinity and the bandgap of material 1 and 2, respectively. To keep ΔE_C and ΔE_V positive, we should have $E_{C2} > E_{C1}$ and $E_{V1} > E_{V2}$ respectively (see Figure 2.1). This means that the material 2 has bigger bandgap than the material 1.

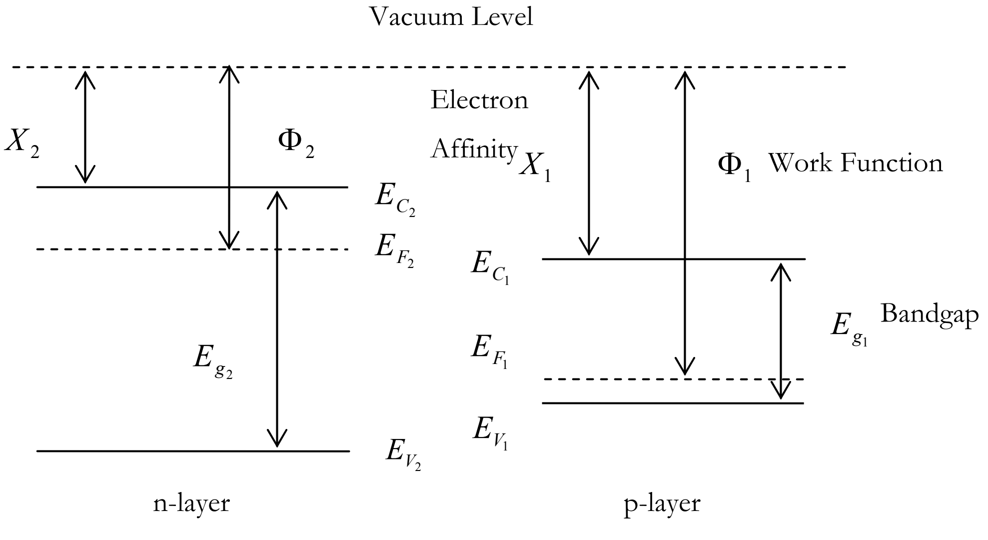

Fig 2.1 Energy band diagram of an n^+p heterojunction for (ΔE_C, ΔE_V)>0, with no physical contact between layers

- In the second type, we have:

Either ΔE_C or ΔE_V is greater than ΔE_g which means that either ΔE_C or ΔE_V is negative:

If $\Delta E_C = X_1 - X_2 > \Delta E_g$ then $\Delta E_V < 0$ or If $\Delta E_C = X_1 - X_2 < 0$ then $\Delta E_V > \Delta E_g$.

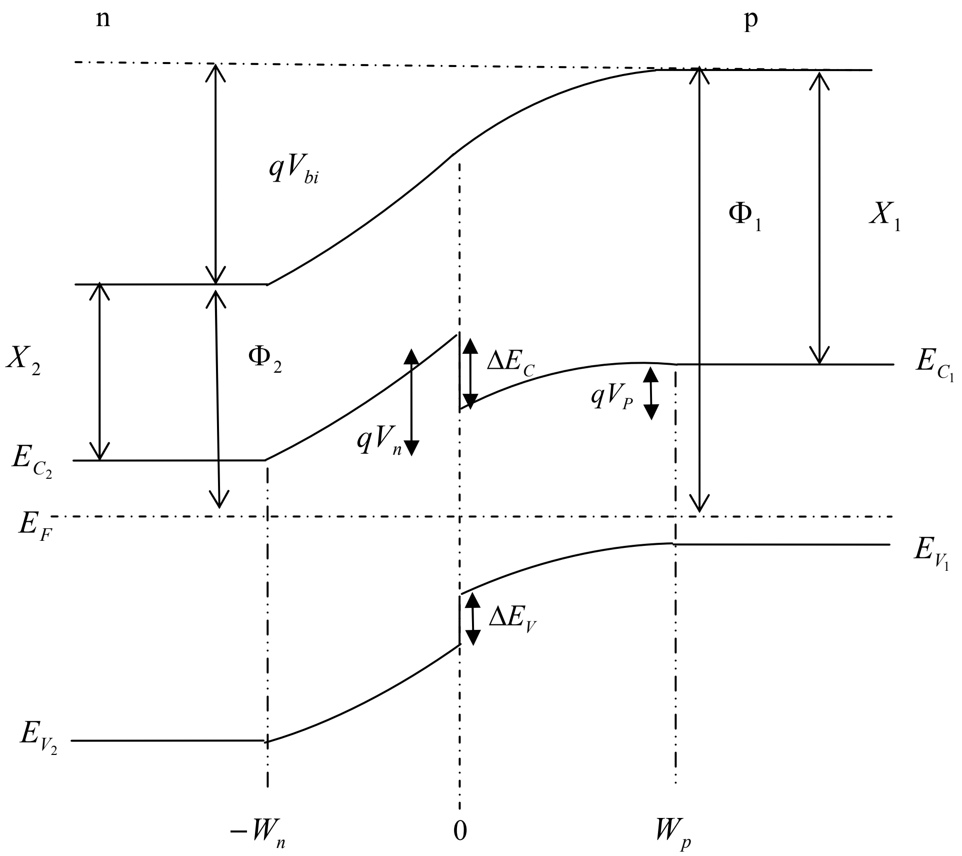

Fig 2.2 Energy band diagram of an n^+p heterojunction in physical contact

In our study, material 2 is amorphous silicon and material 1 is crystalline silicon. This leads us to the following situation:

$E_{g1} = 1.12eV \quad X_1 = 4.05eV$ [3]

$E_{g2} \approx 1.72eV \quad X_2 \approx 3.8eV$ [9]

$\Delta E_g = 0.6eV$

$$X_1 - X_2 = 4.05eV - 3.8eV = 0.25eV$$

$$\Delta E_C = E_{C2} - E_{C1} = X_1 - X_2 = 0.25eV < \Delta E_g$$

therefore $\Delta E_V = \Delta E_g - \Delta E_C = 0.6eV - 0.25eV = 0.35eV > 0$

This means that for a-Si/c-Si heterojunction which is our case, both ΔE_C and ΔE_V will have positive values and consequently for an n-p a-Si/c-Si heterojunction we will have a band diagram like Figure 2.2. As we see from the figure, ΔE_C and ΔE_V are the potential barriers in valence and conduction band that, as we will discuss later, affect the carrier transport in the device

2.2 n^+p Heterojunction: Static Analysis

As it can be seen from Figure 2.2, the heterojunction is assumed to be abrupt. This is what we have already assumed about the a-Si/c-Si heterojunction. This means that there is an abrupt change in the band diagram of the heterojunction at the point of metallurgical junction.

We like to calculate the built in voltage (V_{bi}), the voltage dropped over p- and n-side and also the width of the depletion region ($W_n + W_p$). As we know from the n-p homojunction, the built in voltage is equal to the difference between the work functions of the n- and p-side .i.e, Φ_1 and Φ_2.It is also equal to the voltage drop on both n and p regions. i.e, V_n and V_P. Therefore, we can write:

$$qV_{bi} = \Phi_1 - \Phi_2 = q(V_n + V_p) \tag{2.3}$$

$$qV_{bi} = \Phi_1 - \Phi_2 = q\frac{X_1 + E_{C1} - E_F}{q} - q\frac{X_2 + E_{C2} - E_F}{q} \tag{2.4}$$

and

$$E_{C1} - E_F = E_{g1} - (E_F - E_{V1}) = E_{g1} - kT\ln(\frac{N_{v1}}{N_{a1}}) \tag{2.5}$$

$$E_{C2} - E_F = kT\ln(\frac{N_{c2}}{N_{d2}}) \tag{2.6}$$

so for built in voltage we can write:

$$qV_{bi} = X_1 - X_2 + E_{g1} - kT\ln(\frac{N_{v1}}{N_{a1}}) - kT\ln(\frac{N_{c2}}{N_{d2}}) = \Delta E_C + E_{g1} - kT\ln(\frac{N_{v1}N_{c2}}{N_{a1}N_{d2}})$$

$$V_{bi} = \frac{\Delta E_C}{q} + \frac{E_{g1}}{q} - V_T \ln(\frac{N_{v1}N_{c2}}{N_{a1}N_{d2}}) \qquad (2.7)$$

where N_{v1} and N_{c2} are the effective densities of energy states per unit volume for holes and electron in material 1 and 2 respectively and N_{a1} and N_{d2} are the doping levels of p-type (material 1) and n-type (material 2) materials respectively.

In order to calculate the depletion region width we have to start with electric charge equation:

$$\rho(x) = +qN_d \quad \text{for} \quad -W_n < x < 0 \qquad (2.8)$$

$$\rho(x) = -qN_a \quad \text{for} \quad 0 < x < W_p \qquad (2.9)$$

For $-W_n < x < 0$ we can write the Poisson's equation such:

$$\frac{dE(x)}{dx} = \frac{qN_d}{\varepsilon_2} \Rightarrow E(x) = \frac{qN_d}{\varepsilon_2}(x + W_n) \quad \text{for} \quad -W_n < x < 0 \qquad (2.10)$$

and for $0 < x < W_p$:

$$\frac{dE(x)}{dx} = -\frac{qN_a}{\varepsilon_1} \Rightarrow E(x) = -\frac{qN_a}{\varepsilon_1}(x - W_p) \qquad (2.11)$$

Although the dielectric constants for material 1 and 2 (ε_1 and ε_2) are different but because of the continuity of the electric vector (D), the boundary condition at $x = 0$ gives that:

$$D(0^-) = D(0^+) \Rightarrow \varepsilon_2 E(0^-) = \varepsilon_1 E(0^+) \qquad (2.12)$$

which leads us to

$$N_d W_n = N_a W_p \qquad (2.13)$$

Regarding the relation between electric field and voltage:

$$E(x) = -\frac{dV(x)}{dx} \qquad (2.14)$$

We can calculate the voltage for every interval:

$$V(x)=\begin{cases} 0 & x<-W_n \\ -\dfrac{qN_d}{2\varepsilon_2}(x+W_n)^2 & -W_n<x<0 \\ -\dfrac{qN_d}{2\varepsilon_2}W_n^2-\dfrac{qN_a}{2\varepsilon_1}(2W_px-x^2) & 0<x<W_p \\ -V_{bi} & W_p<x \end{cases} \tag{2.15}$$

From equation 2.15 we can write:

$$V_n=V(-W_n)-V(0)=0+\frac{qN_d}{2\varepsilon_2}W_n{}^2=\frac{qN_d}{2\varepsilon_2}W_n{}^2 \tag{2.16}$$

$$V_p=V(0)-V(W_p)=-\frac{qN_d}{2\varepsilon_2}W_n^2+\frac{qN_d}{2\varepsilon_2}W_n^2+\frac{qN_a}{2\varepsilon_1}W_p^2=\frac{qN_a}{2\varepsilon_1}W_p^2 \tag{2.17}$$

and

$$V_{bi}=V_n+V_p=\frac{qN_d}{2\varepsilon_2}W_n^2+\frac{qN_a}{2\varepsilon_1}W_p^2 \tag{2.18}$$

Using equation 2.13 and by substituting $W_n=\dfrac{N_aW_p}{N_d}$ in 2.18:

$$V_{bi}=\frac{qN_d}{2\varepsilon_2}\times\frac{N_a^2W_p^2}{N_d^2}+\frac{qN_a}{2\varepsilon_1}W_p^2=\frac{q}{2\varepsilon_2}\times\frac{N_a^2W_p^2}{N_d}+\frac{qN_a}{2\varepsilon_1}W_p^2 \quad =>$$

$$W_p=\sqrt{\frac{2\varepsilon_1\varepsilon_2N_dV_{bi}}{qN_a(\varepsilon_1N_a+\varepsilon_2N_d)}} \tag{2.19}$$

and respectively for W_n:

$$W_n=\sqrt{\frac{2\varepsilon_1\varepsilon_2N_aV_{bi}}{qN_d(\varepsilon_1N_a+\varepsilon_2N_d)}} \tag{2.20}$$

A quick look at the calculated relations so far helps us recognize the way we can reach the values of V_{bi}, V_n and V_P. From equation 2.7 we can calculate V_{bi} then by substituting it in 2.19 and 2.20, W_n and W_p will be obtained. Therefore, we can calculate the values of V_n and V_P by using W_n and W_p in equations 2.16 and 2.17 respectively.

In case of p^+n heterojunction, the approach for all the calculation is the same and we will find the following equations for the parameters:

$$V_{bi} = \frac{\Delta E_V}{q} + \frac{E_{g1}}{q} - V_T \ln(\frac{N_{V2}N_{C1}}{N_{a2}N_{d1}}) \tag{2.21}$$

$$W_p = \sqrt{\frac{2\varepsilon_1\varepsilon_2 N_d V_{bi}}{qN_a(\varepsilon_1 N_a + \varepsilon_2 N_d)}} \tag{2.22}$$

$$W_n = \sqrt{\frac{2\varepsilon_1\varepsilon_2 N_a V_{bi}}{qN_d(\varepsilon_1 N_a + \varepsilon_2 N_d)}} \tag{2.23}$$

$$V_n = \frac{qN_d}{2\varepsilon_1} W_n^{\,2} \tag{2.24}$$

$$V_p = \frac{qN_a}{2\varepsilon_2} W_p^2 \tag{2.25}$$

$$V_{bi} = V_n + V_p = \frac{qN_d}{2\varepsilon_1} W_n^2 + \frac{qN_a}{2\varepsilon_2} W_p^2 \tag{2.26}$$

2.3 Inserting an Intrinsic *a-Si* Layer at the Heterojunction

Because of the characteristics of the amorphous silicon, the n-p a-Si/c-Si heterojunction solar cell has lower fill factor and open circuit voltage in comparison to the n-p homojunction c-Si solar cell. The studies show [11] that the recombination process in the SCR (where the heterojunction is located) can be the reason for these poor properties. In fact, the recombination that happens at the a-Si and c-Si interface is because of high density of mid-gap states in the amorphous silicon. The high density of trap centers in a-Si also increases the leakage current due to tunneling process [11]. Therefore, to improve the efficiency of the a-Si/c-Si heterojunction solar cell, the quality of the heterointerface is very crucial. To suppress the interface recombination, a very thin intrinsic a-Si layer is inserted at the a-Si/c-Si heterojunction. In order to insert the i-layer in the a-Si/c-Si heterojunction, a good passivation at the c-Si surface is necessary. Because the trap density of intrinsic amorphous silicon is significantly smaller than that of doped layer, inserting a thin layer of it reduces the surface recombination as well as the leakage current. This results in higher open circuit voltage and short circuit current.

Higher efficiency is the main reason for the heterojunction solar cell fabricators to introduce the i-layer in the heterojunction. However, adding an intrinsic amorphous silicon layer affects the depletion region width and the way that the built in voltage is divided between SCR regions. As we will discuss later, it also affects the transport of the carriers flowing through the i-layer by limiting their effective velocities.

2.3.1 Static Analysis of the n^+ *a-Si/i a-Si/p c-Si* Heterostructure

The equation of built in voltage of n^+ip heterojunction is similar to of the n^+p heterojunction without intrinsic layer. For the n^+ip heterojunction in Figure 2.3, we can write:

$$qV_{bi} = \Phi_1 - \Phi_2 = q(V_n + V_p + V_i) \tag{2.27}$$

$$qV_{bi} = \Phi_1 - \Phi_2 = q\frac{X_1 + E_{C1} - E_F}{q} - q\frac{X_2 + E_{C2} - E_F}{q} \tag{2.28}$$

and

$$E_{C1} - E_F = E_{g1} - (E_F - E_{V1}) = E_{g1} - kT\ln(\frac{N_{v1}}{N_{a1}}) \tag{2.29}$$

$$E_{C2} - E_F = kT\ln(\frac{N_{c2}}{N_{d2}}) \tag{2.30}$$

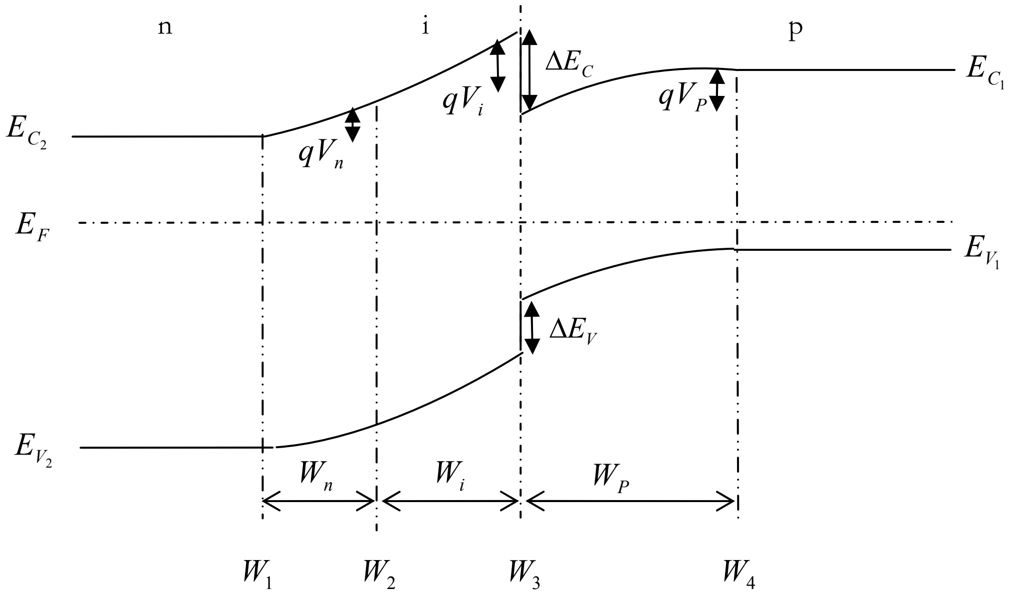

Fig 2.3 Energy band diagram of an n^+ip heterojunction

So for built in voltage we can write:

$$qV_{bi} = X_1 - X_2 + E_{g1} - kT\ln(\frac{N_{v1}}{N_{a1}}) - kT\ln(\frac{N_{c2}}{N_{d2}}) = \Delta E_C + E_{g1} - kT\ln(\frac{N_{v1}N_{c2}}{N_{a1}N_{d2}})$$

$$V_{bi} = \frac{\Delta E_C}{q} + \frac{E_{g1}}{q} - V_T\ln(\frac{N_{v1}N_{c2}}{N_{a1}N_{d2}}) \tag{2.31}$$

where N_{v1} and N_{c2} are the effective densities of energy states per unit volume for holes and electron in material 1 and 2 respectively and N_{a1} and N_{d2} are the doping levels of p-type (material 1) and n-type (material 2) materials respectively.

We need to have the electric field equations for different regions for Poisson's equation,

$$\rho(x) = \begin{cases} 0 & x < W_1 \\ qN_d & W_1 < x < W_2 \\ 0 & W_2 < x < W_3 \\ -qN_a & W_3 < x < W_4 \\ 0 & x > W_4 \end{cases} \tag{2.32}$$

Using Gauss' law: $\nabla(\varepsilon \vec{E}) = \rho$

$$\frac{d\vec{E}(x)}{dx} = \begin{cases} 0 & x < W_1 \\ \dfrac{qN_d}{\varepsilon_2} & W_1 < x < W_2 \\ 0 & W_2 < x < W_3 \\ -\dfrac{qN_a}{\varepsilon_1} & W_3 < x < W_4 \\ 0 & x > W_4 \end{cases} \tag{2.33}$$

and

$$\vec{E}(x) = \begin{cases} \dfrac{qN_d}{\varepsilon_2}(x - W_1) & W_1 < x < W_2 \\ \dfrac{qN_d}{\varepsilon_2} W_n & W_2 < x < W_3 \\ -\dfrac{qN_a}{\varepsilon_1}(x - W_4) & W_3 < x < W_4 \end{cases} \tag{2.34}$$

Boundary conditions give:

$$\varepsilon_2 E(W_3^{\ -}) = \varepsilon_1 E(W_3^{\ +}) \tag{2.35}$$

hence:

$$N_d W_n = N_a W_p \tag{2.36}$$

As before, we can obtain the voltage equations:

$$V(x) = \begin{cases} -\dfrac{qN_d}{2\varepsilon_2}(x-W_1)^2 & W_1 < x < W_2 \\ -\dfrac{qN_d}{\varepsilon_2}W_n(x-W_2) - \dfrac{qN_d}{2\varepsilon_2}W_n^2 & W_2 < x < W_3 \\ -\dfrac{qN_a}{2\varepsilon_1}(x-W_3)^2 - \dfrac{qN_d}{\varepsilon_2}W_nW_i - \dfrac{qN_d}{2\varepsilon_2}W_n^2 & W_3 < x < W_4 \end{cases} \tag{2.37}$$

Now we can calculate the voltage drops across n, p and i regions:

$$V_n = V(W_1) - V(W_2) = \frac{qN_d}{2\varepsilon_2}W_n^2 \tag{2.38}$$

$$V_p = V(W_3) - V(W_4) = \frac{qN_a}{2\varepsilon_1}W_p^2 \tag{2.39}$$

$$V_i = V(W_2) - V(W_3) = \frac{qN_d}{\varepsilon_2}W_nW_i \tag{2.40}$$

$$V_{bi} = V_n + V_p + V_i = \frac{qN_d}{2\varepsilon_2}W_n^2 + \frac{qN_a}{2\varepsilon_1}W_p^2 + \frac{qN_d}{\varepsilon_2}W_nW_i \tag{2.41}$$

Using $W_n = \dfrac{N_aW_p}{N_d}$ we reach: $(\dfrac{qN_a^2}{2\varepsilon_2N_d} + \dfrac{qN_a}{2\varepsilon_1})W_p^2 + \dfrac{qN_aW_i}{\varepsilon_2}W_p - V_{bi} = 0$ which gives us:

$$W_p = \frac{-\dfrac{W_i}{\varepsilon_2} + \sqrt{(\dfrac{W_i}{\varepsilon_2})^2 + \dfrac{2V_{bi}}{q}(\dfrac{1}{\varepsilon_2N_d} + \dfrac{1}{\varepsilon_1N_a})}}{\dfrac{N_a}{\varepsilon_2N_d} + \dfrac{1}{\varepsilon_1}} \tag{2.42}$$

and consequently

$$W_n = \frac{-\dfrac{W_i}{\varepsilon_2} + \sqrt{(\dfrac{W_i}{\varepsilon_2})^2 + \dfrac{2V_{bi}}{q}(\dfrac{1}{\varepsilon_1N_a} + \dfrac{1}{\varepsilon_2N_d})}}{\dfrac{N_d}{\varepsilon_1N_a} + \dfrac{1}{\varepsilon_2}} \tag{2.43}$$

where the subscript 1 stands for p-region (c-Si) and 2 for n, i-region (a-Si).
These equations let us calculate the space charge region width on the n- and p-side as well as the voltage dropped over n, p and intrinsic layer by having the width of the intrinsic layer, W_i.

2.3.2 Static Analysis of the p^+ *a-Si/i a-Si/n c-Si* Heterostructure

We will repeat the same scenario to calculate the equations for p^+in heterojunction (Figure 2.4).

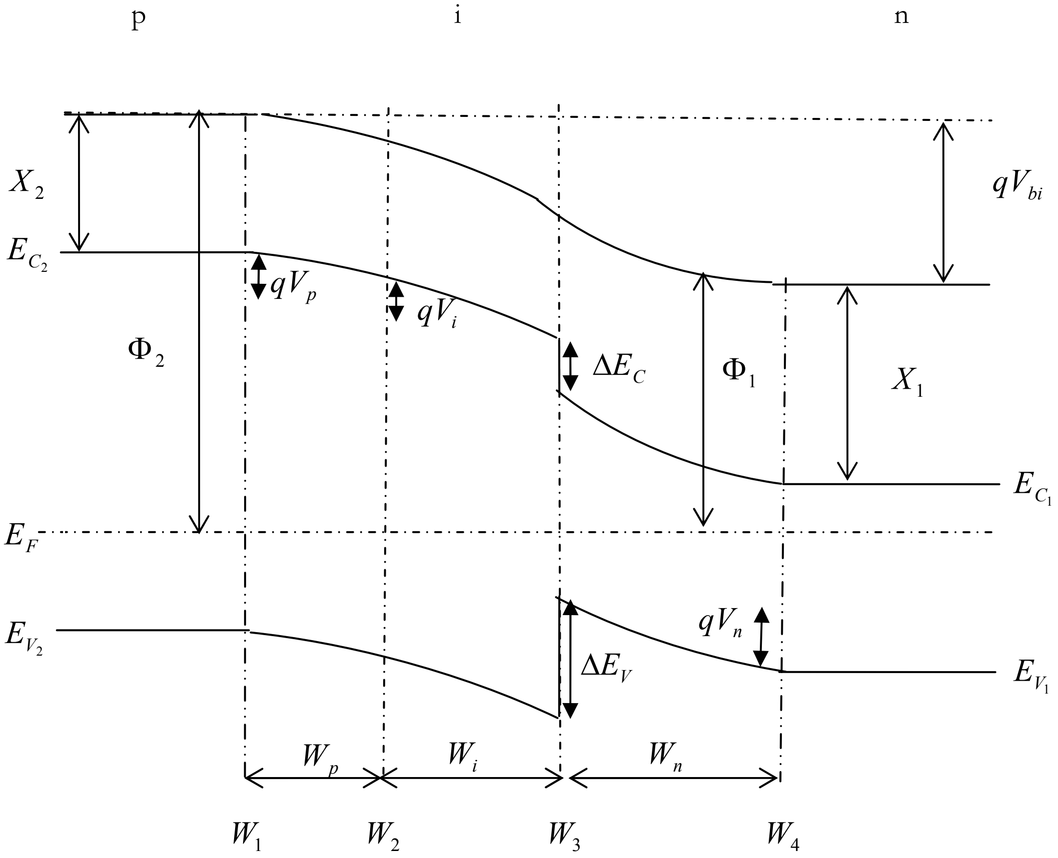

Fig 2.4 Energy band diagram of a p^+in heterojunction

$$qV_{bi} = \Phi_2 - \Phi_1 = q(V_n + V_p + V_i) \tag{2.44}$$

$$qV_{bi} = \Phi_2 - \Phi_1 = q\frac{X_2 + E_{C2} - E_F}{q} - q\frac{X_1 + E_{C1} - E_F}{q} \tag{2.45}$$

and

$$E_{C2} - E_F = E_{g2} - (E_F - E_{V2}) = E_{g2} - kT\ln(\frac{N_{v2}}{N_{a2}}) \tag{2.46}$$

$$E_{C1} - E_F = kT\ln(\frac{N_{c1}}{N_{d1}}) \tag{2.47}$$

so for built in voltage we can write:

$$qV_{bi} = X_2 - X_1 + E_{g2} - kT\ln(\frac{N_{v2}}{N_{a2}}) - kT\ln(\frac{N_{c1}}{N_{d1}}) = -\Delta E_C + E_{g1} + \Delta E_C + \Delta E_V - kT\ln(\frac{N_{v2}N_{c1}}{N_{a2}N_{d1}})$$

$$V_{bi} = \frac{\Delta E_V}{q} + \frac{E_{g1}}{q} - V_T\ln(\frac{N_{v2}N_{c1}}{N_{a2}N_{d1}}) \tag{2.48}$$

where N_{c1} and N_{v2} are the effective densities of energy states per unit volume for electrons and holes in material 1 and 2 respectively and N_{d1} and N_{a2} are the doping levels of n-type (material 1) and p-type (material 2) materials respectively.

In order to use the Poisson's equation, we need to have the electric field equations:

$$\rho(x) = \begin{cases} 0 & x < W_1 \\ -qN_a & W_1 < x < W_2 \\ 0 & W_2 < x < W_3 \\ qN_d & W_3 < x < W_4 \\ 0 & x > W_4 \end{cases} \tag{2.49}$$

Using Gauss' law:

$$\frac{d\vec{E}(x)}{dx} = \begin{cases} 0 & x < W_1 \\ \dfrac{-qN_a}{\varepsilon_2} & W_1 < x < W_2 \\ 0 & W_2 < x < W_3 \\ \dfrac{qN_d}{\varepsilon_1} & W_3 < x < W_4 \\ 0 & x > W_4 \end{cases} \tag{2.50}$$

Integrating equation 2.50, we obtain:

$$\vec{E}(x) = \begin{cases} \dfrac{-qN_a}{\varepsilon_2}(x - W_1) & W_1 < x < W_2 \\ \dfrac{-qN_a}{\varepsilon_2}W_p & W_2 < x < W_3 \\ \dfrac{qN_d}{\varepsilon_1}(x - W_4) & W_3 < x < W_4 \end{cases} \tag{2.51}$$

Using boundary conditions:

$$\varepsilon_2 E(W_3^{\;-}) = \varepsilon_1 E(W_3^{\;+}) \tag{2.52}$$

we have:

$$N_a W_p = N_d W_n \tag{2.53}$$

Also using equation 2.51, we will have:

$$V(x) = \begin{cases} \dfrac{qN_a}{2\varepsilon_2}(x - W_1)^2 & W_1 < x < W_2 \\ \dfrac{qN_a}{\varepsilon_2}W_p(x - W_2) + \dfrac{qN_a}{2\varepsilon_2}W_p^2 & W_2 < x < W_3 \\ \dfrac{qN_d}{2\varepsilon_1}(x - W_3)^2 + \dfrac{qN_a}{\varepsilon_2}W_pW_i + \dfrac{qN_a}{2\varepsilon_2}W_p^2 & W_3 < x < W_4 \end{cases} \tag{2.54}$$

and consequently:

$$V_n = V(W_4) - V(W_3) = \frac{qN_d}{2\varepsilon_1} W_n{}^2 \tag{2.55}$$

$$V_p = V(W_2) - V(W_1) = \frac{qN_a}{2\varepsilon_2} W_p^2 \tag{2.56}$$

$$V_i = V(W_3) - V(W_2) = \frac{qN_a}{\varepsilon_2} W_p W_i \tag{2.57}$$

$$V_{bi} = V_n + V_p + V_i = \frac{qN_d}{2\varepsilon_1} W_n^2 + \frac{qN_a}{2\varepsilon_2} W_p^2 + \frac{qN_a}{\varepsilon_2} W_p W_i \tag{2.58}$$

Using equation 2.53 ($W_p = \frac{N_d W_n}{N_a}$) and by substituting it in 2.58, we obtain:

$(\frac{qN_d^2}{2\varepsilon_2 N_a} + \frac{qN_d}{2\varepsilon_1}) W_n^2 + \frac{qN_d W_i}{\varepsilon_2} W_n - V_{bi} = 0$ which leads us to the following:

$$W_n = \frac{-\frac{W_i}{\varepsilon_2} + \sqrt{(\frac{W_i}{\varepsilon_2})^2 + \frac{2V_{bi}}{q}(\frac{1}{\varepsilon_2 N_a} + \frac{1}{\varepsilon_1 N_d})}}{\frac{N_d}{\varepsilon_2 N_a} + \frac{1}{\varepsilon_1}} \tag{2.59}$$

and consequently:

$$W_p = \frac{-\frac{W_i}{\varepsilon_2} + \sqrt{(\frac{W_i}{\varepsilon_2})^2 + \frac{2V_{bi}}{q}(\frac{1}{\varepsilon_1 N_d} + \frac{1}{\varepsilon_2 N_a})}}{\frac{N_a}{\varepsilon_1 N_d} + \frac{1}{\varepsilon_2}} \tag{2.60}$$

Where the subscript 1 stands for n-region (c-Si) and 2 for p and i-region (a-Si).

Chapter 3

Carrier Transport Mechanisms in *a-Si/c-Si* Heterojunction

The a-Si/c-Si heterojunction brings new concepts in carrier transport mechanism because the theory of injection in homojunctions fails to account the behaviour of the carriers caused by heterojunction properties.

During past two decades, a few theories have been proposed to explain the transport of carriers in heterojunctions. In this chapter, we have covered these theories literally and have talked about the transport mechanisms that we have chosen to use in our modeling.

First, in section 3.1, we have discussed SCLC (space charge limited current) and have talked about the reasons why it is not suitable for our case. MTCE (multi tunneling capture emission) is another transport modeling that has been discussed literally in section 3.2. In sections 3.3 and 3.5, we have covered two transport mechanisms of the drift-diffusion and thermionic emission that play the most important role in carriers transport in heterojunctions. These two mechanisms deal directly with the effects of the potential barriers in conduction or valence band on the carriers transport and therefore, the result of modeling appears in the I-V characteristics of the heterojunction. Lundstorm [12,13] has discussed the above mentioned factors in heterojunction bipolar transistors and he has also extended his work in a more general way for graded heterojunctions. Furlan et. al. [14,15] have used this idea in simulation of a-Si/c-Si heterojunction solar cell.

We have included direct tunneling (section 3.4) while modeling the thermionic emission in our model as well as the surface recombination current (section 3.6) at the interface of a-Si and c-Si junction. The later becomes important in low forward biases.

3.1 Space Charge Limiting Current (SCLC)

For a heterojunction between c-Si and a-Si:H, the carrier transport model based on space charge limited current (SCLC) in a-Si:H was reported by Smid et al. in 1985 [16]. SCLC originates from high-level injection of carriers to a low-doped semiconductor. In this case, the density of the injected carriers is so high that it exceeds the majority carriers density, and thus the bulk material cannot neutralize the injected carriers. This leads to a space charge region (non-zero electric field) in the bulk region and band bending in the energy band diagram of the low-doped side [17]. The high injection of carriers into low doped bulk region occurs at high-applied voltages (higher than 0.6V) and results in the relation between forward bias and the current to be no longer exponential. In this case, the I-V relation is rather superlinear:

$$I = KV^{m} \tag{3.1}$$

where *m* depends on the density of states in a-Si:H bandgap and *K* depends on the film thickness, trap distribution and conductivity [18]. Figure 3.1 shows the current-voltage characteristics (I-V) of (n)a-Si:H/(p)c-Si measured at 296 K [18] . The electrical model of n a-Si:H/c-Si diode has been proposed by Marsal et. al. [18] as two parallel resistances (one ohmic and the other nonlinear) in series with a normal diode.

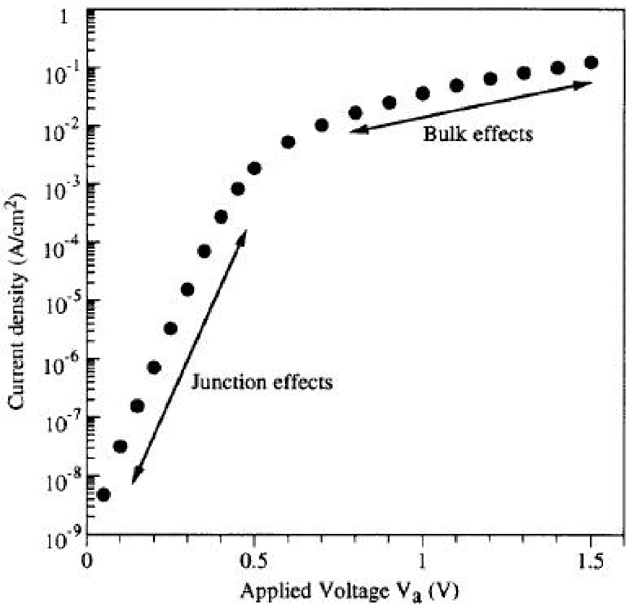

Fig 3.1 Current density–voltage characteristic of an *(n) a-Si:H/(p) c-Si* diode measured at room temperature [18]

As the theory of SCLC defines, the major factor that causes SCLC to happen is high injection of carriers into the low-doped bulk. In our case, which is $n^{+}ip$ or $p^{+}in$ a-Si/c-Si heterojunction, it is unlikely to have a high injection. This is because of the intrinsic amorphous layer in SCR that as we will discuss later on, limits the transport of the carriers by drift-diffusion effective velocity factor. Also because of presence of a potential barrier in heterojunction band (valence or conduction), there will be another limiting factor (interface effective velocity) which prevents the carriers to be highly injected. Another point that is worth to mention is the applied voltage in which this mechanism (SCLC) operates that is more than 0.6V. As we will see later, the emission-diffusion theory affects the current at high voltages (in presence of intrinsic layer) which makes it unnecessary to include the SCLC in our model.

3.2 Multi-Tunneling Capture Emission (MTCE)

Matsuura et al. [9] proposed this model in 1984 to overcome the problems that the earlier tunneling models had to face. Before Matsuura, a few tunneling models had been proposed including direct tunneling and multi step tunneling.

In Matsuura's work, a variety of tunneling transport processes has been assessed and finally the multi tunneling capture-emission model has been confirmed by the experiments. Since the localized states are quasi-continuously distributed within the gap of a-Si:H spatially as well as energetically, it is reasonable to expect a multi step tunneling process to be dominant rather than a one step tunneling [17]. According to this model, a hole in the valence band of p-type c-Si jumps from one localized state to another in a-Si:H located within an energy range of kT from each other by a multi tunneling process and keeps jumping until the tunneling rate becomes smaller than the rate for hole release from the state to the valence band of a-Si:H or for recombination of the hole with an electron in the conduction band of a-Si:H. An ending point of the tunneling might be close to the edge of the depletion layer of a-Si:H, where the tunneling rate decreases due to a decrease of electric field. Figure 3.2 shows the carrier transport phenomenon through multi tunneling capture emission model. [9]

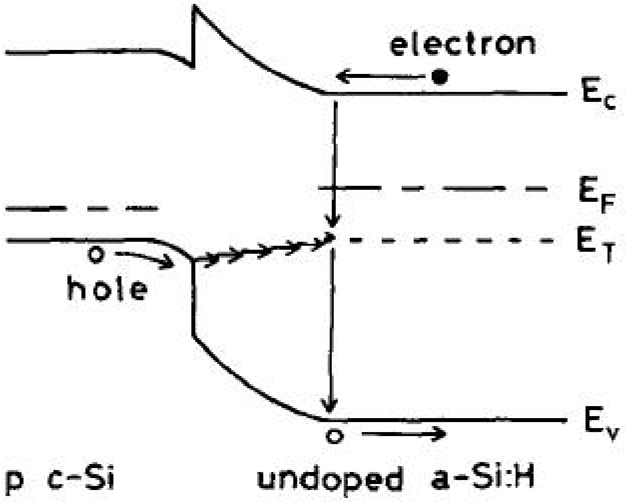

Fig 3.2 MTCE model for heterojunction [9]

In this model the current density flowing from p-type c-Si to undoped a-Si:H is given by [9]:

$$J_{c->a} = B(e_p + \sigma_n v_{th} n)\exp(AV) \tag{3.2}$$

where A is a temperature-independent constant, *B* is a constant independent of applied voltage and temperature and e_p, the hole emission rate given as:

$$e_p = \sigma_p v_{th} N_V \exp(-(E_T - E_V)/kT) \tag{3.3}$$

σ_n is the capture cross section of electrons, v_{th} the thermal velocity, *n* the electron density in the conduction band of a-Si:H, σ_p the capture cross section of holes and E_F and E_T, the energies of Fermi level and trapping level of a-Si:H respectively [9]; and the net current density: $J = J_0[\exp(AV) - 1]$, where [9]:

$$J_0 = B[\sigma_p v_{th} N_V \exp(-\frac{E_T - E_V}{kT}) + \sigma_n v_{th} N_C \exp(-\frac{E_C - E_F}{kT})] \tag{3.4}$$

Although this theory matches the experimental data, we should note that it describes the forward current-voltage characteristics of amorphous-crystalline silicon heterojunction having thick (1μm) undoped a-Si:H layer. However, it is unclear whether this model is also valid for junctions with highly doped ultra thin a-Si layers, as used in solar cells [19]. Therefore, in our case that is the modeling of n^+ip or p^+in a-Si/c-Si heterojunction solar cell, and regarding the fact that the a-Si layer thickness (intrinsic or doped) is not thicker than a few tens nm (at most), this model will not be a good choice to describe the behaviour of the device.

3.3 Thermionic Emission

When two materials with different bandgaps are put together to form a junction, the difference between the bandgaps, which appears as an offset energy band, causes some effects on the transport mechanism of carriers. These kinds of junctions can be Metal-Semiconductor, heterojunction between two different semiconductors or heterojunction between two similar semiconductors with different bandgaps.

The thermionic theory describes the behaviour of carriers when they have to pass over a potential barrier formed by a heterojunction. (Figure 3.3)

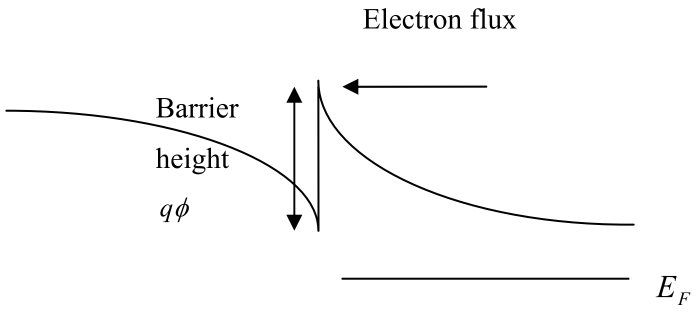

Fig 3.3 Electron transport over the potential barrier

As we have seen in previous chapter, the height of barrier in conduction band is equal to the difference between conduction band levels or the electron affinity of two semiconductors (equation 2.1). The carriers (electrons, for instance) must have minimum energy in order to be able to overcome the barrier. This minimum energy equals the potential of the barrier height plus the Fermi energy. So for the electron current associated to the electron flux shown in Figure 3.3 we can write:

$$J = \int_{E_F+q\varphi}^{\infty} q v_x dn \tag{3.5}$$

where $E_F + q\varphi$ is the minimum energy required for thermionic emission over the barrier and v_x is the velocity of carriers in transport direction [3]. It is found that the current that will pass the barrier has the form of [3]:

$$J = A^* T^2 \exp(-\frac{q\varphi}{kT}) \exp(\frac{qV}{kT}) \tag{3.6}$$

where φ is the barrier height, *V* is the forward bias and

$$A^* = \frac{4\pi q m^* k^2}{h^3} \tag{3.7}$$

is the Richardson constant for thermionic emission and the average velocity of carriers in the direction of transport over the barrier (thermionic emission velocity) will be [3,20]:

$$v_x = \sqrt{\frac{kT}{2\pi m^*}} \tag{3.8}$$

where m^* stands for effective hole or electron mass.

This indicates that when there is a potential barrier in conduction (valence) band of a junction, the average velocity of carriers will be v_x, therefore, as it will be discussed later in chapter four, in case of high forward voltage, this velocity may play a limiting factor role for the transport of the carriers. This velocity is also called thermal velocity of carriers.

3.4 Direct Tunneling in Thermionic Emission

In case of abrupt heterojunction, when the doping level of the emitter is high enough to make the spike in valence or conduction band very sharp, the carriers can tunnel through the energy spike as well as overcome it by thermionic emission.

Grinberg et. al. [21] have calculated this effect by the integration of the range of barrier energies available for tunneling. The result is a multiplicative factor to the interface effective velocity of the carriers (the velocity that carriers have when overcome the potential barrier in conduction or valence band) that causes it to increase a few times and consequently makes additional carrier injection across the heterojunction possible. Figure 3.4 [22] shows the effect of tunneling on the different effective velocities of carriers in a heterojunction bipolar transistor. We see that for the holes effective velocity at the junction (thermionic emission without (○) and with (●) tunneling) , the tunneling increases it by more than a factor of 10 at low bias, but decreases to approximately a factor of 2 at high bias [22].

As we discussed in section 3.2, MTCE is not a suitable choice for our modeling. On the other hand, the direct tunneling describes the behaviour of the carriers in case of narrow band spike in terms of a factor multiplied by the interface effective velocity of carriers. Since we have used the interface effective velocity of carriers in our modeling, we have included direct tunneling in our model to simulate the cases when the tunneling occurs.

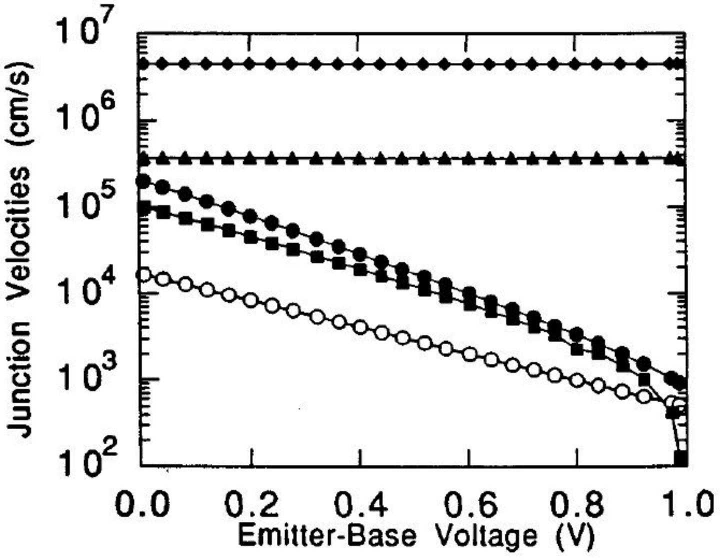

Fig 3.4 Effective hole velocities [emitter space charge region drift diffusion (■), thermionic emission without (○) and with (●) tunneling, quasi-neutral base diffusion (▲) and base-collector saturation velocity (♦)] for InAlAs/InGaAs *Pnp* HBT as a function of emitter-base bias V_{EB} for the case of no compositional base grading.[22]

3.5 Drift-Diffusion

In addition to the thermionic emission that should be considered as the transport mechanism of carriers while passing over the potential barrier, the carriers are scattered when flowing through the SCR in heterojunctions. For homojunctions, it is assumed that the carriers current in SCR is constant and therefore the effective velocity of carriers within the depletion region is taken fixed. Using this method, the current across the SCR is calculated and the term containing the current density inside the SCR is disregarded. Although the experiments prove that the model of injection for homojunctions under low-level injection is accurate, it fails to model the suppression of injected current due to the band spike that occurs in heterojunctions [13]. In fact, the scattering may exist in homojunctions as well but the amount of it is so small that it is neglected. However, a potential barrier in energy band (conduction or valence) causes the effect of scattering to be significant on velocity of minority carriers that diffuse in the base. In chapter four, we will model this phenomenon as an effective velocity of carriers that limits their transport through the depletion region.

3.6 The *a-Si/c-Si* Heterojunction Interface Recombination Current

The experimental data in $n^{+}ip$ ($p^{+}in$) a-Si/C-si heterojunctions show that the dominant transport mechanism for carriers in lower forward bias is interface recombination. Song et. al. [23] showed that for forward voltages below 0.3 V, the dominant conduction mechanism is the recombination current generated by recombining the free electrons (holes) pushed by the forward bias through the intrinsic layer and the trapped holes (electrons) in the amorphous/crystalline interface. The trapped holes (electrons) in the a-Si/c-Si interface are located in the band tails of the a-Si mobility gap and can recombine by free electrons (holes). We will calculate this current in chapter four (section 4.4).

Chapter 4

Modeling the Current-Voltage Characteristics of the *a-Si/c-Si* Heterojunction

The presence of a spike in energy band of heterojunctions introduces additional carrier flow mechanisms for dark current. Thermionic emission deals with carriers flow over the potential barrier and drift-diffusion describes the carriers transport within depletion region. We have modeled these two mechanisms as two effective velocities of carriers (interface effective velocity and drift-diffusion effective velocity) which limit their flow through the heterojunction.

In sections 4.1 and 4.2, we have used the thermionic emission theory (including direct tunneling) to model how the transport of the carriers is affected while passing over the barriers. Our calculations show that the thermal velocity of carriers plays the major role in defining the interface effective velocity. In section 4.3, we have also found out that the mobility and the maximum electric field in depletion region have the major impacts on scattering the flow of the carriers through the SCR. We have found that the potential barrier and the depletion region do not affect the flow of holes and electrons in n-p and p-n heterojunctions respectively.

Adding an intrinsic layer of amorphous silicon, we have recalculated the drift-diffusion effective velocity for this case. Since the potential barrier does not change by adding the intrinsic layer, we do not have to recalculate the interface effective velocity. However, introducing the intrinsic layer affects the carriers flow through the depletion region.

In section 4.4, we have calculated the recombination current of carriers at the a-Si and c-Si interface and have shown that this current is also suppressed with the same limiting factors that suppress the dark current.

Finally, in section 4.5, we have produced the complete I-V equations for $n^{+}ip$ and $p^{+}in$ heterojunction, including the limiting factors as well as the interface recombination current.

In all above-mentioned sections, we have modeled both $n^{+}ip$ and $p^{+}in$ a-Si/c-Si heterojunction solar cells. As we will discuss later in chapter six, the reason is that the effect of limiting factors on the $n^{+}ip$ is significantly different from that of the $p^{+}in$ solar cells.

4.1 Modeling the Thermionic Emission Velocity as a Limiting Factor for Heterojunction Current

In this section, we will derive the equations for the $n^{+}p$ and $p^{+}n$ heterojunction current under the forward voltage, describing the role of thermionic emission velocity in limiting the current.

4.1.1 $n^{+}p$ Heterojunction Current

Suppose that we have an $n^{+}p$ heterojunction device under the forward bias. We like to verify how the forward current would be affected in presence of two different bandgaps. We assume that V_n and V_p are the voltage drops in n- and p-region, respectively, and as we know, the sum of these two voltages will give us the built in voltage of the device. In the text of this discussion, the superscript and/or subscript *'0'* indicate the equilibrium situation, and *'A'* means that the device is under forward bias.

We start our modeling with electron current in $n^{+}p$ heterojunction cell. Regarding the Figure 4.1, in equilibrium situation the sum of the fluxes of electrons at any point should be zero since there is no net current in this state. The flux of carriers at any point can be calculated by multiplying the concentration of the carriers at that point by the average velocity. As we have already seen, the average velocity over the potential barrier is the thermal velocity. Therefore having the concentration of the carriers before the barrier (0^{-}) we can write:

$$F_1(0^-) = n(W_n)v_x e^{\frac{-qV_n}{kT}} \tag{4.1}$$

and

$$F_2(0^-) = n(W_p)v_x e^{\frac{-(\Delta E_C - qV_p)}{kT}} \tag{4.2}$$

Assuming the equilibrium situation, we have: $F_2 = F_1$.

Therefore, $n_0(W_n)v_x e^{\frac{-qV_n^0}{kT}} = n_0(W_p)v_x e^{\frac{-q(\Delta E_C - V_p^0)}{kT}}$ which results:

$$n_0(W_n) = n_0(W_p) e^{\frac{-(\Delta E_C - qV_p^0 - qV_n^0)}{kT}} \tag{4.3}$$

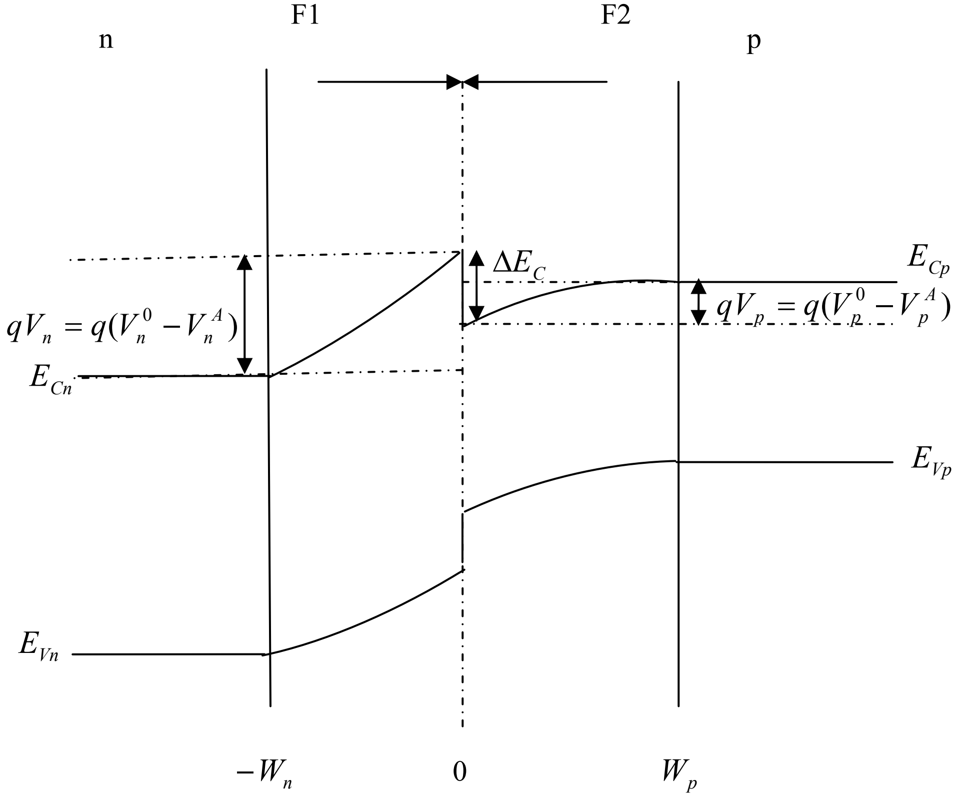

Fig 4.1 Electron fluxes in n^+p heterojunction device

If we apply a forward bias V_A to the device, assuming that this voltage will drop on n- and p-side by V_n^A and V_p^A, respectively, such that:

$$V_A = V_n^A + V_p^A \tag{4.4}$$

then the carrier fluxes will no longer be equal and a carrier flux will flow through the device so that: $F_n = F_1 - F_2$, therefore we will have:

$$F_n = F_1 - F_2 = n(W_n)v_x e^{\frac{-qV_n}{kT}} - n(W_p)v_x e^{-\frac{\Delta E_C - qV_p}{kT}} \tag{4.5}$$

We can also write the following equations between the equilibrium state and the forward biased state:

$$V_n = V_n^0 - V_n^A \tag{4.6}$$

$$V_p = V_p^0 - V_p^A \tag{4.7}$$

and

$$V_n + V_p = V_n^0 + V_p^0 - V_A = V_{bi} - V_A \tag{4.8}$$

Assuming low-level injection on the n-side, we will have:

$$n_0(W_n) \approx n(W_n) \tag{4.9}$$

From equation 4.5 and using 4.9, for the flux under forward bias we can write:

$$F_n = v_x e^{-\frac{\Delta E_C - qV_p}{kT}} [n_0(W_n) e^{\frac{-qV_n + \Delta E_C - qV_p}{kT}} - n(W_p)] \tag{4.10}$$

and substituting $n_0(W_n)$ from equation 4.3 :

$$F_n = v_x e^{-\frac{\Delta E_C - qV_p}{kT}} [n_0(W_p) e^{\frac{-qV_n + \Delta E_C - qV_p - \Delta E_C + qV_p^0 + qV_n^0}{kT}} - n(W_p)] \tag{4.11}$$

Using equations 4.4, 4.6 and 4.7, we can write:

$$-V_n - V_p + V_n^0 + V_p^0 = V_n^A + V_p^A = V_A \tag{4.12}$$

This leads us to:

$$F_n = v_x e^{-\frac{\Delta E_C - qV_p}{kT}} [n_0(W_p) e^{\frac{qV_A}{kT}} - n(W_p)] \tag{4.13}$$

We have:

$$n(W_p) = n_0(W_p) + \Delta n(W_p) \tag{4.14}$$

which means the concentration of carriers under forward bias equals the equilibrium concentration plus the excess carrier concentration injected under forward bias. Thus, we will have:

$$F_n = v_x e^{-\frac{\Delta E_C - qV_p}{kT}} [n_0(W_p)(e^{\frac{qV_A}{kT}} - 1) - \Delta n(W_p)] \tag{4.15}$$

From equation 4.15, we see that if the first expression in right hand ($v_x e^{-\frac{\Delta E_C - qV_p}{kT}}$) becomes very big then the equation will demonstrate the normal n-p homojunction behaviour under forward bias for excess carrier injection, i.e.

$$\Delta n^{hm}(W_p) = n_0(W_p)(e^{\frac{qV_A}{kT}} - 1) \tag{4.16}$$

The superscript '*hm*' indicates the fact that equation 4.16 shows the concentration of excess electrons at W_p in homojunction. This means that the coefficient $v_x e^{-\frac{\Delta E_C - qV_p}{kT}}$ is responsible for the effect that the potential barrier in conduction band causes on electron current. Consequently, $\Delta n(W_p)$ in equation 4.15 (which we will show by superscript '*ht*') stands for the concentration of excess electrons at W_p in heterojunction. Using these definitions, we can rewrite 4.15 as follows:

$$F_n = v_x e^{-\frac{\Delta E_C - qV_p}{kT}} [\Delta n^{hm}(W_p) - \Delta n^{ht}(W_p)] \tag{4.17}$$

We know that if we have the concentration of excess minority carriers at the interface of SCR and the bulk region (W_p), the diffusion length and lifetime of minority carriers in the bulk, we can calculate the current [24]. The diffusion length and lifetime of minority carriers in the bulk are the same for both n-p heterojunction and n-p homojunction since the p-region is the same material. Therefore, we have:

$$J_n^{hm} = q\frac{L_n}{\tau_n}\Delta n^{hm}(W_p) \tag{4.18}$$

for homojunction and

$$J_n^{ht} = q\frac{L_n}{\tau_n}\Delta n^{ht}(W_p) \tag{4.19}$$

for heterojunction. In the equation 4.17, F_n stands for electron flux in heterojunction diode. By multiplying F_n by electron charge (q), we will have the electron current in heterojunction device or J_n^{ht}:

$$qF_n = J_n^{ht} \tag{4.20}$$

Combining equations 4.17, 4.18, 4.19 and 4.20, we can write:

$$J_n^{ht} = \frac{\tau_n}{L_n} v_x e^{-\frac{\Delta E_C - qV_p}{kT}} [q\frac{L_n}{\tau_n}\Delta n^{hm}(W_p) - q\frac{L_n}{\tau_n}\Delta n^{ht}(W_p)] = \frac{\tau_n}{L_n} v_x e^{-\frac{\Delta E_C - qV_p}{kT}} (J_n^{hm} - J_n^{ht}) \tag{4.21}$$

Consequently:

$$J_n^{ht} = \frac{J_n^{hm}}{1 + \frac{L_n / \tau_n}{v_x e^{-\frac{\Delta E_C - qV_p}{kT}}}} \tag{4.22}$$

This shows how the current gets lower in presence of a potential barrier in conduction band. We can simplify this equation by two modifications. First, the expression $\frac{L_n}{\tau_n}$ which is the diffusion length divided by the lifetime of minority carriers, can be represented as diffusion velocity $(\frac{L_n}{\tau_n} = v_n)$ of minority carriers in the bulk region. In other words, v_n indicates how fast the minority carriers will diffuse in the bulk region. Second, Lundstorm defines the expression $v_x e^{-\frac{\Delta E_C - qV_p}{kT}}$ as the interface effective velocity of carriers, v_{in} [12]. With this definition, equation 4.22 can be rewritten as:

$$J_n^{ht} = \frac{J_n^{hm}}{1 + \frac{v_n}{v_{in}}} \tag{4.23}$$

where:

$$v_n = \frac{L_n}{\tau_n} \tag{4.24}$$

$$v_{in} = v_x e^{-\frac{\Delta E_C - qV_p}{kT}} \tag{4.25}$$

From equation 4.23, it is seen that if v_{in} is much greater than v_n, there will be no current reduction compared with the homojunction. The value of v_n is independent of v_{in}, therefore we cannot reach an estimation of how big v_{in} should be in comparison with v_n to get the limiting factor eliminated. We can calculate v_{in} itself to see when this velocity is a large number, in which case we should have: $v_x e^{-\frac{\Delta E_C - qV_p}{kT}} >> 0$ that leads $e^{\frac{\Delta E_C - qV_p}{kT}}$ to be a small number. We see that $e^{\frac{\Delta E_C - qV_p}{kT}}$ will be a small number if ΔE_C becomes zero or very small. This means that the limiting factor will vanish if there is no potential barrier in conduction band or $\Delta E_C = 0$.

It is worth to mention that the coefficient $e^{-\frac{\Delta E_C - qV_p}{kT}}$ should be taken into account if we intend to study the interface effective velocity of electrons at the interface of SCR and p-bulk region (which we do to calculate the current). This means that if we want to mention the interface effective velocity at the potential barrier (x=0), it would only be v_x rather than $v_x e^{-\frac{\Delta E_C - qV_p}{kT}}$.

We can repeat the same approach for holes to figure out the effect of barrier in valence band on holes transport mechanism in $n^+ p$ heterojunction cell.

$$F_1(0^+) = p(W_p) v_x e^{\frac{-qV_p}{kT}} \tag{4.26}$$

and

$$F_2(0^+) = p(-W_n) v_x e^{\frac{\Delta E_V + qV_n}{kT}} \tag{4.27}$$

Assuming the equilibrium situation:

$F_2 = F_1$ we get $p_0(W_p) v_x e^{\frac{-qV_p^0}{kT}} = p_0(-W_n) v_x e^{\frac{\Delta E_V + qV_n^0}{kT}}$ which results:

$$p_0(W_p) = p_0(-W_n) e^{\frac{\Delta E_v + qV_n^0 + qV_p^0}{kT}} \tag{4.28}$$

Applying forward bias V_A to the device and having equation 4.7, a carrier flux will flow through the device, so that: $F_p = F_1 - F_2$, therefore:

$$F_p = F_1 - F_2 = p(W_p) v_x e^{\frac{-qV_p}{kT}} - p(-W_n) v_x e^{\frac{\Delta E_V + qV_n}{kT}} \tag{4.29}$$

Assuming low-level injection on the p-side:

$$p_0(W_p) \approx p(W_p) \tag{4.30}$$

and using equation 4.28, we will have:

$$F_p = v_x e^{\frac{\Delta E_V + qV_n}{kT}} [p_0(-W_n) e^{\frac{\Delta E_v + qV_n^0 + qV_p^0}{kT}} e^{\frac{-qV_p - \Delta E_V - qV_n}{kT}} - p(-W_n)] \tag{4.31}$$

Having also

$$-V_n - V_p + V_n^0 + V_p^0 = V_n^A + V_p^A = V_A \tag{4.32}$$

and

$$p(-W_n) = p_0(-W_n) + \Delta p(-W_n) \tag{4.33}$$

we will have:

$$F_p = v_x e^{\frac{\Delta E_V + qV_n}{kT}} [\Delta p^{hm}(-W_n) - \Delta p^{ht}(-W_n)] \tag{4.34}$$

Therefore:

$$J_p^{ht} = \frac{\tau_p}{L_p} v_x e^{\frac{\Delta E_V + qV_n}{kT}} [q\frac{L_p}{\tau_p}\Delta p^{hm}(-W_n) - q\frac{L_p}{\tau_p}\Delta p^{ht}(-W_n)] = \frac{\tau_p}{L_p} v_x e^{\frac{\Delta E_V + qV_n}{kT}} (J_p^{hm} - J_p^{ht}) \tag{4.35}$$

Then we can write:

$$J_p^{ht} = \frac{J_p^{hm}}{1 + \dfrac{L_p / \tau_p}{v_x e^{\frac{\Delta E_V + qV_n}{kT}}}} \tag{4.36}$$

where v_x is the thermal velocity of holes. It can be seen that $v_x e^{\frac{\Delta E_V + qV_n}{kT}} >> 0$ which leads us to $1 + \dfrac{L_p / \tau_p}{v_x e^{\frac{\Delta E_V + qV_n}{kT}}} \approx 1$ and consequently: $J_p^{ht} = J_p^{hm}$ or in other word, the presence of barrier in the valence band in an $n^+ p$ heterojunction does not affect the hole current.

4.1.2 $p^+ n$ Heterojunction Current

The method that we will use to derive the interface effective velocity of holes in p^+n heterojunction is the same as we did for electrons in n^+p heterojunction. Therefore, in this section we will proceed to derive the equations briefly.

From the Figure 4.2, for the fluxes of holes at (0^-), we can write:

$$F_1(0^-) = p(-W_p)v_x e^{\frac{-qV_P}{kT}} \tag{4.37}$$

and

$$F_2(0^-) = p(W_n)v_x e^{\frac{-(\Delta E_V - qV_n)}{kT}} \tag{4.38}$$

Assuming the equilibrium situation:

$F_2 = F_1$ therefore $p_0(-W_p)v_x e^{\frac{-qV_P^0}{kT}} = p_0(W_n)v_x e^{\frac{-q(\Delta E_V - V_n^0)}{kT}}$ which results:

$$p_0(-W_p) = p_0(W_n)e^{\frac{-(\Delta E_V - qV_P^0 - qV_n^0)}{kT}} \tag{4.39}$$

Applying a forward bias V_A, the carrier fluxes will no longer be equal and there will be a carrier flux such that: $F_p = F_1 - F_2$ and therefore:

$$F_p = F_1 - F_2 = p(-W_p)v_x e^{\frac{-qV_P}{kT}} - p(W_n)v_x e^{-\frac{\Delta E_V - qV_n}{kT}} \tag{4.40}$$

Again, by assuming low-level injection on the p-side we will have:

$$p_0(-W_p) \approx p(-W_p) \tag{4.41}$$

and using equations 4.39 and 4.40 for the hole flux under forward bias we can write

$$F_p = v_x e^{-\frac{\Delta E_V - qV_n}{kT}} [p_0(W_n)e^{\frac{-qV_P + \Delta E_V - qV_n - \Delta E_V + qV_n^0 + qV_P^0}{kT}} - p(W_n)] \tag{4.42}$$

and therefore

$$F_p = v_x e^{-\frac{\Delta E_V - qV_n}{kT}} [p_0(W_n)e^{\frac{qV_A}{kT}} - p(W_n)] \tag{4.43}$$

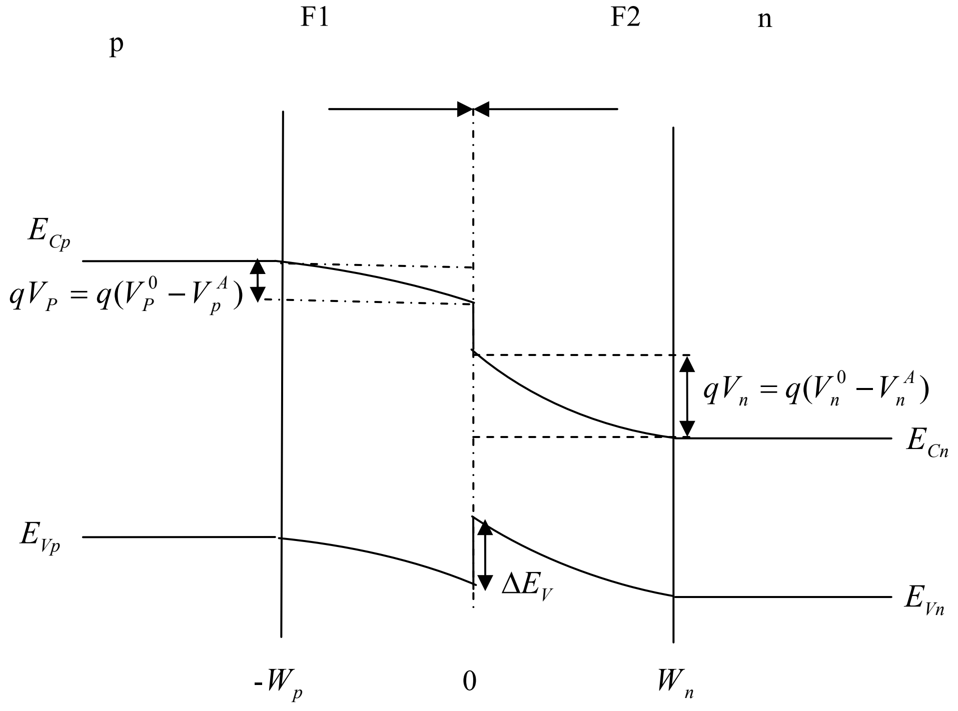

Fig 4.2 Hole fluxes in p^+n heterojunction device

Using

$$p(W_n) = p_0(W_n) + \Delta p(W_n) \tag{4.44}$$

we will have:

$$F_p = v_x e^{-\frac{\Delta E_V - qV_n}{kT}} [p_0(W_n)(e^{\frac{qV_A}{kT}} - 1) - \Delta p(W_n)] \tag{4.45}$$

$\Delta p(W_n)$ is the concentration of the excess holes at W_n in p^+n heterojunction that we show by: $\Delta p^{ht}(W_n)$, and also $p_0(W_n)(e^{\frac{qV_A}{kT}} - 1)$ is the concentration of excess holes at W_n in p^+n homojunction that we show by: $\Delta p^{hm}(W_n)$. Now we can rewrite equation 4.45 as:

$$F_p = v_x e^{-\frac{\Delta E_V - qV_n}{kT}} [\Delta p^{hm}(W_n) - \Delta p^{ht}(W_n)] \tag{4.46}$$

This leads us to the following:

$$J_p^{ht} = \frac{\tau_p}{L_p} v_x e^{-\frac{\Delta E_V - qV_n}{kT}} [q \frac{L_p}{\tau_p} \Delta p^{hm}(W_n) - q \frac{L_p}{\tau_p} \Delta p^{ht}(W_n)] = \frac{\tau_p}{L_p} v_x e^{-\frac{\Delta E_V - qV_n}{kT}} (J_p^{hm} - J_p^{ht}) \tag{4.47}$$

and

$$J_p^{ht} = \frac{J_p^{hm}}{1 + \frac{L_p / \tau_p}{v_x e^{-\frac{\Delta E_V - qV_n}{kT}}}} \tag{4.48}$$

Making the same modifications that we did in n^+p heterojunction for equation 4.22, we will have:

$$J_p^{ht} = \frac{J_p^{hm}}{1 + \frac{v_p}{v_{ip}}} \tag{4.49}$$

where

$$v_p = \frac{L_p}{\tau_p} \tag{4.50}$$

is the diffusion velocity of holes in n-region, and

$$v_{ip} = v_x e^{-\frac{\Delta E_V - qV_n}{kT}} \tag{4.51}$$

the interface effective velocity of holes. It should be noted that v_x is the thermionic emission velocity of holes over the potential barrier in valence band. As we saw for electron current in n^+p heterojunction (section 4.1.1), the limiting factor for hole current in p^+n heterojunction will disappear if the barrier in valence band (ΔE_V) is either small or zero.

By repeating the same steps, we have calculated the interface effective velocity of electrons in p^+n heterojunction as $v_{in} = v_x e^{\frac{\Delta E_C + qV_P}{kT}}$ which as we saw for holes interface effective velocity in n^+p heterojunction (section 4.1.1), has a big value which means that there is no limiting factor for electron current in p^+n heterojunction or: $J_n^{ht} = J_n^{hm}$.

4.2 Modeling the Effect of Tunneling on the Interface Effective Velocity of Carriers

As we discussed in previous chapter, a heavy doping level of the emitter makes the width of the offset in the conduction or valence band narrow and therefore the carriers pass through the barrier by tunneling. Grinberg et. al. [21] calculations show that this can be modeled by multiplying the interface effective velocity of carriers by a factor.

Recently, researches [22] show that this phenomenon is important in the transport mechanism of the carriers since it can reduce the limiting factor of potential barrier by several times for low forward biases.

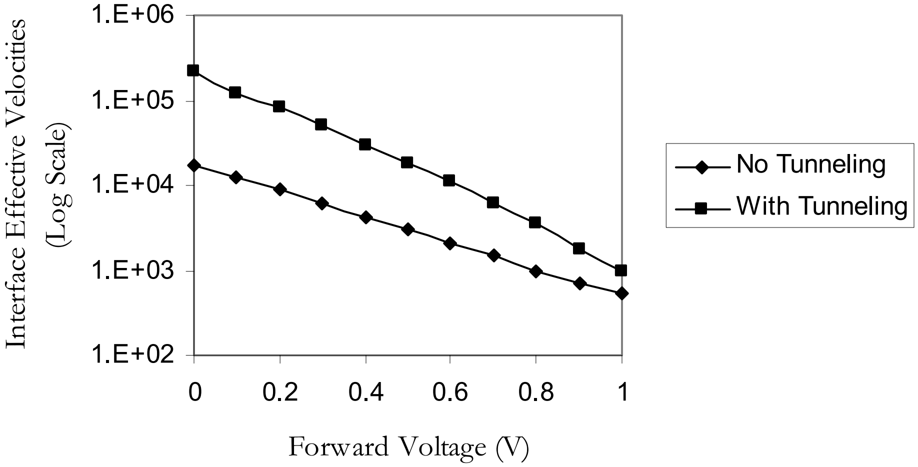

Fig 4.3 Interface effective velocity of holes with and without tunneling [22]

Figure 4.3 shows the data extracted from Figure 3.4 for hole interface effective velocity with and without the effect of tunneling. It is seen that the tunneling increases the interface effective velocity of carriers by more than a factor of 10 at low bias, but approximately by a factor of 2 at high bias. The increase of interface effective velocity of carriers means that the limiting factor of the carriers transport decreases. In other words, by tunneling, the carriers find another way to pass through the potential barrier in valence or conduction band instead of passing over it by thermionic emission and consequently resulting in more injection of carriers across the heterojunction. Using the numerical result of this effect, we can include the effect of tunneling in our model by adding a multiplicative factor γ, for the interface effective velocity of carriers, so that:

$$v_{ip} = \gamma v_x e^{-\frac{\Delta E_V - qV_n}{kT}} \tag{4.52}$$

for holes in p^+n heterojunction and as:

$$v_{in} = \gamma v_x e^{-\frac{\Delta E_C - qV_p}{kT}} \tag{4.53}$$

for electrons in n^+p heterojunction.

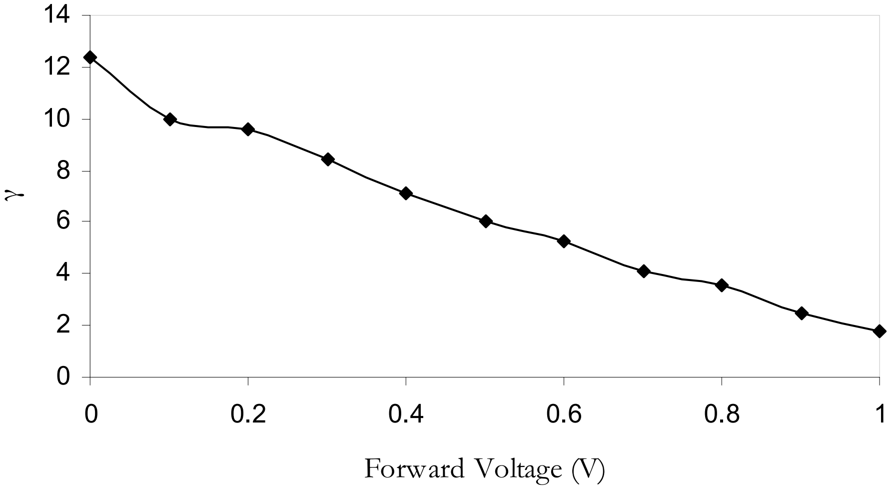

Fig 4.4 Multiplicative factor to interface effective velocity used to model the direct tunneling in our calculations

Figure 4.4 shows the dependence of γ on the forward bias.

The important point in tunneling (direct tunneling) effect is that this phenomenon will exist if the width of band offset is narrow enough. In other words, one side of junction should be heavily doped to make the spike sharp. In case of p^+n or n^+p a-Si/c-Si heterojunction, the emitter or window side of the junction is heavily doped, so this will be the case but if we introduce an intrinsic layer in amorphous side, the spike will not be sharp anymore and therefore, direct tunneling cannot occur. However if the width of intrinsic layer is thin (less than 5nm), then we can still include direct tunneling in our model [25]. Therefore, in our case, which is $p^{+}in$ or $n^{+}ip$ heterojunction solar cell, the slope of energy bands of heterojunction under forward bias is too low to permit any significant contribution of tunneling carriers to cell current [15].

4.3 Modeling the Drift-Diffusion Effective Velocity as Limiting Factor for Heterojunction Current

As we discussed in previous chapter, the carriers are scattered while flowing through the depletion region in heterojunction. In following sections, we will model this effect as a limiting effective velocity of carriers in heterojunctions with and without intrinsic layer.

4.3.1 $n^{+}p$ Heterojunction Current

In an $n^{+}p$ heterojunction (Figure 4.1), we consider the electron current flowing from n-region through the space charge region. The interface effective velocity comes into account when the electrons flow over the potential barrier. We like to see whether there is another limiting factor for current before reaching the barrier. In other words, what is the limiting factor for the electron flux flowing through the space charge region, neglecting the previous discussed interface effective velocity role?

To answer this question, we begin our modeling with the drift-diffusion current equation. If we consider the electron quasi-Fermi level energy (E_{Fn}) as a reference (zero) potential level, then the drift-diffusion current equation in the n space charge region, can be written as:

$$J_n = \mu_n n(x) \frac{dE_{Fn}}{dx} \tag{4.54}$$

Where

$$E_{Fn} = E_C + kT \ln(\frac{n}{N_c}) \tag{4.55}$$

By substituting equation 4.54 in 4.55, we will have:

$$J_n = \mu_n n(x) \frac{dE_C(x)}{dx} + \mu_n kT \frac{dn(x)}{dx} \tag{4.56}$$

If we take the energy level at 0^+ as reference level (Figure 4.1), the relation between energy of the bottom of the conduction band and the voltage dropped on SCR can be written as: $E_C(x) = -qV(x) + C$, while we have the boundary condition: $E_C(0^-) = \Delta E_C$. We can also write: $E_C(0^-) = -qV(0^-) + C$ therefore: $C = E_C(0^-) + qV(0^-) = \Delta E_C + qV(0^-)$ and finally:

$$E_C(x) = \Delta E_C + q[V(0^-) - V(x)] \tag{4.57}$$

where V(0)-V(x) is the potential difference between 0^- (before the potential barrier in conduction band) and any arbitrary point between 0^- and $-W_n$.

We can substitute the equation of V(x) and V(0) by using equation 2.15:

$$V(x) - V(-W_n) = -\tfrac{qN_d}{2\varepsilon_s}(W_n + x)^2 \tag{4.58}$$

It means: $V(0^-) = V(-W_n) - \tfrac{qN_d}{2\varepsilon_s}(W_n)^2$ and $V(x) = V(-W_n) - \tfrac{qN_d}{2\varepsilon_s}(W_n + x)^2$ Therefore:

$$V(0^-) - V(x) = \tfrac{qN_d}{2\varepsilon_s}(x^2 + 2W_n x) \tag{4.59}$$

By substituting equation 4.59 in 4.57, we will have:

$$E_C(x) = \Delta E_C + \tfrac{q^2 N_d}{2\varepsilon_s}(x^2 + 2W_n x) \tag{4.60}$$

Now we can rewrite equation 4.56 as:

$$J_n = kT\mu_n \exp(\frac{-E_C(x)}{kT}) \times d[n(x)\exp(\frac{E_C(x)}{kT})]/dx \tag{4.61}$$

To find the heterojunction electrons current J_n, assuming the depletion approximation, we integrate equation 4.61 across the n-side space charge region [26]:

$$\frac{J_n}{kT\mu_n}\int_{0^-}^{-W_n}\exp(\frac{E_C(x)}{kT})dx=[n(x)\exp(\frac{E_C(x)}{kT})]_{0^-}^{-W_n} \tag{4.62}$$

therefore

$$\frac{J_n}{kT\mu_n}\int_{0^-}^{-W_n}\exp(\frac{E_C(x)}{kT})dx=[n(-W_n)\exp(\frac{E_C(-W_n)}{kT})-n(0^-)\exp(\frac{E_C(0^-)}{kT})] \tag{4.63}$$

Using equation 4.57:

$$\frac{J_n}{kT\mu_n}\int_{0^-}^{-W_n}\exp(\frac{E_C(x)}{kT})dx=[n(-W_n)\exp(\frac{\Delta E_C+q(V(0^-)-V(-W_n))}{kT})-n(0^-)\exp(\frac{\Delta E_C}{kT})] \tag{4.64}$$

In equilibrium state, there is no current flowing, i.e., $J_n=0$ thus:

$$n^0(-W_n)\exp(\frac{\Delta E_C+q(V^0(0^-)-V^0(-W_n))}{kT})=n^0(0^-)\exp(\frac{\Delta E_C}{kT}) \tag{4.65}$$

From equation 4.65 we can write:

$$n^0(-W_n)=n^0(0)\exp(\frac{q(-V^0(0^-)+V^0(-W_n))}{kT})] \tag{4.66}$$

Assuming the low-level injection on the n-side, we can write:

$$n^0(-W_n)\approx n(-W_n) \tag{4.67}$$

By substituting equation 4.66 in 4.64 and considering 4.67, we will have:

$$\frac{J_n}{kT\mu_n}\int_{0^-}^{-W_n}\exp(\frac{E_C(x)}{KT})dx=[n^0(0^-)\exp(\frac{\Delta E_C+q(V(0^-)-V(-W_n)-V^0(0^-)+V^0(-W_n))}{kT})-n(0^-)\exp(\frac{\Delta E_C}{kT})] \tag{4.68}$$

The difference between the voltages at $x=-W_n$ and $x=0^-$ in equilibrium state and under forward bias is equal to a part of applied voltage dropped on n-side, i.e.

$$V(0^-)-V(-W_n)-V^0(0^-)+V^0(-W_n)=[V^0(-W_n)-V^0(0^-)]-[V(-W_n)-V(0^-)]=V_n^0-V_n=V_n^A \tag{4.69}$$

We can also write

$$n(0^-)=\Delta n(0^-)+n^0(0^-) \tag{4.70}$$

Considering equations 4.69 and 4.70, we can rewrite 4.68 as follows:

$$\frac{J_n}{kT\mu_n}\int_{0^-}^{-W_n}\exp(\frac{E_C(x)}{kT})dx=\exp(\frac{\Delta E_C}{kT})[n^0(0^-)[\exp(\frac{q(V_n^A)}{kT})-1]-\Delta n(0^-)] \tag{4.71}$$

The right hand side of above equation gives information about the excess carriers (electrons) of junction with and without potential barrier in conduction band at 0^-. To clarify this discussion, assume that the expression $\frac{J_n}{kT\mu_n}\int_{0^-}^{-W_n}\exp(\frac{E_C(x)}{kT})dx$ goes down to zero. So: $\Delta n(0^-)=n^0(0^-)[\exp(\frac{q(V_n^A)}{kT})-1]$ which is the equation for excess electrons at 0^- in n^+p homojunction or $\Delta n^{hm}(0^-)$. This means that if $\frac{J_n}{kT\mu_n}\int_{0^-}^{-W_n}\exp(\frac{E_C(x)}{kT})dx$ is not zero, then $\Delta n(0^-)$ is the excess electrons concentration at 0^- in n^+p heterojunction or $\Delta n^{ht}(0^-)$. Now we can rewrite equation 4.71 as follows:

$$\frac{J_n}{kT\mu_n}\int_{0^-}^{-W_n}\exp(\frac{E_C(x)}{kT})dx=\exp(\frac{\Delta E_C}{kT})[\Delta n^{hm}(0^-)-\Delta n^{ht}(0^-)] \tag{4.72}$$

If we neglect the effect of potential barrier as a limiting interface velocity, we can calculate the concentration of excess electrons at the interface between SCR and p-region by multiplying the right hand side of equation 4.72 by $\exp(\frac{\Delta E_C-qV_p}{kT})$, which is simply Boltzmann equation for the carrier concentration. This will give us:

$$\frac{J_n}{kT\mu_n}\int_{0^-}^{-W_n}\exp(\frac{E_C(x)}{kT})dx=\exp(\frac{\Delta E_C}{kT})\exp(\frac{-\Delta E_C+qV_p}{kT})[\Delta n^{hm}(W_p)-\Delta n^{ht}(W_p)] \tag{4.73}$$

Having the excess electrons concentration at W_p lets us calculate the currents at the same point. As we did in section 4.1.1, we can write:

$$\frac{J_n^{ht}}{kT\mu_n}q\int_{0^-}^{-W_n}\exp(\frac{E_C(x)}{kT})dx=\frac{1}{v_n}\exp(\frac{\Delta E_C}{kT})\exp(\frac{-\Delta E_C+qV_p}{kT})[J_n^{hm}-J_n^{ht}] \tag{4.74}$$

which can be rewritten as:

$$J_n^{ht}=\frac{J_n^{hm}}{1+\frac{v_n}{v_{effe}}} \tag{4.75}$$

where

$$v_{effe} = \frac{kT\mu_n \exp(\frac{\Delta E_C}{kT})\exp(\frac{-\Delta E_C + qV_p}{kT})}{q\int_{0^-}^{-W_n} \exp(\frac{E_C(x)}{kT})dx} \tag{4.76}$$

is the drift-diffusion effective velocity of electrons and $v_n = \frac{L_n}{\tau_n}$. The equation 4.75 defines that the electron current will be lowered while flowing through the space charge region on n-side if a potential barrier (ΔE_C) is present in the conduction band.

To calculate equation 4.76, first we consider the integral in denominator. By substituting $E_C(x)$ from equation 4.60, we will have:

Denominator=

$$q\int_{0^-}^{-W_n} \exp(\frac{\Delta E_C + \frac{q^2 N_d}{2\varepsilon_s}(x^2 + 2W_n x)}{kT})dx = q\exp(\Delta E_C / kT)\int_{0^-}^{-W_n} \exp(\frac{\frac{q^2 N_d}{2\varepsilon_s}[(x+W_n)^2 - W_n^2]}{kT})dx \tag{4.77}$$

By choosing [27]

$$a = q\sqrt{\frac{N_d}{2\varepsilon_s kT}} \tag{4.78}$$

and $x + W_n = t$, we can write: *dx=dt*, and then:

Denominator

$$= q\exp(\Delta E_C / kT)\int_{W_n}^{0^-} \exp(-a^2 W_n^2).\exp(a^2 t^2)dt = q\exp(\Delta E_C / kT)\exp(-a^2 W_n^2)\int_{W_n}^{0^-} \exp(a^2 t^2)dt \tag{4.79}$$

By changing the variable as*: at=y => adt=dy,* therefore:

$$\text{Denominator} = -q\exp(\Delta E_C / kT).a^{-1}.\exp(-a^2 W_n^2)\int_{0^-}^{aW_n} \exp(y^2)dy \tag{4.80}$$

The third part of this expression ($\exp(-a^2 W_n^2)\int_{0^-}^{aW_n} \exp(y^2)dy$) is Dawson's integral that has already been solved numerically [28]. By applying the approximation of aW_n>2, the solution of the Dawson's integral will be $(2aW_n)^{-1}$. This approximation leads to $qV_{bi} > 4kT$ which is generally the case except for very large values of forward bias [27].

By this approximation, we will have:

$$\text{Denominator}=-q\exp(\Delta E_C/kT).a^{-1}.\frac{1}{2aW_n}=-\frac{q\exp(\Delta E_C/kT)}{2W_n}.\frac{2\varepsilon_s kT}{q^2N_d} \tag{4.81}$$

By substituting equation 4.81 in 4.76:

$$v_{effe}=\frac{kT\mu_n\exp(\frac{\Delta E_C}{kT})\exp(\frac{-\Delta E_C+qV_p}{kT})}{\frac{-\exp(\frac{\Delta E_C}{kT})2\varepsilon_s kT}{2W_nqN_d}}=\frac{-qN_dW_n\mu_n}{\varepsilon_s}\exp(\frac{-\Delta E_C+qV_p}{kT})=-\mu_nE(0^-)\exp(\frac{-\Delta E_C+qV_p}{kT}) \tag{4.82}$$

The negative sign indicates the direction of electrons flux that is opposite to the current direction. Therefore, the magnitude of effective velocity of electrons considered at W_p will be :

$$v_{effe}=\mu_nE(0^-)\exp(-\frac{\Delta E_C-qV_p}{kT}) \tag{4.83}$$

It should be noted again that if we intend to study the electrons drift-diffusion effective velocity at 0^-, it will be:

$$v_{effe}=\mu_nE(0^-) \tag{4.84}$$

We can verify whether the unit of v_{effe} is the same as the unit of velocity.

$$v_{effe}=\mu E=[\frac{cm^2}{Vs}][\frac{V}{cm}]=[\frac{cm}{s}] \tag{4.85}$$

We can repeat the same procedure for the holes and find the drift-diffusion effective velocity of holes in n^+p heterojunction as a lowering factor for hole current as well. We calculated:

$$J_p^{ht} = \frac{J_p^{hm}}{1 + \dfrac{v_p}{v_{effh}}} \tag{4.86}$$

where,

$$v_{effh} = \mu_p E(0^+) e^{\frac{\Delta E_C + qV_n}{kT}} \tag{4.87}$$

and $v_p = \dfrac{L_p}{\tau_p}$. As it can be seen again $v_{effh} = \mu_p E(0^+) e^{\frac{\Delta E_C + qV_n}{kT}} >> 0$ and therefore $J_p^{ht} = J_p^{hm}$. This means that both lowering factors (interface effective velocity and drift-diffusion effective velocity) do not lower the hole current in case of $n^+ p$ heterojunction.

4.3.2 $n^+ ip$ Heterojunction Current

As we have seen in the previous chapters, in most solar cell applications, an intrinsic layer of amorphous silicon is introduced in the space charge region of the device (in $n^+ p$ heterojunction, for instance, the i-layer is inserted in n-side SCR up to the n and p interface, x=0). The width of the intrinsic layer is usually between 3 nm to a few tens nm which is much wider than W_n. This is because, as discussed earlier, n-side is heavily doped. This leads us to calculate the drift-diffusion effective velocity of electrons in i-layer in $n^+ ip$ heterojunction to find out how the electron current will be lowered.

Assuming that the electric field in intrinsic layer is constant and approximately equals to the magnitude of voltage dropped across the intrinsic layer (V_i) divided by the width of the intrinsic layer:

$$E_i = \frac{V_i}{W_i} \tag{4.88}$$

The potential difference between $-W_i$ and an arbitrary point between 0^- and $-W_i$ will be:

$$V_i(x) - V(-W_i) = -\frac{V_i}{W_i}(W_i + x) \tag{4.89}$$

Using this, we can write:

$$V_i(0^-) - V(-W_i) = -V_i \tag{4.90}$$

and thus:

$$V_i(0^-) - V(x) = \frac{V_i}{W_i}x \tag{4.91}$$

and therefore we can rewrite equation 4.57 as:

$$E_C(x) = \Delta E_C + q(\frac{V_i}{W_i}x) \tag{4.92}$$

Regarding equation 4.92, we can recalculate the integral in denominator of equation 4.76 as:

$$q\int_{0^-}^{-W_i}\exp(\frac{E_C(x)}{kT})dx = q\exp(\frac{\Delta E_C}{kT})\int_{0^-}^{-W_i}\exp(\frac{qV_i}{W_ikT}x)dx = q\exp(\frac{\Delta E_C}{kT})[\frac{W_ikT}{qV_i}\exp(\frac{qV_i}{W_ikT}x)]_{0^-}^{-W_i} \tag{4.93}$$

which gives:

$$-\exp(\frac{\Delta E_C}{kT})\frac{W_ikT}{V_i}[1-\exp(\frac{-qV_i}{kT})] \tag{4.94}$$

By substituting equation 4.94 in drift-diffusion effective velocity of electrons equation (4.76), we will have:

$$|v_{effe}| = \frac{kT\mu_n\exp(\frac{\Delta E_C}{kT})\exp(\frac{-\Delta E_C + qV_p}{kT})}{\exp(\frac{\Delta E_C}{kT})\frac{W_ikT}{V_i}[1-\exp(\frac{-qV_i}{kT})]} = \frac{\mu_n\frac{V_i}{W_i}}{1-\exp(\frac{-qV_i}{kT})}\exp(-\frac{\Delta E_C - qV_p}{kT}) \tag{4.95}$$

Equation 4.95 is a simple form of carrier effective velocity in space charge region when the region is intrinsic layer. Therefore, in case of n^+ip, in I-V equation (4.75) instead of electron drift-diffusion effective velocity in SCR (v_{effe}), equation 4.95 (drift-diffusion effective velocity of electrons in intrinsic layer) should be substituted.

4.3.3 $p^+ n$ Heterojunction Current

In this section, we will derive the equations of the drift-diffusion effective velocity of carriers in p^+n heterojunctions. The method that we use here is the same as we did in n^+p heterojunctions section (4.3.1), therefore, this section will mostly be about deriving the equations with less explanation.

Figure 4.2 shows the energy band diagram of a p^+n heterojunction. We calculate the hole current right before the potential barrier in valence band or 0^-. To do so, we need to use the following equation as drift-diffusion current equation in p space charge region [24]:

$$J_p = \mu_p p(x) \frac{dE_{Fp}}{dx} \tag{4.96}$$

where E_{Fp} is hole quasi-Fermi level energy:

$$E_{Fp} = E_V + kT \ln(\frac{N_V}{p}) \tag{4.97}$$

By substituting equation 4.97 in 4.96, we will have:

$$J_p = \mu_p p(x) \frac{dE_V(x)}{dx} - \mu_p kT \frac{dp(x)}{dx} \tag{4.98}$$

If we take the energy level at 0^+ as reference level, the relation between energy of the top of the valence band and the voltage dropped on SCR can be written as: $E_V(x) = -qV(x) + C$ while we have the boundary condition: $E_V(0^-) = -\Delta E_V$. We can also write: $E_V(0^-) = -qV(0^-) + C$ therefore: $C = E_V(0^-) + qV(0^-) = -\Delta E_V + qV(0^-)$ and finally:

$$E_V(x) = -\Delta E_V + q[V(0^-) - V(x)] \tag{4.99}$$

Where $V(0^-) - V(x)$ is the potential difference between the 0^- (before barrier) and any arbitrary point between 0^- and $-W_p$.

We can substitute the equation of V(x) and V(0) by [24]:

$$V(x) - V(-W_p) = \tfrac{qN_a}{2\varepsilon_s}(W_p + x)^2 \tag{4.100}$$

$,V(0^-) = V(-W_p) + \frac{qN_a}{2\varepsilon_s}(W_p)^2$ and $V(x) = V(-W_p) + \frac{qN_a}{2\varepsilon_s}(W_p + x)^2$

therefore:

$$V(0^-) - V(x) = -\frac{qN_a}{2\varepsilon_s}(x^2 + 2W_p x) \tag{4.101}$$

By substituting equation 4.101 in 4.99, we will have:

$$E_V(x) = -\Delta E_V - \frac{q^2 N_a}{2\varepsilon_s}(x^2 + 2W_p x) \tag{4.102}$$

We can rewrite equation 4.98 as follows:

$$J_p = -kT\mu_p \exp(\frac{E_V(x)}{kT}) \times d[p(x)\exp(-\frac{E_V(x)}{kT})]/dx \tag{4.103}$$

To find the hole current, assuming the depletion approximation, we integrate equation 4.103 across the p-space charge region [26].

$$-\frac{J_p}{kT\mu_p}\int_{0^-}^{-W_p} \exp(-\frac{E_V(x)}{kT})dx = [p(x)\exp(-\frac{E_V(x)}{kT})]_{0^-}^{-W_p} \tag{4.104}$$

therefore

$$-\frac{J_p}{kT\mu_p}\int_{0^-}^{-W_p} \exp(-\frac{E_V(x)}{kT})dx = [p(-W_p)\exp(-\frac{E_V(-W_p)}{kT}) - p(0^-)\exp(-\frac{E_V(0^-)}{kT})] \tag{4.105}$$

Using equation 4.99:

$$-\frac{J_p}{kT\mu_p}\int_{0^-}^{-W_p} \exp(-\frac{E_V(x)}{kT})dx = [p(-W_p)\exp(\frac{\Delta E_V + q(-V(0^-) + V(-W_p))}{kT}) - p(0^-)\exp(\frac{\Delta E_V}{kT})] \tag{4.106}$$

In equilibrium state, there is no current flowing, i.e., $J_p = 0$ thus:

$$p^0(-W_p)\exp(\frac{\Delta E_V + q(-V^0(0^-) + V^0(-W_p))}{kT}) = p^0(0^-)\exp(\frac{\Delta E_V}{kT})] \tag{4.107}$$

From equation 4.107, we can write:

$$p^0(-W_p) = p^0(0^-)\exp(\frac{q(V^0(0^-) - V^0(-W_p))}{kT})] \tag{4.108}$$

Assuming the low-level injection on the p-side we can write:

$$p^0(-W_p) \approx p(-W_p) \tag{4.109}$$

By substituting equation 4.108 in 4.106 and considering 4.109, we will have:

$$-\frac{J_p}{kT\mu_p}\int_{0^-}^{-W_p}\exp(-\frac{E_V(x)}{kT})dx=[p^0(0^-)\exp(\frac{\Delta E_V+q(-V(0^-)+V(-W_p)+V^0(0^-)-V^0(-W_p))}{kT})-p(0^-)\exp(\frac{\Delta E_V}{kT})] \tag{4.110}$$

The difference between the voltages at $x=-W_p$ and $x=0^-$ in equilibrium state and under forward bias is equal to a part of applied voltage dropped on p-side, i.e.

$$V(-W_p)-V(0^-)+V^0(0^-)-V^0(-W_p)=[V^0(0^-)-V^0(-W_p)]-[V(0^-)-V(-W_p)]=V_p^0-V_p=V_p^A \tag{4.111}$$

We can also write

$$\Delta p(0^-)=p(0^-)-p^0(0^-) \tag{4.112}$$

therefore:

$$-\frac{J_p}{kT\mu_p}\int_{0^-}^{-W_p}\exp(-\frac{E_V(x)}{kT})dx=\exp(\frac{\Delta E_V}{kT})[p^0(0^-)[\exp(\frac{q(V_{PA})}{kT})-1]-\Delta p(0^-)] \tag{4.113}$$

As we discussed in section 4.3.1, the right hand side of above equation ($p^0(0^-)[\exp(\frac{q(V_{PA})}{kT})-1]-\Delta p(0^-)$) gives information about the concentration of excess holes at (0^-) for p^+n homojunction and heterojunction. It means:

$$-\frac{J_p}{kT\mu_p}\int_{0^-}^{-W_p}\exp(-\frac{E_V(x)}{kT})dx=\exp(\frac{\Delta E_V}{kT})[\Delta p^{hm}(0^-)-\Delta p^{ht}(0^-)] \tag{4.114}$$

To find the concentration of excess holes at W_n, it is enough to multiply the excess carrier concentration at 0^- by $\exp(\frac{\Delta E_V-qV_n}{kT})$:

$$-\frac{J_p}{kT\mu_p}\int_{0^-}^{-W_p}\exp(-\frac{E_V(x)}{kT})dx=\exp(\frac{\Delta E_V}{kT})\exp(-\frac{\Delta E_V-qV_n}{kT})[\Delta p^{hm}(W_n)-\Delta p^{ht}(W_n)] \tag{4.115}$$

Now by neglecting the effect of potential barrier as a limiting interface velocity, we can calculate the current at the interface between SCR and p-region W_n:

$$-\frac{J_p}{kT\mu_p}\int_{0}^{-W_p}\exp(-\frac{E_V(x)}{kT})dx=$$

$$-\frac{J_p^{ht}}{kT\mu_p}q\int_0^{-W_p}\exp(-\frac{E_V(x)}{kT})dx=\frac{1}{v_p}\exp(\frac{\Delta E_V}{kT})\exp(\frac{-\Delta E_V+qV_n}{kT})[J_p^{hm}-J_p^{ht}] \qquad (4.116)$$

Consequently:

$$J_p^{ht}=\frac{J_p^{hm}}{1+\frac{v_p}{v_{effh}}} \qquad (4.117)$$

where,

$$v_{effh}=-\frac{kT\mu_p\exp(\frac{\Delta E_V}{kT})\exp(\frac{-\Delta E_V+qV_n}{kT})}{q\int_{0^-}^{-W_p}\exp(-\frac{E_V(x)}{kT})dx} \qquad (4.118)$$

and $v_p=\frac{L_p}{\tau_p}$.

Equation 4.117 shows that the hole current will be lowered if a potential barrier (ΔE_V) is present in the valence band. To calculate equation 4.118, as we did in section 4.3.1, first we consider the integral in denominator. By substituting $E_V(x)$ from equation 4.102, we will have:

Denominator=

$$q\int_{0^-}^{-W_p}\exp(\frac{\Delta E_V+\frac{q^2N_a}{2\varepsilon_s}(x^2+2W_px)}{kT})dx=q\exp(\Delta E_V/kT)\int_{0^-}^{-W_p}\exp(\frac{\frac{q^2N_a}{2\varepsilon_s}[(x+W_p)^2-W_p^2]}{kT})dx$$

(4.119)

Choosing

$$a=q\sqrt{\frac{N_a}{2\varepsilon_s kT}} \qquad (4.120)$$

and $x+W_p=t$ we can write: *dx*=*dt* ,and then:

Denominator

$$= q\exp(\Delta E_V / kT)\int_{W_p}^{0^-}\exp(-a^2W_p^2).\exp(a^2t^2)dt = q\exp(\Delta E_V / kT)\exp(-a^2W_p^2)\int_{W_p}^{0^-}\exp(a^2t^2)dt \tag{4.121}$$

By changing the variable as *:at=y => adt=dy* ,therefore:

$$\text{Denominator} = -q\exp(\Delta E_V / kT).a^{-1}.\exp(-a^2W_p^2)\int_{0^-}^{aW_p}\exp(y^2)dy \tag{4.122}$$

A part of this expression $(\exp(-a^2W_p^2)\int_{0^-}^{aW_p}\exp(y^2)dy)$ is Dawson's integral [28]. By applying the approximation of aW_p>2 (which leads to $qV_A > 4kT$) the solution of the Dawson's integral will be $(2aW_p)^{-1}$. By this approximation, we will have:

$$\text{Denominator} = -q\exp(\Delta E_V / kT).a^{-1}.\frac{1}{2aW_p} = \frac{q\exp(\Delta E_V / kT)}{2W_p}.\frac{2\varepsilon_s kT}{q^2N_a} \tag{4.123}$$

By substituting equation 4.123 in 4.118:

$$v_{effh} = -\frac{kT\mu_p\exp(\frac{\Delta E_V}{kT})\exp(\frac{-\Delta E_V + qV_n}{kT})}{-\frac{q\exp(\Delta E_V / kT)}{2W_p}.\frac{2\varepsilon_s kT}{q^2N_a}} = \frac{qN_aW_p\mu_p}{\varepsilon_s}\exp(\frac{-\Delta E_V + qV_n}{kT}) = \mu_p\,|E(0^-)|\exp(\frac{-\Delta E_V + qV_n}{kT})$$

and therefore the effective velocity of holes at W_n will be:

$$v_{effh} = \mu_p\,|E(0^-)|\exp(\frac{-\Delta E_V + qV_n}{kT}) \tag{4.124}$$

As we saw in section 4.3.1, the unit of v_{effh} is of the unit of velocity.

$$v_{effh} = \mu E = [\frac{cm^2}{Vs}][\frac{V}{cm}] = [\frac{cm}{s}]$$

Needles to say that drift-diffusion effective velocity of holes at 0^- will be: $v_{effh} = \mu_p\,|E(0^-)|$

By repeating the same procedure, we found the drift-diffusion effective velocity of electrons in p^+n heterojunctions, as

$$v_{effe} = \mu_n\left|E(0^+)\right|e^{\frac{\Delta E_C + qV_p}{kT}} \tag{4.125}$$

and therefore:

$$J_n^{ht} = \frac{J_n^{hm}}{1+\frac{v_n}{v_{effe}}}, \; (v_n = \frac{L_n}{\tau_n}) \tag{4.126}$$

It can be seen that $v_{effe} = \mu_n \left| E(0^+) \right| e^{\frac{\Delta E_C + qV_p}{kT}}$ >>0 and therefore $J_n^{ht} = J_n^{hm}$. This means that both lowering factors (interface effective velocity and drift-diffusion effective velocity) do not lower the electron current in case of p^+n heterojunction.

4.3.4 p^+ *in* Heterojunction Current

Introducing an intrinsic layer of amorphous silicon in the space charge region of the device leads us to calculate the drift-diffusion effective velocity of holes in i-layer in p^+in heterojunction to find out how the hole current will be lowered.

As we did in n^+ip case, we assume that the electric field in intrinsic layer is constant and approximately equals the magnitude of dropped voltage on intrinsic layer over its width with negative sign:

$$E_i = -\frac{V_i}{W_i} \tag{4.127}$$

Therefore the potential difference between $-W_p$ and an arbitrary point between 0^- and $-W_i$ will be:

$$V_i(x) - V(-W_i) = \frac{V_i}{W_i}(W_i + x) \tag{4.128}$$

Using this we can write:

$$V_i(0^-) - V(-W_i) = V_i \tag{4.129}$$

and

$$V_i(0^-) - V(x) = -\frac{V_i}{W_i} x \tag{4.130}$$

Therefore, we can rewrite equation 4.99 as:

$$E_V(x) = -\Delta E_V - q(\frac{V_i}{W_i}x) \tag{4.131}$$

Regarding this, we can recalculate the integral in denominator of equation 4.118:

$$q\int_{0^-}^{-W_i} \exp(-\frac{E_V(x)}{kT})dx = q\exp(\frac{\Delta E_V}{kT})\int_{0^-}^{-W_i} \exp(\frac{qV_i}{W_ikT}x)dx = q\exp(\frac{\Delta E_V}{kT})[\frac{W_ikT}{qV_i}\exp(\frac{qV_i}{W_ikT}x)]_{0^-}^{-W_i} \tag{4.132}$$

which gives:

$$\exp(\frac{\Delta E_V}{kT})\frac{W_ikT}{V_i}[\exp(-\frac{qV_i}{kT})-1] \tag{4.133}$$

By substituting equation 4.133 in the effective velocity of carriers in SCR equation (4.118), we will have:

$$v_{effh} = -\frac{kT\mu_p \exp(\frac{\Delta E_V}{kT})\exp(\frac{-\Delta E_V + qV_n}{kT})}{\exp(\frac{\Delta E_V}{kT})\frac{W_ikT}{V_i}[\exp(-\frac{qV_i}{kT})-1]} = \frac{\mu_p \frac{V_i}{W_i}}{[1-\exp(-\frac{qV_i}{kT})]}\exp(\frac{-\Delta E_V + qV_n}{kT}) \tag{4.134}$$

and therefore at 0^- we will have:

$$v_{effh} = \frac{\mu_p \frac{V_i}{W_i}}{1-\exp(-\frac{qV_i}{kT})} \tag{4.135}$$

4.4 Modeling the Interface Recombination Current in *a-Si/c-Si* Heterojunction

In this section, we will derive the equations of the interface recombination current in n^+ip and p^+in heterojunctions solar cell.

4.4.1 Interface Recombination Current in n^+ip Heterojunction

The electrons pushed by the forward bias in n^+ip heterojunction, face many localized (trapped) holes in a-Si/c-Si interface upon reaching this point. This causes the free electrons to recombine with the trapped holes and produce the recombination current at the interface. On the other hand, the free holes that come from the p-region of the n^+ip will recombine with trapped electrons upon reaching the interface. However, the contribution of this current is very small and can be neglected in our calculation.

The recombination current at a-Si/c-Si interface is calculated by:

$$J_R = q\sigma_c v_{th}(np_t + pn_t) \tag{4.136}$$

where σ_c is the capture cross-section of charged centers, v_{th} is the thermal velocity, *n* and *p* are free carrier concentrations, and n_t and p_t are interface concentration of trapped carriers at the a-Si/c-Si heterojunctions [14]. For n^+ip heterojunction solar cell, the emitter (n-region) is heavily doped, and the recombination current equation at W_3 will become:

$$J_R = q\sigma_c v_{th} n_3 p_{t3} \tag{4.137}$$

This is because that $n_0 >> p_0$ and regarding the fact that the dropped voltage on the base side is much more than that across the intrinsic layer and emitter side, we can definitely conclude that at a-Si/c-Si interface, $n(W_3) >> p(W_3)$. This leads us to equation 4.137.

The localized states in the gap are comprised of donorlike and acceptorlike states with energy dependent densities of $g_D(E)$ and $g_A(E)$, where [29]:

$$g_D(E) = g_{D\min} \exp(-\frac{E - E_{mc}}{E_D}) \tag{4.138}$$

$$g_A(E) = g_{A\min} \exp(\frac{E - E_{mc}}{E_A}) \tag{4.139}$$

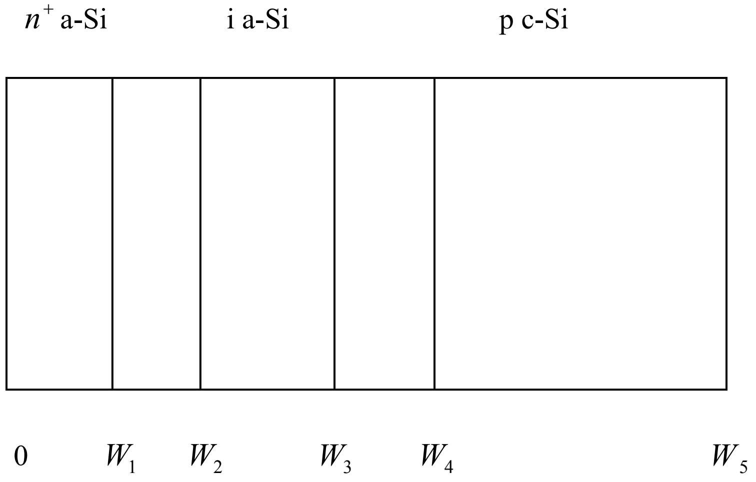

Fig 4.5 n^+ip heterojunction solar cell

Here, E_D and E_A are the characteristic energy slopes of the exponential distribution of donorlike and acceptorlike localized states and E_{mc} is the energy difference between the minimum in the density of states and the conduction band edge [29].

In case of n^+ip (p^+in) a-Si/c-Si heterojunction, assuming symmetric tails of donorlike and acceptorlike surface states at the a-si/c-si heterojunction interface, E_{mc} can be replaced by the valence band level and conduction band level of the amorphous silicon respectively [14,15]. Therefore, equation 4.138 and 4.139 for densities of states can be rewritten as:

$$g_D(E) = g_{D\min} \exp(-\frac{E - E_V}{E_D}) \tag{4.140}$$

$$g_A(E) = g_{A\min} \exp(\frac{E - E_C}{E_A}) \tag{4.141}$$

In case of n^+ip heterojunctions, we should calculate the concentration of trapped (localized) holes (donorlike) in the interface. For this purpose, we can write [29]:

$$p_t = \int_{E_c}^{E_{tn}^d} g_D(E)dE + \frac{p}{nC+p}\int_{E_{tp}^d}^{E_{tn}^d} g_D(E)dE \tag{4.142}$$

The parameter '*C*' is the ratio of the cross-section of a charged trap to the cross-section of a neutral trap [29] or:

$$C = \frac{\sigma_c}{\sigma_N} \tag{4.143}$$

The first term in equation 4.142 is typically much smaller than the second term because $g_D(E)$ varies rapidly with energy. Therefore, we can eliminate the first part of equation 4.142. The boundaries in the second term integral are the hole quasi-Fermi levels which are given by: [29]

$$E_{tn}^d = E_c + kT\ln(\frac{n+p/C}{N_c}) \tag{4.144}$$

$$E_{tp}^d = E_v - kT\ln(\frac{nC+p}{N_v}) \tag{4.145}$$

Where E_c and E_v are the energies corresponding to the bottom of the conduction band and to the top of the valence band respectively. N_c and N_v are the effective state densities in the conduction and valence band as well. Using equation 4.137 and by substituting 4.140 into 4.142 and solving the integral, we can write: (the subscript 3 stands for the value of the parameter at W_3 in Figure 4.5)

$$J_R = q\sigma_c v_{th} n_3 \frac{p_3}{n_3C+p_3}\int_{E_{tp}^d}^{E_{tn}^d} g_{D\min}\exp(-\frac{E-E_{mc}}{E_D})dE =$$

$$= q\sigma_c v_{th} n_3 \frac{p_3}{n_3C+p_3}(-g_{D\min}E_D)[\exp(-\frac{E-E_{mc}}{E_D})]_{E_v-kT\ln(\frac{n_3C+p_3}{N_v})}^{E_c+kT\ln(\frac{n_3+p_3/C}{N_c})} =$$

$$= q\sigma_c v_{th} n_3 \frac{p_3}{n_3C+p_3}(-g_{D\min}E_D)[\exp(-\frac{E_c+kT\ln(\frac{n_3+p_3/C}{N_c})-E_V}{E_D}) - \exp(-\frac{E_V-kT\ln(\frac{n_3C+p_3}{N_v})-E_V}{E_D})] =$$

$$= q\sigma_c v_{th} n_3 \frac{p_3}{n_3C+p_3}(-g_{D\min}E_D)[\exp(-\frac{E_g}{E_D})(\frac{n_3+p_3/C}{N_c})^{-\frac{kT}{E_D}} - (\frac{n_3C+p_3}{N_v})^{\frac{kT}{E_D}}] \tag{4.146}$$

The term $\exp(-\frac{E_g}{E_D})(\frac{n_3+p_3/C}{N_c})^{-\frac{kT}{E_D}}$ is small enough to be negligible. Also, p_3 in $(\frac{n_3C+p_3}{N_v})^{\frac{kT}{E_D}}$ is much smaller than n_3C so we can eliminate it too. By these simplifications, we can rewrite equation 4.146 as:

$$J_R = q\sigma_c v_{th} n_3 \frac{p_3}{n_3C+p_3}(g_{D\min}E_D)[(\frac{n_3C}{N_v})^{\frac{kT}{E_D}}] \tag{4.147}$$

Again, because $p_3 << n_3C$, we can eliminate p_3 in the denominator of the fraction.

$$J_R = q\sigma_c v_{th} n_3 \frac{p_3}{n_3C}(g_{D\min}E_D)(\frac{n_3C}{N_v})^{\frac{kT}{E_D}} = q\sigma_c v_{th} n_3 \frac{p_3}{C}(g_{D\min}E_D)(\frac{n_3C}{N_v})^{\frac{kT}{E_D}} \tag{4.148}$$

n_3 and p_3 are representing the free carrier densities in the a-Si/c-Si interface at W_3 . We can replace these parameters with those that are more familiar to us. The density of free electrons at W_4 is:

$$n_4 = n_{p0}\exp(qV_F/kT) \tag{4.149}$$

and for n_3 we can write:

$$n_3 = n_4\exp(qV_p/kT) \tag{4.150}$$

and also

$$p_4 = N_a \tag{4.151}$$

and

$$p_3 = p_4\exp(-qV_p/kT) \tag{4.152}$$

Therefore, we can write:

$$n_3 = n_{p0}\exp(\frac{q(V_F+V_p)}{kT}) \tag{4.153}$$

and

$$p_3 = N_a\exp(-qV_p/kT) \tag{4.154}$$

By substituting equations 4.153 and 4.154 in 4.148, we can write:

$$=q\sigma_c v_{th}\frac{N_a\exp(-qV_p/kT)}{C}(g_{D\min}E_D)\left(\frac{Cn_{p0}\exp(\frac{q(V_F+V_p)}{kT})}{N_v}\right)^{\frac{kT}{E_D}}$$

$$=q\sigma_c v_{th}\frac{N_a\exp(-qV_p/kT)}{C}(g_{D\min}E_D)\left(\frac{Cn_{p0}}{N_v}\right)^{\frac{kT}{E_D}}\exp\left(\frac{q(V_F+V_p)}{E_D}\right)$$

$$J_R=q\sigma_c v_{th}g_{D\min}E_D\frac{N_a}{C}\left(\frac{Cn_{p0}}{N_v}\right)^{\frac{kT}{E_D}}\exp\left[\frac{q(V_F+V_p)}{E_D}-\frac{qV_p}{kT}\right] \tag{4.155}$$

Equation 4.155 gives the a-Si/c-Si interface recombination current in n^+ip heterojunction. The values for the parameters in this equation are:

$E_D=0.052eV$ [14]

$g_{D\min}=10^{14}cm^{-2}eV^{-1}$ [14]

$\sigma_c v_{th}=5\times10^{-10}cm^3\sec^{-1}$ [30]

C=0.01 [31]

4.4.2 Interface Recombination Current in p^+in Heterojunction

We can redo all the calculations to obtain p^+in heterojunction interface recombination current. From Figure 4.6, assuming the same approximation that we took in previous section for n^+ip interface recombination current ($p_0 >> n_0$ and $p(W_3) >> n(W_3)$), we can write:

$$J_R=q\sigma_c v_{th}pn_t \tag{4.156}$$

We should calculate the concentration of trapped (localized) electrons (acceptorlike) in the interface. For this purpose, we can write [29]:

$$n_t=\frac{n}{n+Cp}\int_{E_{tp}^a}^{E_{tn}^a}g_A(E)dE \tag{4.157}$$

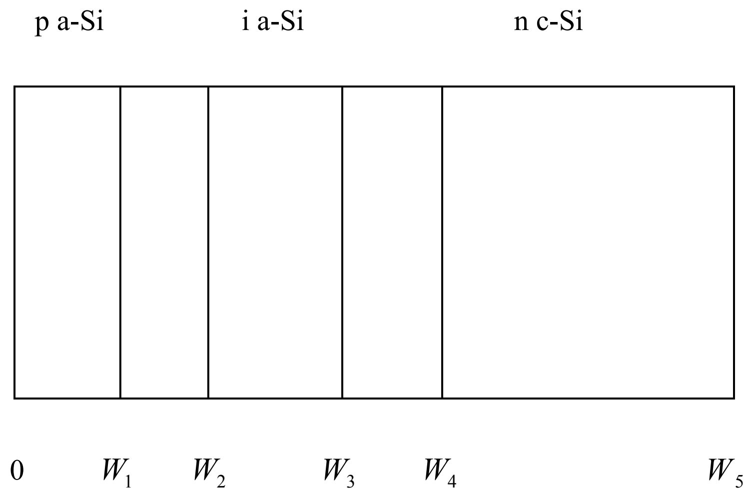

Fig 4.6 p^+in heterojunction solar cell

The boundaries in the integral are the electron quasi-Fermi levels given by [29]:

$$E_{tn}^a = E_c + kT\ln(\frac{n+Cp}{N_c}) \tag{4.158}$$

$$E_{tp}^a = E_v - kT\ln(\frac{p+n/C}{N_v}) \tag{4.159}$$

Where E_c and E_v are the energies corresponding to the bottom of the conduction band and to the top of the valence band respectively. N_c and N_v are the effective state densities in the conduction and valence band as well and the parameter '*C*' is the ratio of the cross-section of a charged trap to the cross-section of a neutral trap [29]. Using equation 4.156 and by substituting 4.141 in 4.157 and solving the integral, for recombination current at W_3, we can write:

$$J_R = q\sigma_c v_{th} p_3 \frac{n_3}{n_3 + Cp_3}\int_{E_{tp}^a}^{E_{tn}^a} g_{A\min}\exp(\frac{E-E_c}{E_A})dE =$$

$$= q\sigma_c v_{th} p_3 \frac{n_3}{n_3 + Cp_3}(g_{A\min}E_A)[\exp(\frac{E-E_c}{E_A})]_{E_v - kT\ln(\frac{p_3+n_3/C}{N_v})}^{E_c + kT\ln(\frac{n_3+Cp}{N_c})} =$$

$$= q\sigma_c v_{th} p_3 \frac{n_3}{n_3 + Cp_3}(g_{A\min} E_A)[\exp(\frac{E_c + kT\ln(\frac{n_3 + Cp_3}{N_c}) - E_c}{E_A}) - \exp(\frac{E_v - kT\ln(\frac{p_3 + n_3 / C}{N_v}) - E_c}{E_A})] =$$

$$= q\sigma_c v_{th} p_3 \frac{n_3}{n_3 + Cp_3}(g_{A\min} E_A)[(\frac{n_3 + Cp_3}{N_c})^{\frac{kT}{E_A}} - \exp(-\frac{E_g}{E_D})(\frac{p_3 + n_3 / C}{N_v})^{-\frac{kT}{E_D}}] \qquad (4.160)$$

By a few simplifications, we obtain:

$$J_R = q\sigma_c v_{th} p_3 \frac{n_3}{Cp}(g_{A\min} E_A)[(\frac{Cp_3}{N_c})^{\frac{kT}{E_A}}] \qquad (4.161)$$

We have:

$$p_4 = p_{n0}\exp(qV_F / kT) \qquad (4.162)$$

$$p_3 = p_4\exp(qV_n / kT) \qquad (4.163)$$

and also:

$$n_4 = N_d \qquad (4.164)$$

$$n_3 = n_4\exp(-qV_n / kT) \qquad (4.165)$$

Therefore, we can write:

$$p_3 = p_{n0}\exp(\frac{q(V_F + V_n)}{kT}) \qquad (4.166)$$

$$n_3 = N_d\exp(-qV_n / kT) \qquad (4.167)$$

By substituting equations 4.166 and 4.167 in 4.161, we can write:

$$J_R = q\sigma_c v_{th}\frac{N_d\exp(-qV_n / kT)}{C}(g_{A\min} E_A)(\frac{Cp_{n0}\exp(\frac{q(V_F + V_n)}{kT})}{N_c})^{\frac{kT}{E_A}} =$$

$$= q\sigma_c v_{th} g_{A\min} E_A \frac{N_d}{C}(\frac{Cp_{n0}}{N_c})^{\frac{kT}{E_A}}\exp[\frac{q(V_F + V_n)}{E_A} - \frac{qV_n}{kT}] \qquad (4.168)$$

The values for the parameters are:

$E_A = 0.052eV$ [15]

$g_{A\min} = 5\times 10^{15} cm^{-2} eV^{-1}$ [15]

$\sigma_c v_{th} = 5\times 10^{-10} cm^3 \sec^{-1}$ [30]

C=0.01 [31]

4.5 Total Effective Velocities as Limiting Factors in $n^+ ip$ and $p^+ in$ Heterojunction Current

So far, we have modeled the thermionic emission and drift-diffusion transport mechanisms as two effective velocities of carriers that limit the carriers flow in heterojunctions. The final model for I-V characteristics of an n^+ip heterojunction includes the forward dark current suppressed by these two effective velocities in addition to interface recombination current. The later (J_R) is lowered by the same factors as the electrons current is decreased. This is explained by the fact that the electrons recombining at the heterointerface travel the same path as the electrons injected into c-Si base layer [14]. Therefore, the I-V equation for n^+ip a-Si/c-Si heterojunction is obtained as:

$$J = J_n^{ht} + J_p^{ht} + \frac{J_R}{1+A_n} = \frac{J_n^{hm}}{1+A_n} + J_p^{hm} + \frac{J_R}{1+A_n} = (\frac{qv_n n_{p0}}{1+A_n} + qv_p p_{n0})(e^{\frac{qV_F}{kT}} - 1) + \frac{J_R}{1+A_n} \qquad (4.169)$$

where

$$A_n = \frac{v_n}{v_{effe}} + \frac{v_n}{v_{in}} \qquad (4.170)$$

and the equations for v_{effe} and v_{in} are $\dfrac{\mu_n \dfrac{V_i}{W_i}}{1-\exp(\dfrac{-qV_i}{kT})} e^{-\frac{\Delta E_c - qV_p}{kT}}$ and $\gamma v_x e^{-\frac{\Delta E_C - qV_p}{kT}}$, respectively.

Similarly, for p^+in we can write:

$$J = J_p^{ht} + J_n^{ht} + \frac{J_R}{1+A_p} = \frac{J_p^{hm}}{1+A_p} + J_n^{hm} + \frac{J_R}{1+A_p} = (\frac{qv_p p_{n0}}{1+A_p} + qv_n n_{p0})(e^{\frac{qV_F}{kT}} - 1) + \frac{J_R}{1+A_p} \qquad (4.171)$$

where

$$A_p = \frac{v_p}{v_{effh}} + \frac{v_p}{v_{ip}} \tag{4.172}$$

and the equations for v_{effh} and v_{ip} are $\dfrac{\mu_p \dfrac{V_i}{W_i}}{1-\exp(\dfrac{-qV_i}{kT})} e^{-\frac{\Delta E_V - qV_n}{kT}}$ and $\gamma v_x e^{-\frac{\Delta E_V - qV_n}{kT}}$, respectively.

Chapter 5

Development of Analytical Models for $n^+ ip$ and $p^+ in$ *a-Si/c-Si* Heterojunction Solar Cells under Illumination

So far, we have modeled the current-voltage characteristics of a-Si/c-Si heterojunctions including the lowering factors that affect the current. In this chapter, we have developed an analytical model for n^+ip and p^+in under illumination and also under forward bias.

To model the n^+ip cell under illumination, we have calculated the quantum efficiency equations for every region of the cell in section 5.1. By having the quantum efficiency, we are able to calculate the photocurrent and develop the complete I-V curve under forward bias and illumination. In developing the I-V characteristics of n^+ip cell in section 5.1, we have used the lowering factors of current that we calculated in previous chapters including the interface and drift-diffusion effective velocities. As discussed earlier, we have also included the direct tunneling in our model by adding a multiplicative to the interface effective velocity. a-Si/c-Si interface recombination current has also been taken into account when completing the I-V equation. Therefore, the I-V equation contains the forward current, interface recombination current and the photocurrent which all are affected by the interface effective velocity of carriers (including direct tunneling) and the effective velocity of carriers within the depletion region.

Section 5.2 contains all the above-mentioned discussions for p^+in cell.

5.1 Analytical Model for the $n^+ ip$ *a-Si/c-Si* Heterojunction Solar Cell under Illumination

We consider a solar cell constituted of an intrinsic a-Si layer at the top of p-region c-Si (base) and a heavily doped n-region a-Si (emitter) over the intrinsic layer (Figure5.1). For the sake of consistency, we modify the labels in Figure 5.1 as follows:

$W_5 - W_4 = W_b \quad W_4 - W_3 = W_p, \quad W_3 - W_2 = W_i, \quad W_2 - W_1 = W_n \quad W_1 - 0 = W_1$

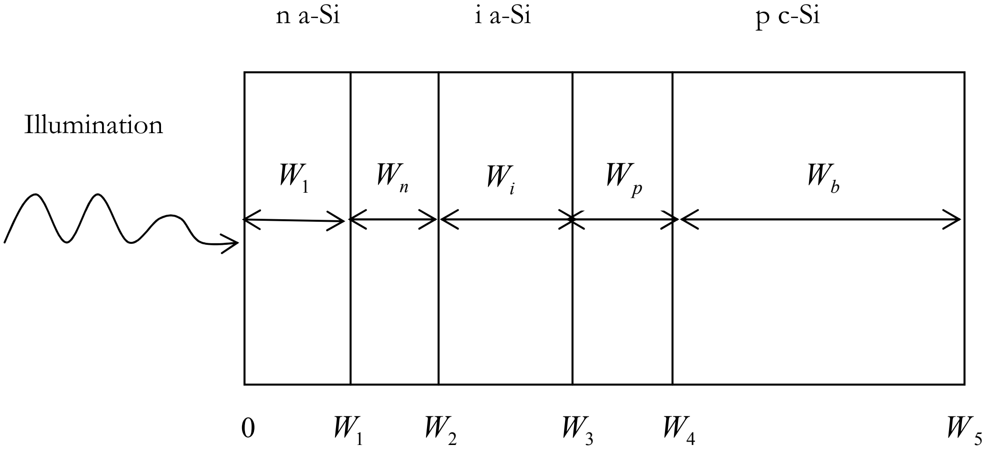

Fig 5.1 n^+ip cell structure used to develop the analytical model

To model the above shown n^+ip heterojunction solar cell, we should take into account dark and photocurrent in addition to the interface recombination current. We discussed the dark and the interface recombination current and derived the related equations in chapter 4. We will derive the equations of the photocurrent in coming sections.

5.1.1 Model for the Internal Quantum Efficiency and Photocurrent

The method for calculating the photocurrents is the same as for the homojunction solar cell using the drift-diffusion equation as well as the continuity equation. Solving these equations with respect to the boundary conditions will lead us to the equation of internal quantum efficiency for each region. Having the quantum efficiency and the intensity of light in each region, we can calculate the photocurrent generated in that region in the same way that we discussed in chapter 1 for homojunction solar cell.

Figure 5.2 shows the energy diagram of an n^+ip heterojunction cell. As we can see, we must calculate all the electron and hole currents generated by light in different regions. There are four regions (p-region, W_p, W_n and W_i) where the electron photogenerated currents will contribute to the total photocurrent of the device. The equation of electron photogenerated current in base (p-region) is the same as the one calculated for the electron photocurrent of n^+p homojunction solar cell, generated in p-side of the cell or:

$$J_{n4}(W_4) = q\frac{\alpha_c L_n e^{-[\alpha_a(W_1+W_p+W_i)+\alpha_c W_n]}}{1-\alpha_c^2 L_p^2}\left[\frac{\frac{s_n\tau_n}{L_n}Cosh(\frac{W_b}{L_n})+Sinh(\frac{W_b}{L_n})+(\alpha_c L_n-\frac{s_n\tau_n}{L_n})e^{-\alpha_c W_b}}{Cosh(\frac{W_b}{L_n})+\frac{s_n\tau_n}{L_n}Sinh(\frac{W_b}{L_n})}-\alpha_c L_n\right] \tag{5.1}$$

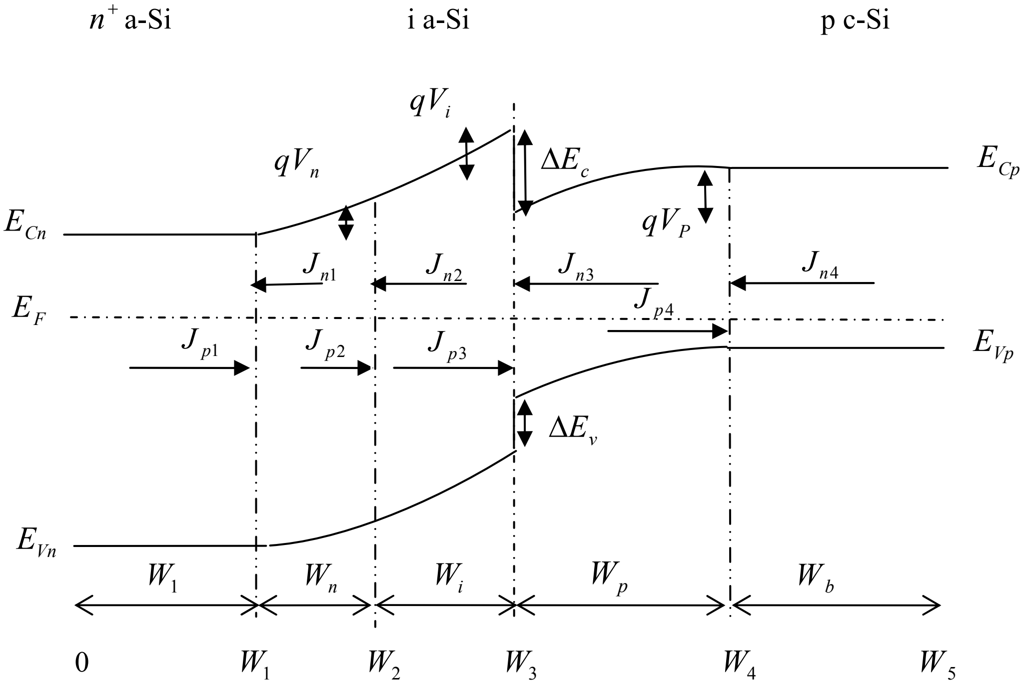

Fig 5.2 n^+ip *a-Si/c-Si* heterojunction solar cell energy band diagram

where, the subscript '*c*' stands for crystalline silicon and '*a*' for amorphous silicon. In every part of SCR, there is also hole photogenerated current. This means that the total photocurrent in each part of SCR will be the sum of the hole and electron photogenerated currents. Therefore, we should calculate both electron and hole photocurrents in each region of SCR at the same point. For instance, in region W_p, if we calculate the hole photocurrent at point W_4, then we should calculate the electron photocurrent at the same point, W_4, and sum of these two photocurrents will give us the total photogenerated current in W_p region. Taking this into account, we calculate the electron and hole photocurrents J_{n1}, J_{p2} at W_2, J_{n2}, J_{p3} at W_3 and J_{n3}, J_{p4} at W_4 . As we can see from Figure 5.2, all these regions are located in depletion region. Regarding the fact that in this region there is a strong electric field, all the photogenerated carriers will be swept away immediately by this filed. This fact is important in defining boundary conditions.

In calculating the photocurrents, we will consider drift current while writing the drift-diffusion current equation to combine with continuity equation but in final stage, when we derive the final equation for the current, we will only consider diffusion current equation. The reason for this is that when we combine drift-diffusion equation with continuity equation and derive the equation for excess carrier profile, we should only be concerned about how this profile will diffuse, which means to consider the diffusion equation. In other words, the effect of electric field on the profile of the excess carrier is taken into account when we write the drift-diffusion equation in steady state at the beginning. By determining how this profile diffuses, we obtain the final photogenerated current.

We start calculating the electron photocurrents J_{n1} at W_2, J_{n2} at W_3 and J_{n3} at W_4. We want to solve the equations in a general way for an arbitrary region of the width W inside SCR. This will help us use the calculated equation to derive all the three electron photocurrents, J_{n1}, J_{n2} and J_{n3}, just by changing the appropriate parameters.

The drift-diffusion and continuity equation in steady state for electrons are: $J_n = qn\mu_n E + qD_n \dfrac{dn}{dx}$ and $0 = \dfrac{1}{q}\dfrac{dJ_n(x)}{dx} + G_n(x) - R_n(x)$ where $G_n(x) = \alpha e^{-\alpha x}$ and

$$R_n(x) = 0 \tag{5.2}$$

Because of high electric field, it is assumed that there is no recombination in space charge region (equation 5.2). We take this assumption in both a-Si and c-Si part of the device for space charge region. Combining drift-diffusion current equation and continuity equation, we will have:

$$\frac{d^2n(x)}{dx^2} + \frac{\mu_n E(x)}{D_n}\frac{dn(x)}{dx} + \frac{\alpha e^{-\alpha x}}{D_n} = 0 \tag{5.3}$$

Using the equations $(\dfrac{dn(x)}{dx} = \dfrac{d\Delta n(x)}{dx})$ and $(D_n = V_T \mu_n)$ we will have:

$$\frac{d^2\Delta n(x)}{dx^2}+\frac{E(x)}{V_T}\frac{d\Delta n(x)}{dx}+\frac{\alpha e^{-\alpha x}}{D_n}=0 \tag{5.4}$$

The general solution of this second order differential equation is:

$$\Delta n(x)=c_1 e^{-\frac{E}{V_T}x}+c_2-\frac{e^{-\alpha x}}{D_n(\alpha-\frac{E}{V_T})} \tag{5.5}$$

The boundary conditions at W_2, W_3 and W_4 are:

$$\Delta n(W_2)=\Delta n(W_3)=0 \tag{5.6}$$

and

$$\Delta n(W_3)=\Delta n(W_4)=0 \tag{5.7}$$

respectively. For W_n region, we make an approximation and assume that

$$W_2-(W_1+\Delta x)=W_n \tag{5.8}$$

This allows us to have the boundary condition:

$$\text{Lim}\left[\Delta n(W_1+\Delta x)\right]_{\Delta x\to 0}=0 \tag{5.9}$$

From equations 5.6, 5.7 and 5.9, we can conclude that for our general model for an arbitrary region in SCR with width of *W*, the boundary conditions will be:

$$\Delta n(0)=\Delta n(W)=0 \tag{5.10}$$

therefore, using equation 5.5 we will have:

$$\Delta n(0)=c_1+c_2-\frac{1}{D_n(\alpha-\frac{E}{V_T})}=0 \tag{5.11}$$

and

$$\Delta n(W)=c_1 e^{-\frac{E}{V_T}W}+c_2-\frac{e^{-\alpha W}}{D_n(\alpha+\frac{E}{V_T})}=0 \tag{5.12}$$

Consequently:

$$c_1=\frac{1-e^{-\alpha W}}{D_n(\alpha-\frac{E}{V_T})(1-e^{-\frac{E}{V_T}W})} \tag{5.13}$$

Now by having the equation for the excess electron profile, $\Delta n(x)$, we can calculate the electron photocurrent generated in a region of width W inside SCR:

$$J_n(W) = qD_n \frac{d\Delta n(x)}{dx}\Big|_{x=W} = qD_n\left(-\frac{E}{V_T}c_1 e^{-\frac{E}{V_T}W} + \frac{\alpha e^{-\alpha W}}{D_n(\alpha - \frac{E}{V_T})} \right) \tag{5.14}$$

Thus

$$J_n(W) = q\left(\frac{-\frac{E}{V_T}e^{-\frac{E}{V_T}W}(1-e^{-\alpha W})}{(\alpha - \frac{E}{V_T})(1-e^{-\frac{E}{V_T}W})} + \frac{\alpha e^{-\alpha W}}{(\alpha - \frac{E}{V_T})} \right) \tag{5.15}$$

It should be noted that to calculate equation 5.15, in drift-diffusion equation (1.35), instead of electric field equation that is a function of distance, x, in a region inside SCR, the average value of electric field has been used. We have done this to simplify the differential equation 5.4 to be solvable. Therefore, for J_{n1} (electron photocurrent generated in W_n and calculated at W_2) we can write:

J_{n1}: $W = W_n$,

$$E = E_n = \frac{qN_d}{2\varepsilon_n}W_n \tag{5.16}$$

and $\alpha = \alpha_a$ resulting in:

$$J_{n1}(W_2) = qe^{-\alpha_a(W_1)}\left(\frac{-\frac{E_n}{V_T}e^{-\frac{E_n}{V_T}W_n}(1-e^{-\alpha_a W_n})}{(\alpha_a - \frac{E_n}{V_T})(1-e^{-\frac{E_n}{V_T}W_n})} + \frac{\alpha_a e^{-\alpha_a W_n}}{(\alpha_a - \frac{E_n}{V_T})} \right) \tag{5.17}$$

and for J_{n3} (electron photocurrent generated in W_p and calculated at W_4):

$W = W_p$,

$$E = E_p = \frac{qN_a}{2\varepsilon_p}W_p \tag{5.18}$$

and $\alpha = \alpha_c$. Therefore

$$J_{n3}(W_4) = qe^{-\alpha_a(W_1+W_n+W_i)}\left(\frac{-\frac{E_p}{V_T}e^{-\alpha_a W_n}(1-e^{-\alpha_c W_p})}{(\alpha_c-\frac{E_p}{V_T})(1-e^{-\frac{E_p}{V_T}W_p})}+\frac{\alpha_c e^{-\alpha_c W_p}}{(\alpha_c-\frac{E_p}{V_T})}\right) \tag{5.19}$$

The equation for electron photocurrent generated in intrinsic layer and calculated right before the potential barrier in conduction band (W_3^-) will be slightly different. It is because the electric filed in this region is fixed and can be calculated by: $E_i = \frac{V_i}{W_i}$ (equation 4.88), so the electron photocurrent equation for intrinsic layer will be:

$W = W_i$, $E = E_i = \frac{V_i}{W_i}$ and $\alpha = \alpha_a$ resulting in:

$$J_{n2}(W_3^-) = qe^{-\alpha_a(W_1+W_n)}\left(\frac{-\frac{E_i}{V_T}e^{-\frac{E_i}{V_T}W_i}(1-e^{-\alpha_a W_i})}{(\alpha_a-\frac{E_i}{V_T})(1-e^{-\frac{E_i}{V_T}W_i})}+\frac{\alpha_a e^{-\alpha_a W_i}}{(\alpha_a-\frac{E_i}{V_T})}\right) \tag{5.20}$$

Now that we have calculated electron photocurrents, we start with the hole photocurrents, J_{p2}, J_{p3} and J_{p4} in SCR. Regarding the previous discussion, the boundary conditions for an arbitrary region in SCR of width W will be:

$$\Delta p(0) = \Delta p(W) = 0 \tag{5.21}$$

Using the continuity equation in steady state for holes (equation 1.5) while $G_p(x) = \alpha e^{-\alpha x}$ and $R_p(x) = 0$ (because of high electric field, it is assumed that there is no recombination in space charge region) and combining it with drift-diffusion current equation of holes will give us:

$$\frac{d^2 p(x)}{dx^2} - \frac{\mu_p E(x)}{D_p}\frac{dp(x)}{dx} + \frac{\alpha e^{-\alpha x}}{D_p} = 0 \tag{5.22}$$

Using the equations ($\frac{dp(x)}{dx} = \frac{d\Delta p(x)}{dx}$) and ($D_p = V_T \mu_p$), we will have:

$$\frac{d^2 \Delta p(x)}{dx^2} - \frac{E(x)}{V_T}\frac{d\Delta p(x)}{dx} + \frac{\alpha e^{-\alpha x}}{D_p} = 0 \tag{5.23}$$

Here we will use the average value of electric field in n and p-side of SCR. The general solution of this second order differential equation is:

$$\Delta p(x) = c_1 e^{\frac{E}{V_T}x} + c_2 - \frac{e^{-\alpha x}}{D_p(\alpha + \frac{E}{V_T})} \tag{5.24}$$

Applying the boundary conditions (equation 5.21), we will have:

$$\Delta p(0) = c_1 + c_2 - \frac{1}{D_p(\alpha + \frac{E}{V_T})} = 0 \tag{5.25}$$

and

$$\Delta p(W) = c_1 e^{\frac{E}{V_T}W} + c_2 - \frac{e^{-\alpha W}}{D_p(\alpha + \frac{E}{V_T})} = 0 \tag{5.26}$$

Therefore:

$$c_1 = \frac{1 - e^{-\alpha W}}{D_p(\alpha + \frac{E}{V_T})(1 - e^{\frac{E}{V_T}W})} \tag{5.27}$$

Now we can write:

$$J_p(W) = -qD_p \frac{d\Delta p(x)}{dx}|_{x=W} = -qD_p \left(\frac{E}{V_T} c_1 e^{\frac{E}{V_T}W} + \frac{\alpha e^{-\alpha W}}{D_p(\alpha + \frac{E}{V_T})} \right) \tag{5.28}$$

and therefore:

$$J_p(W) = -q \left(\frac{\frac{E}{V_T} e^{\frac{E}{V_T}W} (1 - e^{-\alpha W})}{(\alpha + \frac{E}{V_T})(1 - e^{\frac{E}{V_T}W})} + \frac{\alpha e^{-\alpha W}}{(\alpha + \frac{E}{V_T})} \right) \tag{5.29}$$

Having the general equation for hole current as above, we can calculate the current equations for holes generated by light in different regions of SCR.

For J_{p2}, the hole photocurrent, which generated in W_n, and which we have calculated at W_2, we can write: $W = W_n$, $E = E_n = \dfrac{qN_d}{2\varepsilon_n} W_n$ and $\alpha = \alpha_a$

$$J_{p2}(W_2) = -qe^{-\alpha_a(W_1)} \left(\frac{\frac{E_n}{V_T} e^{\frac{E_n}{V_T} W_n} (1 - e^{-\alpha_a W_n})}{(\alpha_a + \frac{E_n}{V_T})(1 - e^{\frac{E_n}{V_T} W_n})} + \frac{\alpha_a e^{-\alpha_a W_n}}{(\alpha_a + \frac{E_n}{V_T})} \right) \tag{5.30}$$

Similarly for J_{p4} (hole photocurrent generated in W_p and calculated at W_4):

$W = W_p, E = E_p = \dfrac{qN_a}{2\varepsilon_p} W_p$ and $\alpha = \alpha_c$

$$J_{p4}(W_4) = -e^{-\alpha_a(W_1 + W_n + W_i)} q \left(\frac{\frac{E_p}{V_T} e^{-\alpha_c W_p} (1 - e^{-\alpha_c W_p})}{(\alpha_c + \frac{E_p}{V_T})(1 - e^{\frac{E_p}{V_T} W_p})} + \frac{\alpha_c e^{-\alpha_c W_p}}{(\alpha_c + \frac{E_p}{V_T})} \right) \tag{5.31}$$

For J_{p3} we can write: $W = W_i$, $E = E_i = \dfrac{V_i}{W_i}$ and $\alpha = \alpha_a$

$$J_{p3}(W_3) = -qe^{-\alpha_a(W_1 + W_n)} \left(\frac{\frac{E_i}{V_T} e^{\frac{E_i}{V_T} W_i} (1 - e^{-\alpha_a W_i})}{(\alpha_a + \frac{E_i}{V_T})(1 - e^{\frac{E_i}{V_T} W_i})} + \frac{\alpha_a e^{-\alpha_a W_i}}{(\alpha_a + \frac{E_i}{V_T})} \right) \tag{5.32}$$

For the hole photocurrent generated in n-side, J_{p1}, where the material is amorphous silicon, the analysis of a-Si:H/c-Si solar cells with different emitter thicknesses shows in all cases that the recombination probability of charge carriers generated in the amorphous emitter is close to unity. Therefore, the a-Si emitter does not significantly contribute to the photocurrent [32]. This means that for hole photogenerated currents we only need to calculate the currents generated in W_p, W_n and W_i; and as a conclusion, for total photocurrent in n^+ip heterojunction solar cell, when there is no applied bias, we can write:

$$J_{ph} = J_{sc} = J_{n1} + J_{n2} + J_{n3} + J_{n4} + J_{p2} + J_{p3} + J_{p4} \tag{5.33}$$

5.1.2 Model for the I-V Characteristics under Forward Bias and Illumination

In chapter four we showed that the electron dark current in $n^{+}ip$ will be suppressed by two effective velocities (equation 4.169). When we apply a forward voltage to $n^{+}ip$ solar cell, dark current flows through the device compensating the photocurrent. In worse case, we can imagine that the photogenerated electrons will reach the n-region before the dark electron current compensates them. Therefore, the dark electron current that reaches the p-side has already compensated the electron photocurrent and thus the electron photocurrent will be lowered by the same lowering factor that affects the dark electron current.

Even if the dark current is not big enough to compensate the photocurrent completely, the photocurrent is still suppressed by the same lowering factors that affect dark current. Since the photocurrent is carried by electrons over the offset barrier ΔE_C and the intrinsic layer, the collected photocurrent is suppressed by the same velocity limitations as the dark current of electrons in the opposite direction [14] or in other words:

$$J^{ht} = \frac{J_n^{hm} - J_n^{ph}}{1 + A_n} + J_p^{hm} - J_p^{ph} + \frac{J_R}{1 + A_n} \tag{5.34}$$

where $A_n = \frac{v_n}{v_{effe}} + \frac{v_n}{v_{in}}$ (equation 4.170).

However, the equation 5.34 needs to be modified due to following reasons:

The direction of electron photocurrent is against the direction of electric field in space charge region. Thus, it flows from p-side to the n-side. However, when there is an applied voltage, the electrons are forced to move in direction of the electric field in SCR, i.e. in opposite direction of photocurrent. To interpret the word "compensation" into mathematic form, we will subtract the electron photocurrent from the dark electron current to gain the total current. To subtract the electron photocurrent from its dark current, we should have both current values at the same location of the device. Recalling the equation for dark electron and hole currents across p-n junction under forward bias V_F [3]:

$$J = (q\frac{L_n}{\tau_n}n_{p0} + q\frac{L_p}{\tau_p}p_{n0})(e^{\frac{qV_F}{kT}} - 1) \tag{5.35}$$

we calculate the dark currents at the interface of SCR and p-region (W_4 for electrons) and at the interface of SCR and n-region (W_1 for holes), respectively. However, parts of the electron and hole photocurrents that we calculated in previous section, have been calculated at locations different than W_4 and W_1, i.e. W_2 and W_3. Therefore we must recalculate those photocurrents at W_4 and W_1. To do so, we will use the concept of effective velocities and the concentrations of carriers at each point [33].

We start with electron photocurrents J_{n1}, J_{n2}, J_{n3} and J_{n4}. We have calculated J_{n1} (generated at W_n) at W_2, J_{n2} (generated at W_i) at W_3^-, J_{n3} (generated at W_p) and J_{n4} (generated at p-region) at W_4. So we can subtract J_{n3} and J_{n4} from electron dark current directly (electron dark current is calculated at W_4 as well). For J_{n1}, J_{n2} we need to calculate the effective velocities of electrons at W_2, W_3^-. Using the equations that we derived in chapter four (equations 4.84 and 4.95), we can write:

$$v_{effe}(W_2) = \mu_n E(W_2) = \frac{\mu_n q N_d W_n}{\varepsilon_n} \tag{5.36}$$

$$v_{effe}(W_3^-) = \frac{\mu_n \frac{V_i}{W_i}}{1 - \exp(-\frac{qV_i}{kT})} \tag{5.37}$$

For J_{n1} we can write:

$$J_{n1}(W_2) = v_{effe}(W_2) n(W_2) \tag{5.38}$$

$$J_{n1}(W_4) = v_n n(W_2) \exp(\frac{-qV_i + \Delta E_C - qV_p}{kT}) \tag{5.39}$$

, ($v_n = \frac{L_n}{\tau_n}$). So we can write:

$$J_{n1}(W_4) = A_{n1} J_{n1}(W_2) \tag{5.40}$$

where

$$A_{n1} = \frac{v_n}{v_{effe}(W_2)} \exp(\frac{-qV_i + \Delta E_C - qV_p}{kT}) \tag{5.41}$$

This means that the equivalent value of J_{n1} (electron photocurrent at W_2) at W_4 is $J_{n1} \times A_{n1}$.

Consequently for J_{n2}:

$$J_{n2}(W_3^-) = v_{effe}(W_3^-)n(W_3^-) \tag{5.42}$$

and

$$J_{n2}(W_4) = v_n n(W_3^-)\exp(\frac{\Delta E_C - qV_p}{kT}) \tag{5.43}$$

Therefore:

$$J_{n2}(W_4) = A_{n2}J_{n2}(W_3^-) \tag{5.44}$$

where

$$A_{n2} = \frac{v_n}{v_{effe}(W_3^-)}\exp(\frac{\Delta E_C - qV_p}{kT}) \tag{5.45}$$

and consequently the value of J_{n2} (electron photocurrent at W_3^-) at W_4 is $J_{n2} \times A_{n2}$.

Similarly for holes photocurrents J_{p2}, J_{p3} and J_{p4}, generated in W_n, W_i and W_p and calculated at W_2, W_3^-, W_4 respectively, we should find the equivalent values of them at SCR and n-region interface or W_1 where the hole dark current has been calculated in dark current equation (equation 5.35). In calculating the equation for hole dark current, it is assumed that the value of hole dark current is the same at W_1 and W_4 [24]. Thus as far as we have calculated J_{p4} at W_4, we can simply subtract it from the hole dark current.

For J_{p2}, J_{p3}, we find the effective velocity of holes at W_2, W_3^-.

$$v_{effh}(W_2) = \frac{\mu_p \frac{V_i}{W_i}}{1 - \exp(-\frac{qV_i}{kT})} \tag{5.46}$$

$$v_{effh}(W_3^-) = \gamma v_{xh} \tag{5.47}$$

where $v_x = \sqrt{\frac{kT}{2\pi m_h^*}}$ (equation 3.8) and γ represents direct tunneling in thermionic emission (Figure 4.4).

Now we can write:

$$J_{p2}(W_2) = v_{effh}(W_2)p(W_2) \tag{5.48}$$

$$J_{p2}(W_1) = v_p p(W_2) \exp(\frac{-qV_n}{kT}) \tag{5.49}$$

then we can write:

$$J_{p2}(W_1) = A_{p2} J_{p2}(W_2) \tag{5.50}$$

where

$$A_{p2} = \frac{v_p}{v_{effh}(W_2)} \exp(\frac{-qV_n}{kT}) \tag{5.51}$$

Also:

$$J_{p3}(W_3^-) = v_{xh} p(W_3^-) \tag{5.52}$$

$$J_{p3}(W_1) = v_p p(W_3^-) \exp(\frac{-qV_n - qV_i}{kT}) \tag{5.53}$$

Therefore:

$$J_{p3}(W_1) = A_{p3} J_{p3}(W_3^-) \tag{5.54}$$

where

$$A_{p3} = \frac{v_p}{v_{xh}} \exp(\frac{-qV_n - qV_i}{kT}) \tag{5.55}$$

At this point, we have calculated all the photocurrents at SCR and n-bulk region interface (W_1) for holes and SCR and p-bulk region interface (W_4) for electrons. Therefore, regarding the dark current and interface recombination current of the cell in addition to the lowering factors that we calculated for electron current in n^+ip cell in chapter four, we can write:

$$J = (\frac{qv_n n_{p0}}{1+A_n} + qv_p p_{n0})(e^{\frac{qV_F}{kT}} - 1) + \frac{J_R}{1+A_n} - \left[\frac{J_{n4} + J_{n3} + J_{n2}A_{n2} + J_{n1}A_{n1}}{1+A_n} + J_{p2}A_{p2} + J_{p3}A_{p3} + J_{p4} \right] \tag{5.56}$$

where $A_n = \frac{v_n}{v_{in}} + \frac{v_n}{v_{effe}}$, $v_{effe} = \frac{\mu_n \frac{V_i}{W_i}}{1 - \exp(-\frac{qV_i}{kT})} e^{-\frac{\Delta E_C - qV_p}{kT}}$, $v_{in} = \gamma v_x e^{-\frac{\Delta E_C - qV_p}{kT}}$, $v_n = \frac{L_n}{\tau_n}$ and $v_p = \frac{L_p}{\tau_p}$.

The equation 5.56 shows how the total current of the cell is affected by the properties of the a-Si/c-Si heterojunction. The term A_n indicates the ratio of the interface and drift-diffusion effective velocities with respect to the diffusion velocity of electrons in p-region. v_{effe} indicates the effective velocity of electrons inside the i-layer within the depletion region. This factor shows that because the electrons are scattered within i-layer, their velocity is limited to this velocity and therefore, the current is suppressed. v_{in}, on the other hand, indicates that the velocity of electrons is limited while passing over the potential barrier in the conduction band. However, the tunneling (represented by γ) can occur when the barrier is sharp and the band spike is thin. In this case, the carriers flow will be less suppressed in comparison with the case that there is no tunneling. We have included the effect of tunneling in equation of carriers velocity when passing over the barrier (interface effective velocity) by adding a multiplicative (γ in equation 4.53).

5.2 Analytical Model for the $p^+ in$ *a-Si/c-Si* Heterojunction Solar Cell under Illumination

In this section, we will calculate all the photocurrent equations needed for complete model of p^+in heterojunction solar cell.

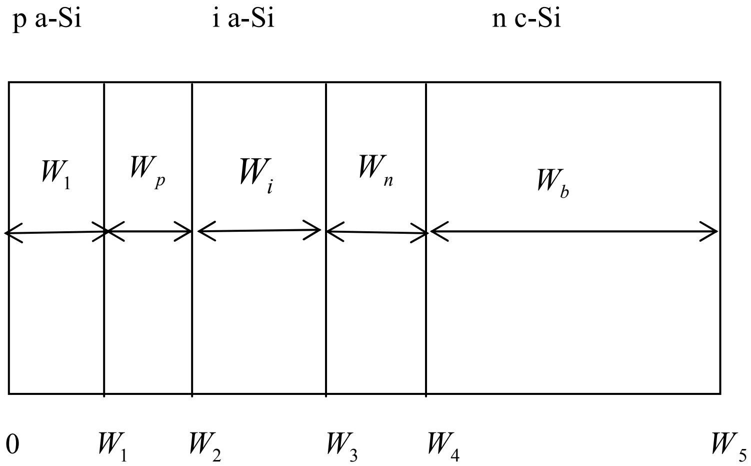

Fig 5.3 p^+in cell structure used to develop the analytical model

The method we use here is the same as we used in previous section for deriving the equations for $n^{+}ip$ heterojunction solar cell. Concerning the Figure 5.3, we define:

$W_5 - W_4 = W_b \quad W_4 - W_3 = W_n, \quad W_3 - W_2 = W_i, \quad W_2 - W_1 = W_p \quad W_1 - 0 = W_1$

5.2.1 Model for Internal Quantum Efficiency and Photocurrent

On Figure 5.4, there are four regions the hole photogenerated current within which will contribute to the photocurrent of the device. The equation for hole photogenerated current in n-region is the same as the hole photocurrent in $p^{+}n$ homojunction solar cell, generated in n-side of the cell or:

$$J_p(W_4) = q\frac{\alpha_c L_p e^{-[\alpha_a(W_1+W_p+W_i)+\alpha_c W_n]}}{1-\alpha_c^2 L_p^2}\left[\frac{\frac{s_p\tau_p}{L_p}Cosh(\frac{W_b}{L_p}) + Sinh(\frac{W_b}{L_p}) + (\alpha L_p - \frac{s_p\tau_p}{L_p})e^{-\alpha_c W_b}}{Cosh(\frac{W_b}{L_p}) + \frac{s_p\tau_p}{L_p}Sinh(\frac{W_b}{L_p})} - \alpha_c L_p\right] \tag{5.57}$$

where the subscript '*c*' stands for crystalline silicon and '*a*' for amorphous silicon.

As we did for $n^{+}ip$ cell, we want to calculate the currents formed by the holes, generated in W_p, W_n and W_i by light. The fact that all these regions are located in space charge region SCR helps us define the boundary conditions easily. In every region, there is also electron photogenerated current that means the total photocurrent in each region will be the sum of the hole and electron photogenerated current. We calculate the electron and hole photocurrents J_{p1}, J_{n2} at W_2; J_{p2}, J_{n3} at W_3^{-} and J_{n4}, J_{p3} at W_4.

We start with the hole photocurrents J_{p1}, J_{p2} and J_{p3} in SCR. Regarding the previous discussion, the boundary conditions will be:

$$\mathrm{Lim}\left[\Delta p(W_1 + \Delta x)\right]_{\Delta x \to 0} = \Delta p(W_2) = \Delta p(W_3) = \Delta p(W_4) = 0 \tag{5.58}$$

We intend to solve the equations in a general way for an arbitrary region of the width *W* inside SCR. Therefore the boundary conditions will be: $\Delta p(0) = \Delta p(W) = 0$ (equation 5.21).

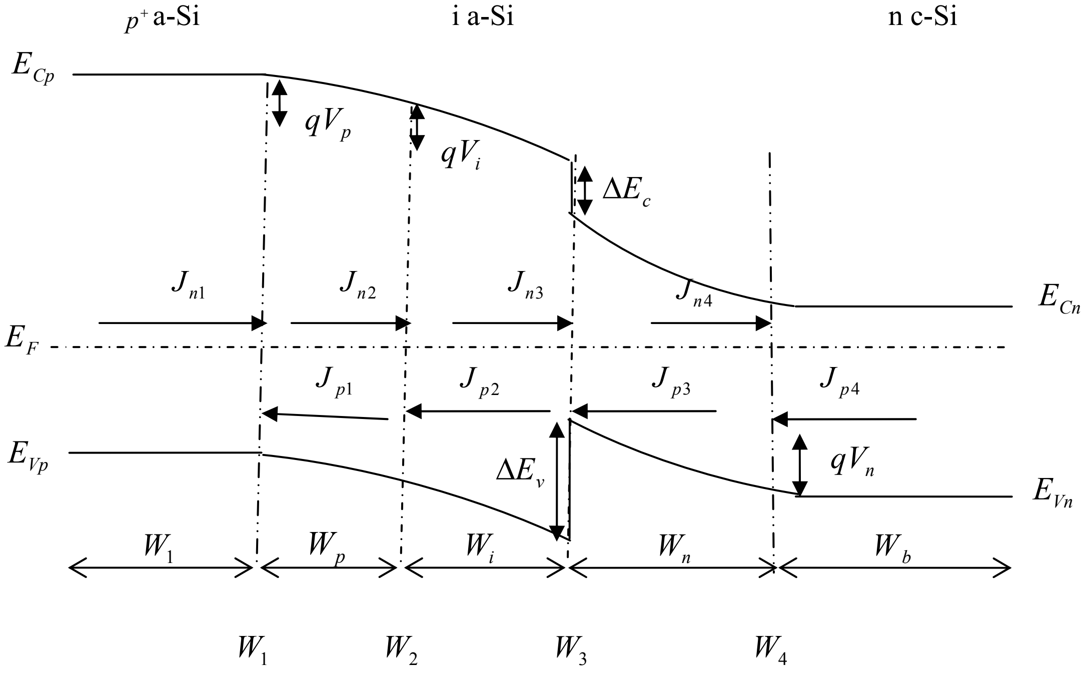

Fig 5.4 $p^{+}in$ *a-Si/c-Si* heterojunction solar cell energy band diagram

Combining the continuity equation in steady state and drift-diffusion equation for holes, assuming $G_p(x) = \alpha e^{-\alpha x}$ and $R_p(x) = 0$, we will have:

$$\frac{d^2 p(x)}{dx^2} - \frac{\mu_p E(x)}{D_p}\frac{dp(x)}{dx} + \frac{\alpha e^{-\alpha x}}{D_p} = 0 \tag{5.59}$$

Using the equations ($\frac{dp(x)}{dx} = \frac{d\Delta p(x)}{dx}$) and ($D_p = V_T \mu_p$), we will have:

$$\frac{d^2 \Delta p(x)}{dx^2} - \frac{E(x)}{V_T}\frac{d\Delta p(x)}{dx} + \frac{\alpha e^{-\alpha x}}{D_p} = 0 \tag{5.60}$$

The general solution of this second order differential equation is:

$$\Delta p(x) = c_1 e^{\frac{E}{V_T}x} + c_2 - \frac{e^{-\alpha x}}{D_p(\alpha + \frac{E}{V_T})} \tag{5.61}$$

Applying the boundary conditions (equation 5.21), we can write :

$$\Delta p(0)=c_1+c_2-\frac{1}{D_p(\alpha+\frac{E}{V_T})}=0 \tag{5.62}$$

$$\Delta p(W)=c_1e^{\frac{E}{V_T}W}+c_2-\frac{e^{-\alpha W}}{D_p(\alpha+\frac{E}{V_T})}=0 \tag{5.63}$$

Therefore:

$$c_1=\frac{1-e^{-\alpha W}}{D_p(\alpha+\frac{E}{V_T})(1-e^{\frac{E}{V_T}W})} \tag{5.64}$$

and

$$J_p(W)=-qD_p\frac{d\Delta p(x)}{dx}\Big|_{x=W}=-qD_p\left(\frac{E}{V_T}c_1e^{\frac{E}{V_T}W}+\frac{\alpha e^{-\alpha W}}{D_p(\alpha+\frac{E}{V_T})}\right) \tag{5.65}$$

Substituting equation 5.64 in 5.65:

$$J_p(W)=-q\left(\frac{\frac{E}{V_T}e^{\frac{E}{V_T}W}(1-e^{-\alpha W})}{(\alpha+\frac{E}{V_T})(1-e^{\frac{E}{V_T}W})}+\frac{\alpha e^{-\alpha W}}{(\alpha+\frac{E}{V_T})}\right) \tag{5.66}$$

Now for J_{p1} we can write:

$W=W_p$, $E=E_p=-\frac{qN_a}{2\varepsilon_p}W_p$ and $\alpha=\alpha_a$ resulting:

$$J_{p1}(W_2)=-qe^{-\alpha_a(W_1)}\left(\frac{\frac{E_p}{V_T}e^{\frac{E_p}{V_T}W_p}(1-e^{-\alpha_aW_p})}{(\alpha_a+\frac{E_p}{V_T})(1-e^{\frac{E_p}{V_T}W_p})}+\frac{\alpha_ae^{-\alpha_aW_p}}{(\alpha_a+\frac{E_p}{V_T})}\right) \tag{5.67}$$

Consequently, for J_{p3} we can also write:

$W=W_n$, $E_n=-\frac{qN_d}{2\varepsilon_n}W_n$ and $\alpha=\alpha_c$ resulting:

$$J_{p3}(W_4) = -qe^{-\alpha_a(W_1+W_p+W_i)}\left(\frac{\frac{E_n}{V_T}e^{\frac{E_n}{V_T}W_n}(1-e^{-\alpha_a W_n})}{(\alpha_c+\frac{E_n}{V_T})(1-e^{\frac{E_n}{V_T}W_n})}+\frac{\alpha_c e^{-\alpha_c W_n}}{(\alpha_c+\frac{E_n}{V_T})}\right) \tag{5.68}$$

For the equation of hole photocurrent generated in intrinsic layer we can write: $E_i = -\frac{V_i}{W_i}$, therefore the hole photocurrent equation in intrinsic layer will be:

$$J_{p2}(W_3^-) = -qe^{-\alpha_a(W_1+W_p)}\left(\frac{\frac{E_i}{V_T}e^{\frac{E_i}{V_T}W_i}(1-e^{-\alpha_a W_i})}{(\alpha_a+\frac{E_i}{V_T})(1-e^{\frac{E_i}{V_T}W_i})}+\frac{\alpha_a e^{-\alpha_a W_i}}{(\alpha_a+\frac{E_i}{V_T})}\right) \tag{5.69}$$

For electron photocurrents, generated in each region of space charge region (SCR), as we saw in the previous section, we need to calculate the currents generated in W_p, W_n and W_i in addition to the photogenerated electron current in p-region:

$$J_{n1}(W_1) = q\frac{\alpha_a L_n}{1-\alpha_a^2 L_n^2}\left[\alpha_a L_n e^{-\alpha_a W_1} - \frac{\alpha_a L_n + \frac{s_n\tau_n}{L_n}[1-e^{-\alpha_a W_1}.Cosh(\frac{W_1}{L_n})]-e^{-\alpha_a W_1}Sinh(\frac{W_1}{L_n})}{Cosh(\frac{W_1}{L_n})+\frac{s_n\tau_n}{L_n}Sinh(\frac{W_1}{L_n})}\right] \tag{5.70}$$

As discussed earlier, we will calculate J_{n2}, J_{n3} and J_{n4} at W_2, W_3^- and W_4 respectively.

Once again, we solve the equations in a general way for an arbitrary region of the width *W* inside SCR. Using the continuity equation in steady state assuming there is no recombination in space charge region and combining it with drift-diffusion current equation, we will have:

$$\frac{d^2n(x)}{dx^2}+\frac{\mu_n E(x)}{D_n}\frac{dn(x)}{dx}+\frac{\alpha e^{-\alpha x}}{D_n}=0 \tag{5.71}$$

and consequently:

$$\frac{d^2\Delta n(x)}{dx^2}+\frac{E(x)}{V_T}\frac{d\Delta n(x)}{dx}+\frac{\alpha e^{-\alpha x}}{D_n}=0 \tag{5.72}$$

The general solution to this second order differential equation is:

$$\Delta n(x) = c_1 e^{-\frac{E}{V_T}x} + c_2 - \frac{e^{-\alpha x}}{D_n(\alpha - \frac{E}{V_T})} \tag{5.73}$$

Applying the boundary conditions, $\Delta n(0) = \Delta n(W) = 0$ (equation 5.10), we will have:

$$\Delta n(0) = c_1 + c_2 - \frac{1}{D_n(\alpha - \frac{E}{V_T})} = 0 \tag{5.74}$$

$$\Delta n(W) = c_1 e^{-\frac{E}{V_T}W} + c_2 - \frac{e^{-\alpha W}}{D_n(\alpha + \frac{E}{V_T})} = 0 \qquad \text{Equ 5.75}$$

Therefore:

$$c_1 = \frac{1 - e^{-\alpha W}}{D_n(\alpha - \frac{E}{V_T})(1 - e^{-\frac{E}{V_T}W})} \tag{5.76}$$

and we can write:

$$J_n(W) = qD_n \frac{d\Delta n(x)}{dx}\Big|_{x=W} = qD_n\left(-\frac{E}{V_T}c_1 e^{-\frac{E}{V_T}W} + \frac{\alpha e^{-\alpha W}}{D_n(\alpha - \frac{E}{V_T})}\right) \tag{5.77}$$

Therefore,

$$J_n(W) = q\left(\frac{-\frac{E}{V_T}e^{-\frac{E}{V_T}W}(1 - e^{-\alpha W})}{(\alpha - \frac{E}{V_T})(1 - e^{-\frac{E}{V_T}W})} + \frac{\alpha e^{-\alpha W}}{(\alpha - \frac{E}{V_T})}\right) \tag{5.78}$$

Now we can write:

For J_{n2}: $W = W_p$, $E = E_p = -\frac{qN_a}{2\varepsilon_p}W_p$ and $\alpha = \alpha_a$

$$J_{n2}(W_2) = qe^{-\alpha_a(W_1)}\left(\frac{-\frac{E_p}{V_T}e^{-\frac{E_p}{V_T}W_p}(1 - e^{-\alpha_a W_p})}{(\alpha_a - \frac{E_p}{V_T})(1 - e^{-\frac{E_p}{V_T}W_p})} + \frac{\alpha_a e^{-\alpha_a W_p}}{(\alpha_a - \frac{E_p}{V_T})}\right) \tag{5.79}$$

For J_{n3}: $W = W_i$, $E = E_i = -\frac{V_i}{W_i}$ and $\alpha = \alpha_a$

$$J_{n3}(W_3^-) = qe^{-\alpha_a(W_1+W_p)}\left(\frac{-\frac{E_i}{V_T}e^{-\frac{E_i}{V_T}W_i}(1-e^{-\alpha_a W_i})}{(\alpha_a-\frac{E_i}{V_T})(1-e^{-\frac{E_i}{V_T}W_i})}+\frac{\alpha_a e^{-\alpha_a W_i}}{(\alpha_a-\frac{E_i}{V_T})}\right) \tag{5.80}$$

and for J_{n4}: $W = W_n$, $E = E_n = -\frac{qN_a}{2\varepsilon_p}W_p$ and $\alpha = \alpha_c$

$$J_{n4}(W_4) = qe^{-\alpha_a(W_1+W_p+W_i)}\left(\frac{-\frac{E_n}{V_T}e^{-\alpha_a W_p}(1-e^{-\alpha_c W_n})}{(\alpha_c-\frac{E_n}{V_T})(1-e^{-\frac{E_n}{V_T}W_n})}+\frac{\alpha_c e^{-\alpha_a W_p}}{(\alpha_c-\frac{E_n}{V_T})}\right) \tag{5.81}$$

Therefore, for total photocurrent when there is no applied bias, we can write:

$$J_{ph} = J_{n1} + J_{n2} + J_{n3} + J_{n4} + J_{p1} + J_{p2} + J_{p3} + J_{p4} \tag{5.82}$$

5.2.2 Model for the I-V Characteristics under Forward Bias and Illumination

In calculating the total current of the solar device under study, we should take into account the lowering factors, which we have already calculated. As we have discussed earlier, these lowering factors come from the presence of a potential barrier in valence band in case of p^+in heterojunction. As we discussed in section 5.1.2, the photocurrent is lowered with the same rate as the dark current. Therefore,

$$J^{ht} = \frac{J_p^{hm} - J_p^{ph}}{1+A_p} + J_n^{hm} - J_n^{ph} + \frac{J_R}{1+A_p} \tag{5.83}$$

where $A_p = \frac{v_p}{v_{effh}} + \frac{v_p}{v_{ip}}$ (equation 4.171).

However, this equation should be modified by including the effect of the location where we calculate a photocurrent. In other words, we should calculate the equivalent of the hole photocurrent calculated in different regions at the point that we calculate hole dark current, W_4, and the equivalent of the electron photocurrent calculated in different regions at the point that we calculate electron dark current, W_1. To do so, as we did for n^+ip, we will use the concept of effective velocities and the concentrations of carriers in each point.

We start with hole photocurrents J_{p1}, J_{p2}, J_{p3} and J_{p4}. We have calculated J_{p1} (generated in W_p) at W_2, J_{p2} (generated in W_i) at W_3^-, J_{p3} (generated in W_n) at W_4 and J_{p4} (generated in n-region) at W_4 as well. Thus J_{p4} and J_{p3} can be subtracted from dark current as they are.

For J_{p1} and J_{p2}, we need to calculate the effective velocities of holes at W_2 and W_3^- or:

$$v_{effh}(W_2) = \mu_p \mid E(W_2) \mid = \frac{\mu_p q N_a W_p}{\varepsilon_p} \tag{5.84}$$

$$v_{effh}(W_3^-) = \frac{\mu_p \dfrac{V_i}{W_i}}{1 - \exp(-\dfrac{qV_i}{kT})} \tag{5.85}$$

For J_{p1} we can write:

$$J_{p1}(W_2) = v_{effh}(W_2) p(W_2) \tag{5.86}$$

$$J_{p1}(W_4) = v_p p(W_2) \exp(\frac{-qV_i + \Delta E_V - qV_n}{kT}) \tag{5.87}$$

So we can write:

$$J_{p1}(W_4) = A_{p1} J_{p1}(W_2) \tag{5.88}$$

where:

$$A_{p1} = \frac{v_p}{v_{effh}(W_2)} \exp(\frac{-qV_i + \Delta E_V - qV_n}{kT}) \tag{5.89}$$

For J_{p2}:

$$J_{p2}(W_3^-) = v_{effh}(W_3^-) p(W_3^-) \tag{5.90}$$

$$J_{p2}(W_4) = v_p p(W_3^-) \exp(\frac{\Delta E_V - qV_n}{kT}) \tag{5.91}$$

Therefore:

$$J_{p2}(W_4) = A_{p2}J_{p2}(W_3^-) \tag{5.92}$$

where

$$A_{p2} = \frac{v_p}{v_{effh}(W_3^-)}\exp(\frac{\Delta E_V - qV_n}{kT}) \tag{5.93}$$

Consequently for electron photocurrents J_{n2}, J_{n3} and J_{n4} generated in W_p, W_i and W_n and calculated at W_2, W_3^-, W_4 respectively, we should do the same as we did for the hole photocurrents. We have calculated J_{n4} at W_4. Regarding the assumption that is taken to derive the dark current of electrons [24], we can assume that the dark current of electrons has the same values both at W_1 and W_4. So we can subtract J_{n4} from electron dark current directly. For J_{n2} and J_{n3},we find the effective velocity of electrons at W_2, W_3^-.

$$v_{effe}(W_2) = \frac{\mu_n \frac{V_i}{W_i}}{1 - \exp(-\frac{qV_i}{kT})} \tag{5.94}$$

$$v_{effe}(W_3^-) = \gamma v_{xe} \tag{5.95}$$

where $v_x = \sqrt{\frac{kT}{2\pi m_e^*}}$ (equation 3.7).

Now we can write:

$$J_{n2}(W_2) = v_{effe}(W_2)n(W_2) \tag{5.96}$$

$$J_{n2}(W_1) = v_n n(W_2)\exp(\frac{-qV_p}{kT}) \tag{5.97}$$

then we can write:

$$J_{n2}(W_1) = A_{n2}J_{n2}(W_2) \tag{5.98}$$

where

$$A_{n2} = \frac{v_n}{v_{effe}(W_2)}\exp(\frac{-qV_p}{kT}) \tag{5.99}$$

$$J_{n3}(W_3^-) = v_{xe}n(W_3^-) \tag{5.100}$$

$$J_{n3}(W_1) = v_n n(W_3^-)\exp(\frac{-qV_p - qV_i}{kT}) \tag{5.101}$$

Therefore:

$$J_{n3}(W_1) = A_{n3} J_{n3}(W_3^-) \tag{5.102}$$

where

$$A_{n3} = \frac{v_n}{v_{xe}}\exp(\frac{-qV_p - qV_i}{kT}) \tag{5.103}$$

So far, we have calculated all the photocurrents at SCR and n-bulk regions (W_4) for holes and SCR and p-bulk region (W_1) for electrons. Therefore, regarding the lowering factors that we calculated for hole current in p^+in cell in chapter four, for total current (dark+photo), including the a-Si, c-Si interface recombination current(equation 4.168 for J_R), we can write :

$$J = (\frac{qv_p p_{n0}}{1+A_p} + qv_n n_{p0})(e^{\frac{qV_F}{kT}} - 1) + \frac{J_R}{1+A_p} - \left[\frac{J_{p4} + J_{p3} + J_{p2}A_{p2} + J_{p1}A_{p1}}{1+A_p} + J_{n1} + J_{n2}A_{n2} + J_{n3}A_{n3} + J_{n4}\right] \tag{5.104}$$

where $A_p = \frac{v_p}{v_{ip}} + \frac{v_p}{v_{effh}}$, $v_{effh} = \frac{\mu_p \frac{V_i}{W_i}}{1 - \exp(-\frac{qV_i}{kT})} e^{-\frac{\Delta E_V - qV_n}{kT}}$, $v_{ip} = \gamma v_x e^{-\frac{\Delta E_V - qV_n}{kT}}$, $v_p = \frac{L_p}{\tau_p}$ and $v_n = \frac{L_n}{\tau_n}$.

Chapter 6

Simulation Results and Analysis of the Developed Models

In this chapter, we will discuss the results that we have obtained by using our analytical model for both n^+ip and p^+in a-Si/c-Si heterojunction solar cells. As we discussed in previous chapters, the main reason that causes the current of heterojunction solar cell to be suppressed is the potential barrier in conduction and/or valence band. The potential barrier in n^+ip is smaller than the one in p^+in cell. Therefore, the effect of limiting factors on n^+ip and p^+in solar cells is significantly different. In n^+ip, because of small potential barrier, the carriers flow is not scattered too much neither within depletion region nor when they pass over the barrier. However, in p^+in the band spike is big and affects the carriers transport both in depletion region (drift-diffusion effective velocity) and when they pass over the potential barrier (interface effective velocity).

We have simulated n^+ip solar cell and produced the quantum efficiency and I-V curves in section 6.1. In section 6.2, we have done the same for p^+in solar cell. Finally, we have used AMPS software [34] to simulate n^+ip and p^+in heterojunction solar cells and have compared the results with the ones that we have obtained form our model.

6.1 Simulation and Analysis of n^+ip Heterojunction Solar Cell

6.1.1 Internal Quantum Efficiency

We start our modeling with internal quantum efficiency of n^+ip heterojunction solar cell. Figure 6.1 shows the simulated internal quantum efficiency with the following device parameters:

$n^{+}-region = 31nm$, $p-region = 250\mu m, W_{i} = 3nm$ (width of the amorphous intrinsic layer)

$N_{d} = 8\times 10^{18} cm^{-3}$, $N_{a} = 10^{16} cm^{-3}$, $L_{n} = 300\mu m$.

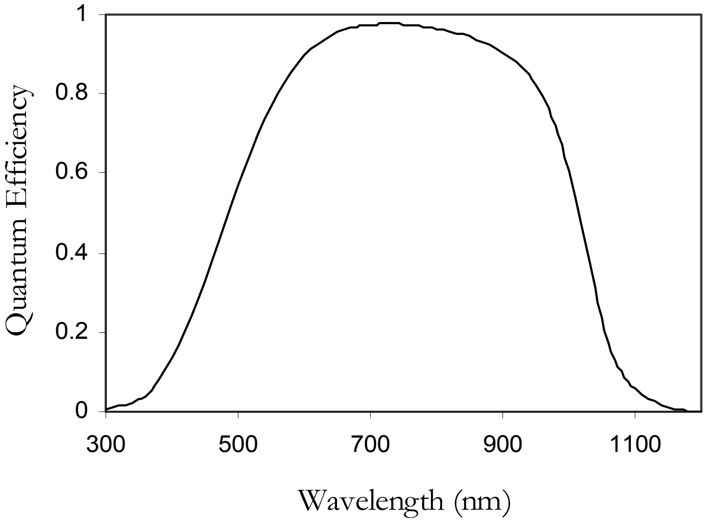

Fig 6.1 Total internal quantum efficiency of $n^{+}ip$ solar cell

For a cell with the above-mentioned parameters chosen, we calculated 1.09eV as built in voltage. However, due to the gap state density in a-Si and c-Si interface, which has not been included in built in voltage equation (equation 2.31), we modify this amount with the built in voltage that AMPS calculated: 1.04eV. The other important parameter is the discontinuity in conduction band or: ΔE_{C}. A few references give different values for ΔE_{C} in $n^{+}ip$ or $n^{+}p$ heterojunction devices. For instance, Furlan et. al. give the value of 0.13eV for ΔE_{C} [14] while Froizheim et. al. give a range between 0.1eV and 0.3eV [31]. We found out that the reasonable value for this parameter could be 0.25eV. This was calculated by finding the difference between the electron affinities of intrinsic amorphous silicon and the p-type doped crystalline silicon: $X_{c-Si} - X_{a-Si} \approx 4.05 - 3.80 \approx 0.25eV$

Due to high recombination rate in amorphous n-region [32], the p-region and the SCR (including the intrinsic layer) make the main contribution to the final quantum efficiency. Figure 6.2 shows these quantum efficiencies separately:

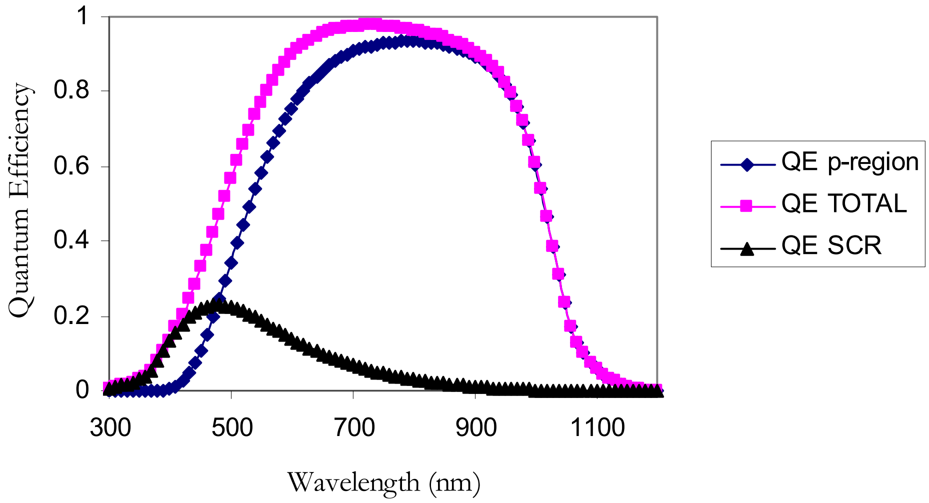

Fig 6.2 Internal quantum efficiency of SCR, p-region and the whole $n^{+}ip$ solar cell

Comparing the curves in Figure 6.2, we can see that the p-region quantum efficiency has the major role in final spectral response.

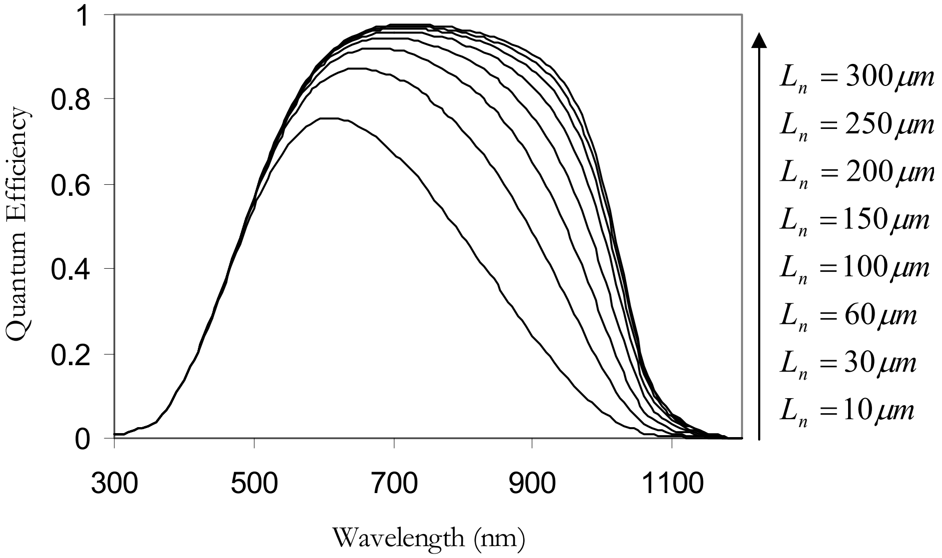

Fig 6.3 Effect of diffusion length in bulk on $n^{+}ip$ solar cell quantum efficiency

It is also obvious (from Figure 6.2) that the generation of electron-hole pairs, for absorbed photons with wavelength between 0.53 and 1.01μm takes place in p-bulk region with probability of 50% and higher with respect to the number of absorbed photons while the space charge region converts (in the best case) only 10% toward 20% of absorbed photons with the wavelength range of 0.39 to 0.64μm into electron-hole pairs.

Since the diffusion length of minority carriers (electrons) in base (p-region) has enormous effect on the internal quantum efficiency of this region, it will not be surprising if this parameter has significant role in total quantum efficiency of the device. Figure 6.3, for instance, shows that by reducing the diffusion length of electrons in p-bulk region from 300μm to 10μm, the rate of electron-hole pairs generation reduces from 88% to 20% for the absorbed photons with wavelengths of 0.92μm. Figure 6.3 also shows the internal quantum efficiency of the cell for different levels of bulk quality. Heterojunction fabrication process can use temperature-degradable, defective Si, whose L_n is low. The low-T nature of the process allows bulk passivation techniques such as hydrogenation prior to cell fabrication. Figure 6.3 shows that even small improvement in bulk quality (longer diffusion length) can lead to significant gains in internal quantum efficiency of solar cell.

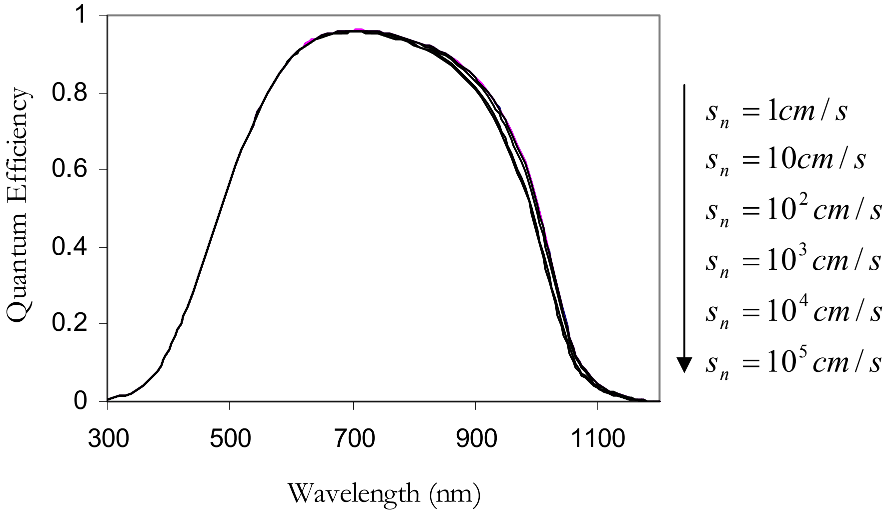

Fig 6.4 n^+ip solar cell internal quantum efficiency of a thicker, moderate quality base region showing no sensitivity to surface passivation (150μm L_n with a 250 μm thick wafer)

Another parameter that influences the base internal quantum efficiency is the rear surface recombination velocity (s_n), which can be reduced by an appropriate surface passivation scheme.

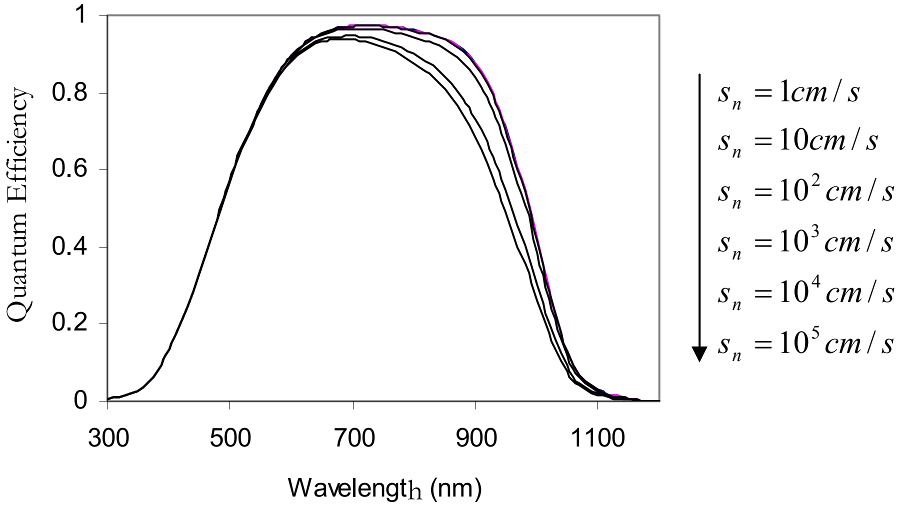

Fig 6.5 n^+ip solar cell internal quantum efficiency of a thinner, moderate quality base region showing increased sensitivity to surface passivation (150μm L_n with a 100 μm thick wafer)

However, the rear surface passivation can be beneficial only if L_n is comparable to the wafer thickness. This is illustrated in Figures 6.4 and 6.5. Figure 6.4 shows that for thicker wafers with moderate L_n (i.e., L_n < wafer thickness), the passivation has only a negligible effect on internal quantum efficiency. However, if the wafer is thinned down to values comparable to L_n, (i.e. a 150μm L_n with a 100 μm thick wafer) then surface passivation can be very beneficial (Figure 6.5). Since low-T surface passivation options are available (pip^+ heterojunction, or PECVD nitride) in the heterojunction process, it would be advantageous to use thinner wafers if the bulk L_n is not very high.

As we have seen before, the intrinsic layer inside SCR and the SCR itself play role in final quantum efficiency of device. A part of SCR that lies in bulk p-region is wide enough to have high amount of photogeneration. This is because n-region is heavily doped and therefore the space charge region will extend mostly in lower doped region, i.e. p-region. Figure 6.6 shows the variation of SCR quantum efficiency with respect to the change in width of the intrinsic layer.

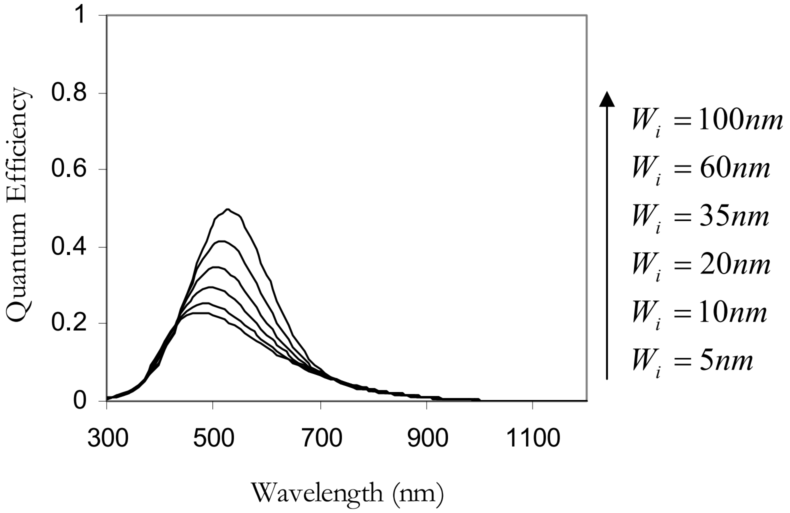

Fig 6.6 $n^{+}ip$ solar cell quantum efficiency of SCR for different intrinsic layer widths

As we can see, it is obvious that by having wider intrinsic layer, the contribution of SCR to total quantum efficiency will increase, but this does not mean that it will have the final quantum efficiency of cell increased. The reason is that by widening the intrinsic layer, the amount of photons that reach the bulk p-region decreases and therefore the quantum efficiency of p-region decreases as well. This results in the change in total quantum efficiency of cell to be negligible. Figure 6.7 shows this fact.

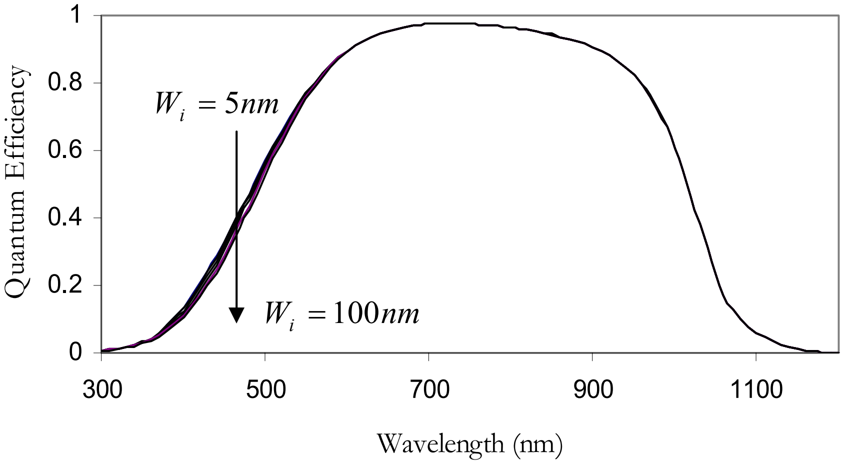

Fig 6.7 Total quantum efficiency of the n^+ip solar cell for different intrinsic layer widths

6.1.2 I-V Characteristics under Illumination

Although the increase in the width of the intrinsic layer does not affect the total quantum efficiency of solar cell but it somehow affects the I-V characteristics of the device. Back to chapter four, equation 4.95, the reason is that the intrinsic layer limits the velocity of the carriers and hence lowers the cell current. The wider the intrinsic layer, or the smaller voltage drop on intrinsic layer (V_i) that can be obtained by increasing the forward bias, the lower the effective velocity of the carriers, which means the lower current. However, due to the small discontinuity of conduction band in n^+ip a-Si/c-Si heterojunction, (0.25 eV) this lowering effect is almost annihilated for intrinsic layers thinner than 100nm. It is worth to mention that the direct tunneling that is included in our modeling is taken into account when the intrinsic layer is very thin (less than 5nm). Figure 6.8 shows the I-V curves for n^+ip heterojunction solar cell for intrinsic layers up to 100nm wide. As we can see, the current is not suppressed significantly.

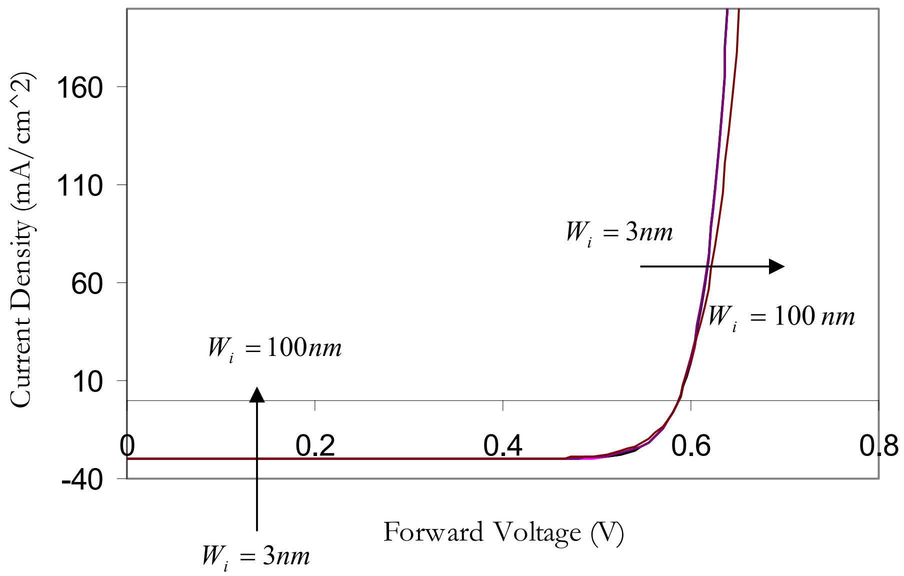

Fig 6.8 I-V graph of $n^{+}ip$ solar cell for different intrinsic layer widths

Table 6.1 shows how open circuit voltage (V_{oc}), short circuit current (J_{sc}) and the fill factor (FF) change by changing the intrinsic layer width. What we observe is that for small range of intrinsic layer widths (<100nm), the V_{oc} and J_{sc} almost remain unchanged.

$W_i(nm)$	$V_{oc}(mV)$	$J_{sc}(mA/cm^2)$	FF
3	587.0	30.15	82.49%
5	587.0	30.15	82.49%
15	587.0	30.10	82.50%
30	587.0	30.01	82.48%
50	587.0	29.92	82.44%
100	586.5	29.77	80.82%

Table 6.1 J_{sc}, V_{oc} and FF of $n^{+}ip$ solar cell for different W_i

However if we increase the intrinsic layer width by a few hundred nano meters, the effect of lowering factors on I-V characteristics of the cell will increase enormously (Figure 6.9).

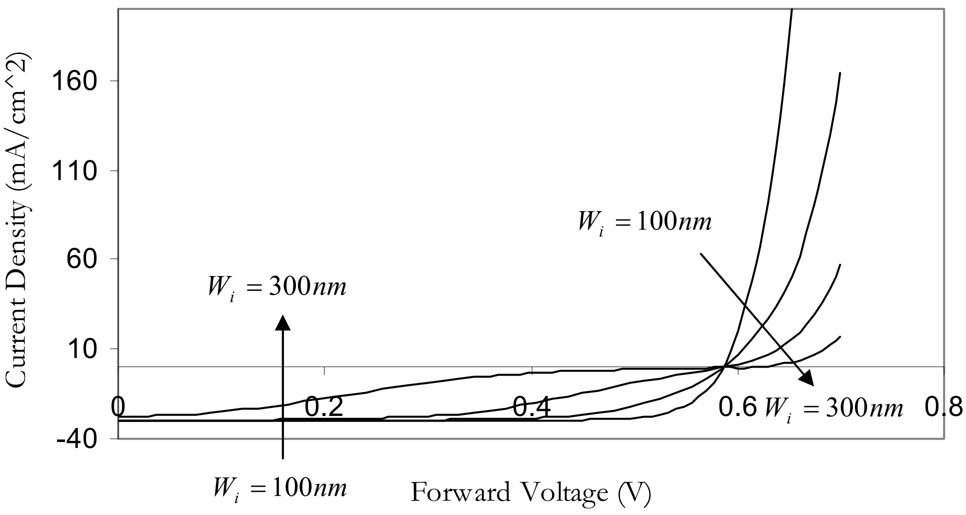

Fig 6.9 I-V graph of n^+ip solar cell with wider intrinsic layers

In this case, V_{oc} will increase by increasing W_i while J_{sc} will decrease slightly (Table 6.2). We see that although for wide intrinsic layer ($W_i = 300nm$), V_{oc} and J_{sc} are high, the FF is significantly low. The reason is that for wide intrinsic layers the maximum achievable power ($V_m I_m$) is very low. Therefore the fill factor ($FF = \frac{V_m J_m}{V_{oc} J_{sc}}$) will be low as well.

$W_i(nm)$	$V_{oc}(mV)$	$J_{sc}(mA/cm^2)$	FF
100	586.5	29.77	80.82%
150	587.0	29.66	68.05%
200	588.0	29.56	49.92%
300	619.0	28.15	20.11%

Table 6.2 J_{sc}, V_{oc} and FF of n^+ip solar cell for wider W_i

Changing the doping level of the base can affect the way the current is lowered. Recalling the equation 4.170, we see that the dropped voltage on the p-side of SCR (V_p) can change the lowering factors exponentially. Equation 2.39 ($V_p = \frac{qN_a}{2\varepsilon_1} W_p^2$) shows that V_p is strongly dependent on N_a. Therefore, if we increase N_a, V_p will be increased as well. This means that a small change on doping level of p-region will affect the I-V characteristics significantly (Figure 6.10). In fact increasing V_p causes the effective velocities of interface and drift-diffusion to become very small and consequently, the current is suppressed drastically. This is not the case for N_d because in equation 4.170, there is no V_n which might be affected by changing N_d.

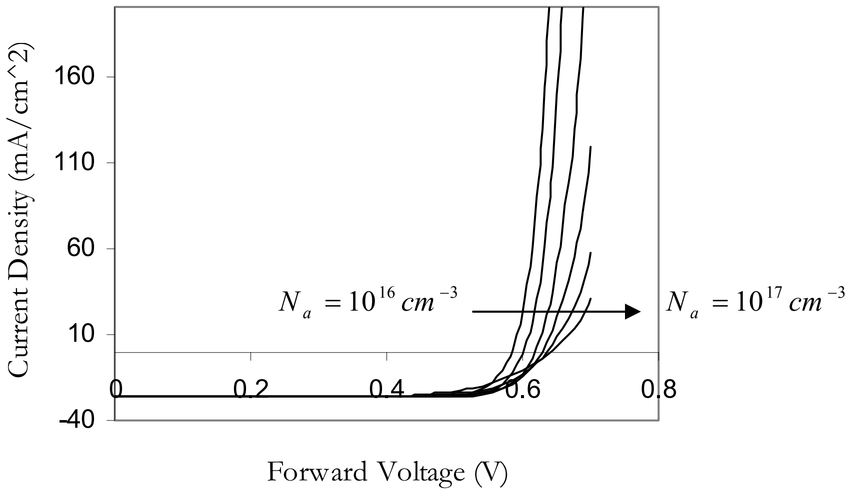

Fig 6.10 I-V graph of n^+ip solar cell for different doping levels (N_a)

Due to the fact that by changing the built in voltage there will be changes in SCR widths (equation 2.42 and 2.43) and consequently in V_p (equation 2.39), we can conclude that V_{bi} can have important role in lowering the current. In other words, if we assume that V_{bi} changes without any change in ΔE_C or other parameters in equation 2.31 such as doping levels and etc., this change will be directly transferred to the dropped voltages on intrinsic layer and p-side of SCR and therefore the lowering factors will be affected. This can happen because of existence of gap defect densities in a-Si and c-Si interface. Figure 6.11 shows how the I-V graph is affected by only changing V_{bi} rather than ΔE_C or doping levels. Decreasing the built in voltage causes W_p to decrease (equation 2.42) and this results in V_p to decrease as well (equation 2.39). The reduction of V_p, as discussed earlier, results in more suppression of the current (equation 4.170).

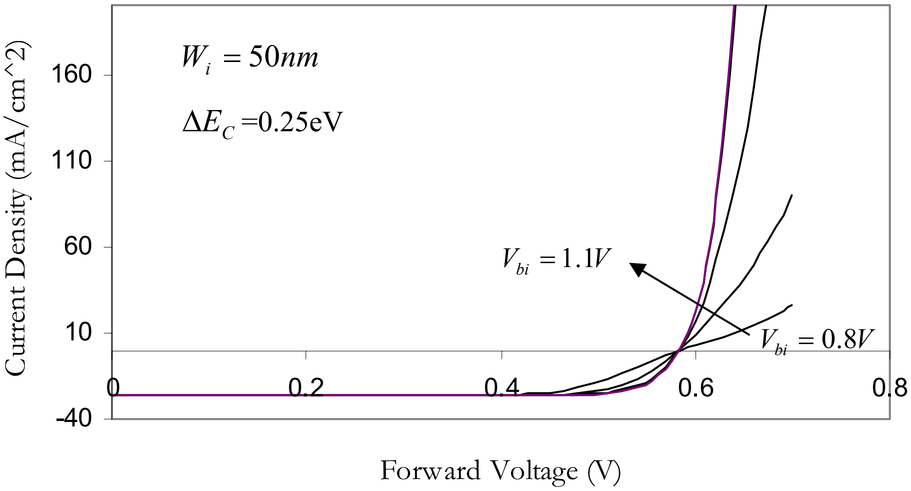

Fig 6.11 I-V graph of n^+ip solar cell for different built in voltages

6.2 Simulation and Analysis of p^+in Heterojunction Solar Cell

6.2.1 Internal Quantum Efficiency

We have simulated a p^+in heterojunction solar cell with the following device parameters:

$p^+ - region = 31nm$, $n - region = 250\mu m$, $W_i = 3nm$ (width of the amorphous intrinsic layer)

$N_a = 3\times10^{18} cm^{-3}$, $N_d = 10^{16} cm^{-3}, L_p = 300\mu m$.

Figure 6.12 shows how different regions of $p^{+}in$ solar cell contribute to the complete quantum efficiency of cell. We see that for the wavelengths range of (520<λ<1010nm), the quantum efficiency of n-region is more than 0.5, while for p-region, the wavelength range in which the quantum efficiency is more than 0.5 is λ<510nm. The SCR contribution to total quantum efficiency of cell is small and only for the wavelength range of (430<λ<520nm), the quantum efficiency of this region is more than 0.2.

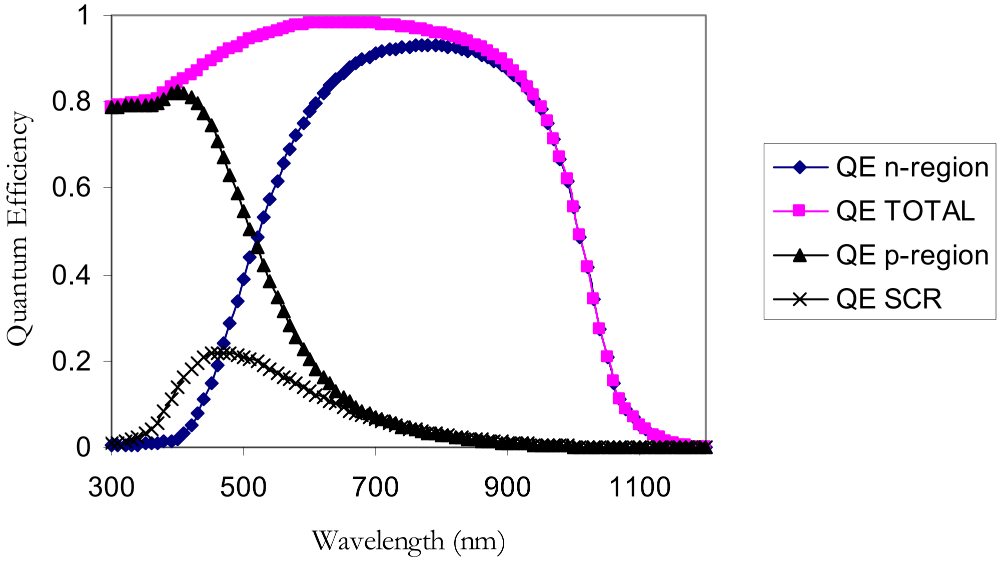

Fig 6.12 Internal quantum efficiency of $p^{+}in$ solar cell for different regions

Many references [14,35,36] have given a value of almost 0.45eV for the discontinuity in valence band, ΔE_V in $p^{+}in$ heterojunction. We have chosen 0.44eV for ΔE_V, which matches what we extracted with AMPS. By this set of data, we calculated the value of 1.24V for built in voltage. However, for the reason that we discussed about in section 6.1.1, we modified this value with the result that AMPS gave us: $V_{bi} = 0.92eV$.

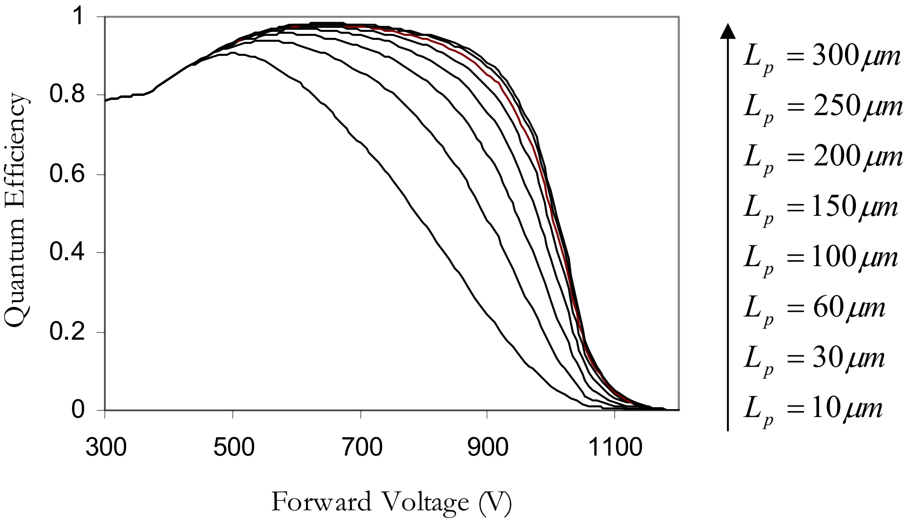

Fig 6.13 Effect of diffusion length in bulk on p^+in solar cell quantum efficiency

As we saw in n^+ip case, the sensitivity of total internal quantum efficiency of cell with respect to the diffusion length of minority carriers in bulk base region is significant. From Figure 6.13, we see that having a good quality bulk region helps us gain very good quantum efficiency (or photocurrent) while the bulk with poor quality, means that minority carriers cannot diffuse into the space charge region when they are far from the SCR and bulk-region interface, which results in lower percentage of photons transformation into electron-hole pairs.

The quality of back surface and the front surface can influence the total quantum efficiency significantly. As we discussed earlier, this is the case when the diffusion length of the minority carriers in n and p-region are long enough in comparison to the width of these regions respectively. Figures 6.14 and 6.15 show how the changes in surface qualities, which we show by surface recombination velocities, affect the total internal quantum efficiency of cell. It is seen that for long diffusion lengths in bulk, the increase in surface recombination velocity (poor quality of the surface) decreases the total quantum efficiency of the solar cell.

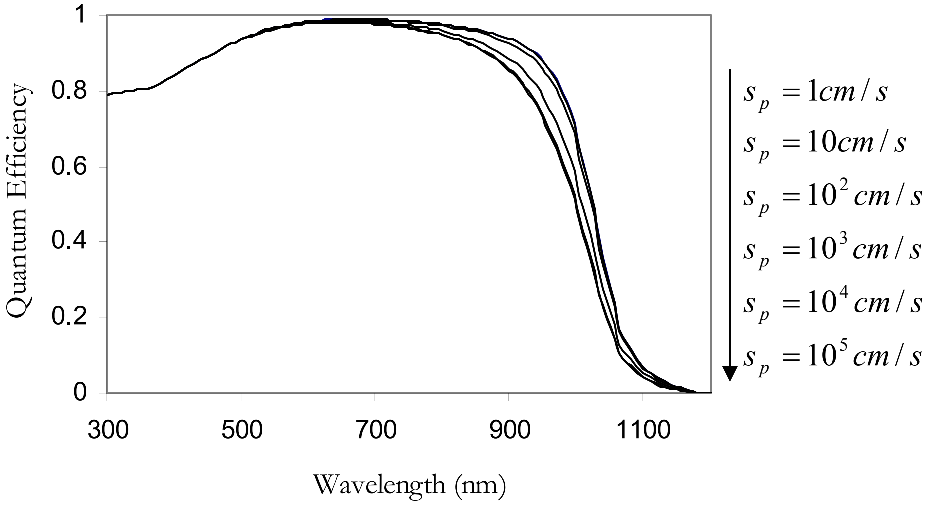

Fig 6.14 p^+in solar cell quantum efficiency change due to change in back surface recombination velocity (s_p)

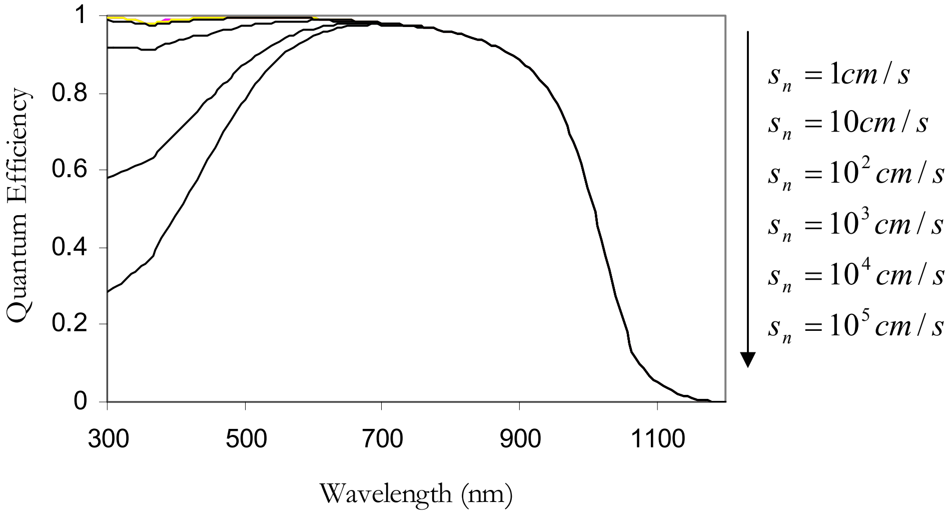

Fig 6.15 p^+in solar cell quantum efficiency change due to change in front surface recombination velocity (s_n)

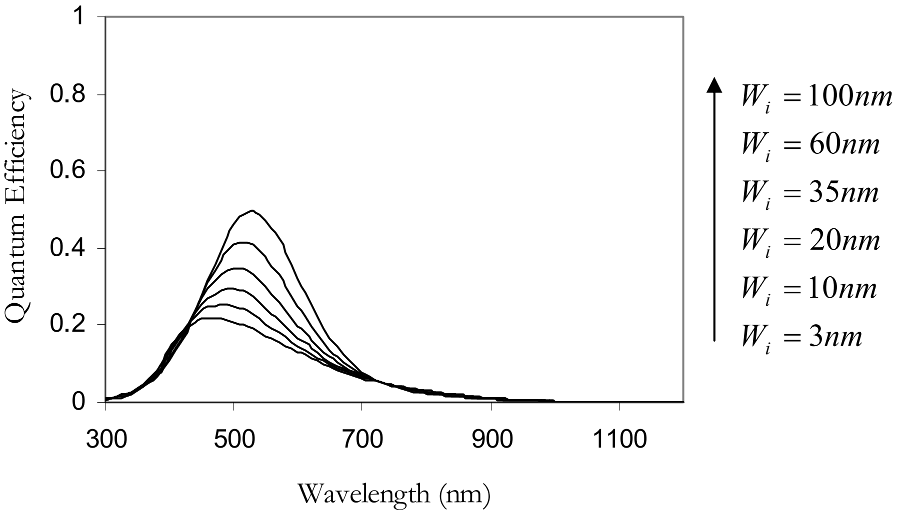

Fig 6.16 p^+in solar cell SCR quantum efficiency for different intrinsic layer widths

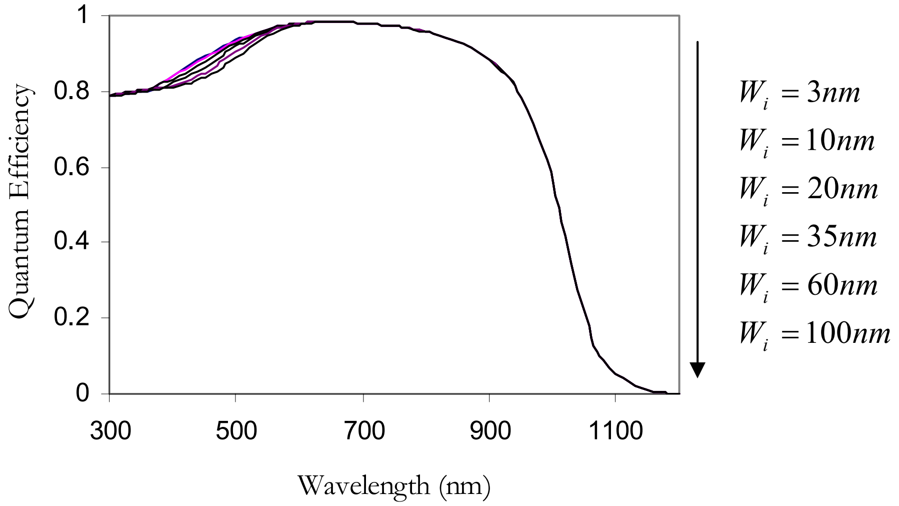

Fig 6.17 Total QE of the p^+in solar cell for different intrinsic layer widths

As we saw in n^+ip solar cell, the SCR width affects the total quantum efficiency of cell. This contribution changes by changing the width of the intrinsic layer, but, as we discussed earlier for n^+ip cell, it will not affect the total quantum efficiency so much. (Figures 6.16, 6.17)

6.2.2 I-V Characteristics under Illumination

Due to a big discontinuity in valence band in $p^{+}in$ heterojunction, we expect the lowering factors to affect the I-V curve of the cell significantly.

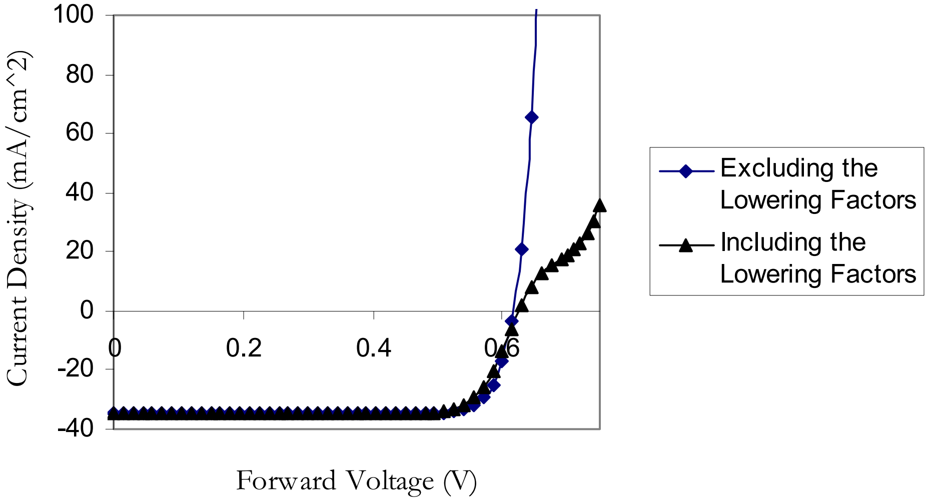

Fig 6.18 I-V graph of $p^{+}in$ solar cell

Recalling the equation 4.172, having a large ΔE_V will cause the interface and drift-diffusion effective velocities of holes to be lowered significantly. This makes the total lowering factor (A_p) become big enough to limit the current (dark and photo) of the cell. Figure 6.18 shows that even for ultra thin intrinsic layer $(W_i = 3nm)$, the current is lowered very significantly in comparison to the current of a cell without discontinuity in valence band (no limiting factors). By increasing the width of the intrinsic layer, the I-V curve will be affected enormously and the cell current will be reduced significantly. Figure 6.19 shows how the I-V curve changes by increasing the intrinsic layer.

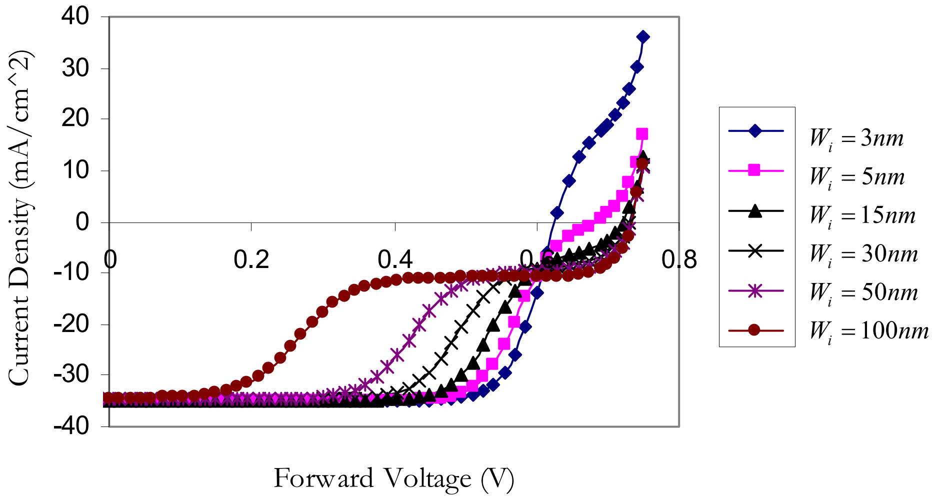

Fig 6.19 I-V graph of p^+in solar cell for different intrinsic layer widths

Table 6.3 shows the values of open circuit voltage (V_{oc}), short circuit current (J_{sc}) and the fill factor (FF) dependence on the intrinsic layer width. We can see that as the width of the intrinsic layer increases, the open circuit voltage increases as well while the short circuit current almost remains unchanged. Although with wide intrinsic layer (100nm), J_{sc} and V_{oc} appear to be very high but the performance of the device will be bad because of low fill factor. The reason is that for wide intrinsic layers the maximum achievable power ($V_m I_m$) is very low. Therefore the fill factor ($FF = \frac{V_m J_m}{V_{oc} J_{sc}}$) will be low as well.

$W_i (nm)$	$V_{oc} (mV)$	$J_{sc} (mA/cm^2)$	FF
3	626.0	34.87	78.98%
5	685.5	34.87	68.93%
15	722.0	34.82	61.02%
30	730.5	34.73	53.79%
50	734.0	34.63	45.06%
100	738.0	34.45	26.82%

Table 6.3 J_{sc}, V_{oc} and FF of p^+in solar cell for different W_i

Changing the doping level of the n-region (N_d) affects the I-V curve. From the equation 2.55, this change will cause the dropped voltage on n-region (V_n) to change significantly. Therefore, the effect of effective velocities will increase in I-V curve (equation 4.172). Figure 6.20 shows that by increasing the doping level of n-region, the current suppression increases.

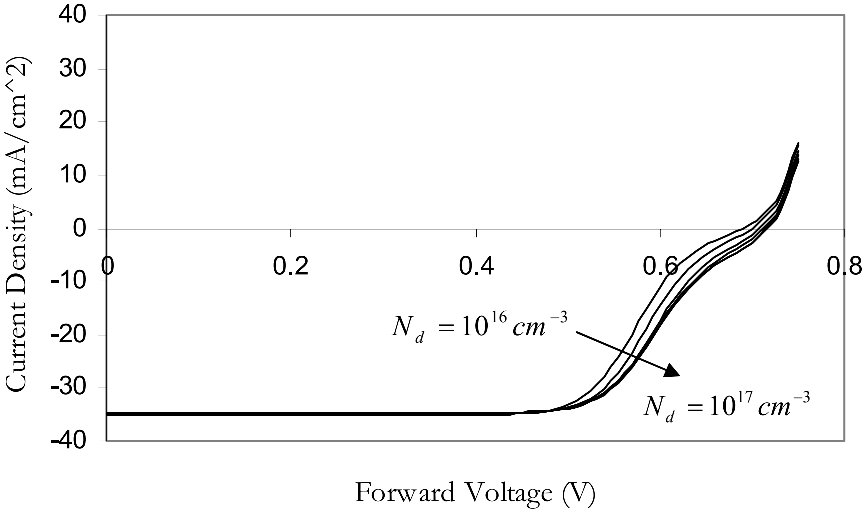

Fig 6.20 I-V graph of p^+in solar cell for different doping levels (N_d)

6.3 Simulation of *a-Si/c-Si* Heterojunction Solar Cells Using AMPS Numerical Simulator and Comparison with Our Analytical Results

AMPS [34] that stands for "Analysis of Microelectronic and Photonic **S**tructures", has been designed by Professor Fonash at the Pennsylvania state university. It was engineered to be a very general and versatile computer simulation tool for the analysis of device physics and for device design. It is a tool to simulate the optoelectronic devices in a very general way.

In this section, we have attempted to use AMPS software to simulate the n^+ip and p^+in heterojunction solar cells and compare the results with our model simulation results.

6.3.1 AMPS Simulation of $n^+ ip$ Heterojunction Solar Cells

We have used AMPS by setting a cell with the same parameters that we used in our modeling in section 6.1.1. Figure 6.21 shows the complete internal quantum efficiency of an n^+ip cell produced by AMPS in comparison with our modeling result. We observe that the two curves match each other. We have also used AMPS to simulate the solar cell I-V curve for different intrinsic layer widths.

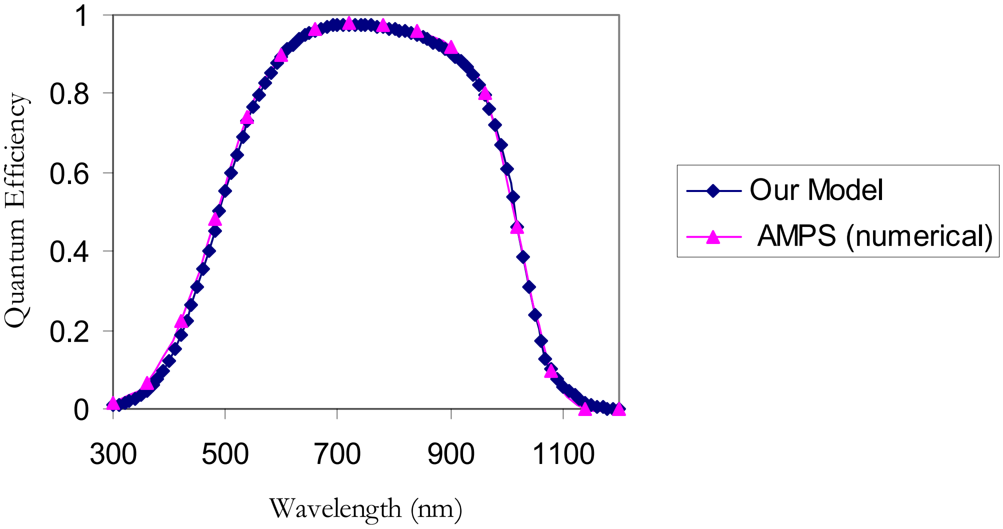

Fig 6.21 Total internal quantum efficiency of n^+ip solar cell (AMPS & our model)

What we see from the result (Figure 6.22), is that in n^+ip heterojunction solar cell, the current is not affected in intrinsic layers thinner than 100 nm. This is the same result that we saw in our modeling simulation result (Figure 6.8 and 6.9). Figure 6.23 shows the comparison between the I-V curves of our modeling result with AMPS result for n^+ip soar cell with intrinsic layer width of 50 nm. Although we observe that there is a difference between the open circuit voltages of two results, the short circuit currents and the fill factors of both results match reasonably. We see that the difference comes from the open circuit voltage.

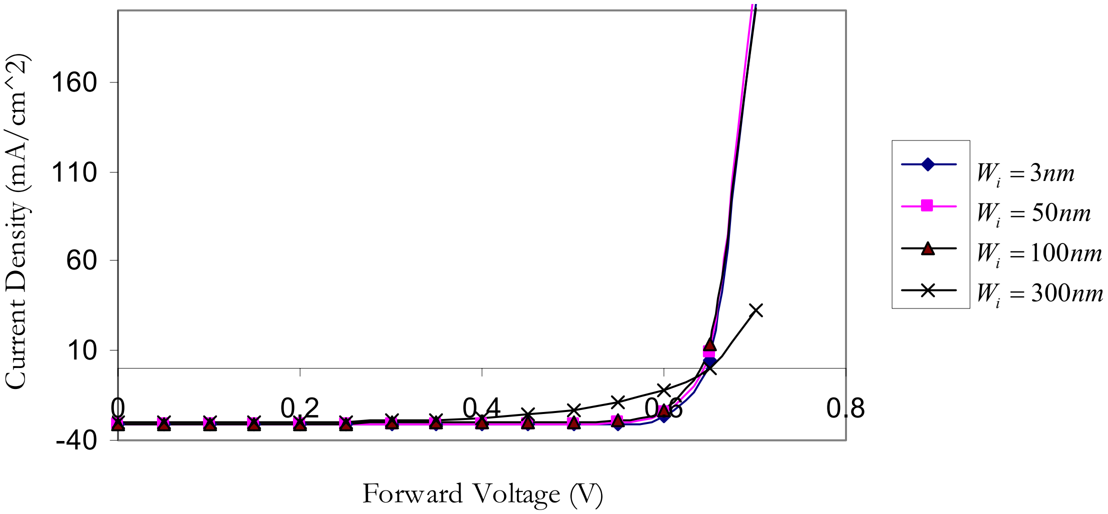

Fig 6.22 I-V graph of n^+ip solar cell for different intrinsic layer widths (AMPS)

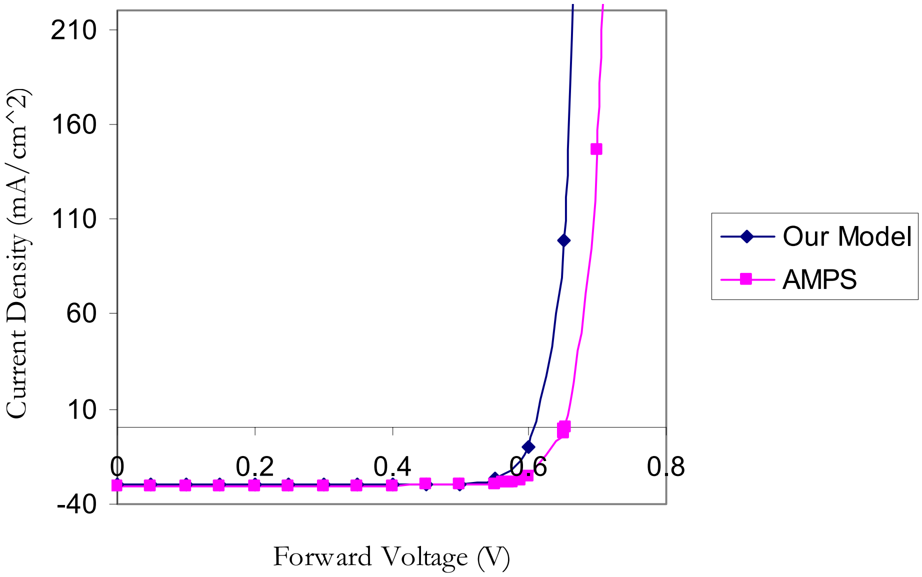

Fig 6.23 Comparison between AMPS and our model I-V results of n^+ip solar cell for $W_i = 50nm$

The difference between our model and AMPS results can be explained as follows: The AMPS program uses "density of defects" to simulate the device instead of carrier lifetime or diffusion length. The defects densities used in AMPS for crystalline side is such that implies good quality of substrate. In our modeling, however, the quality of substrate is modeled by the diffusion length that we have chosen to be 300μm. To model the substrate with high quality, the diffusion length can be chosen much higher than what we have used. Therefore, if we choose the value of electron diffusion length in p-region such that: L_n >>wafer thickness ($L_n = 1000\mu m$), the results will match reasonably. Figure 6.24 shows this fact.

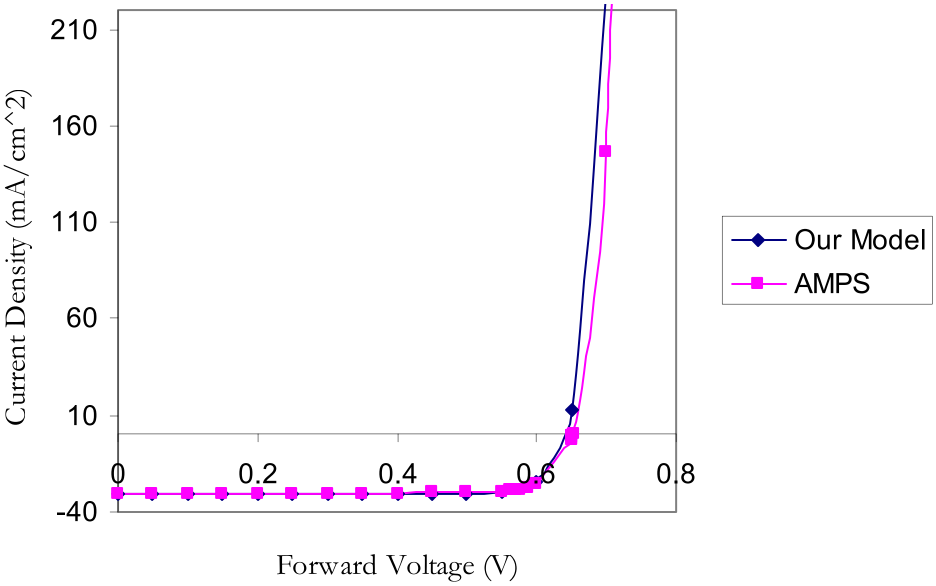

Fig 6.24 Comparison between AMPS and our model I-V results of $n^{+}ip$ solar cell for $W_i = 50nm$ with higher diffusion length in bulk ($L_n = 1000\mu m$)

As we saw from Figure 6.10, the increase of bulk doping level will reduce the solar cell current under forward bias and increase the open circuit voltage. What we see from the AMPS result matches with what we have found from our modeling result (Figure 6.25).

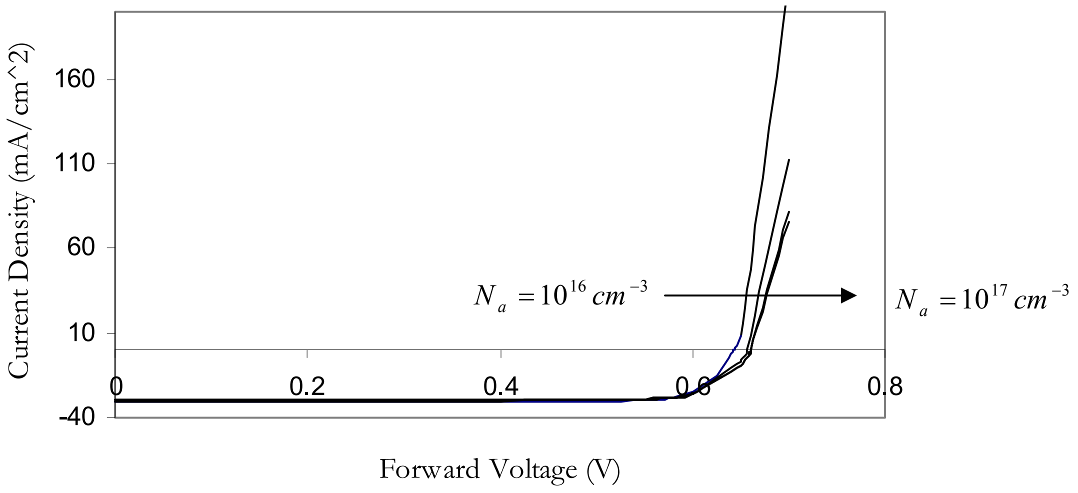

Fig 6.25 AMPS result of I-V graph of n^+ip solar cell for different doping levels (N_a) (AMPS)

6.3.2 AMPS Simulation of p^+in Heterojunction Solar Cells

We have used the same parameters that we used in our modeling in section 6.2.1 to run AMPS for simulating the p^+in heterojunction solar cell. Figure 6.26 shows the total quantum efficiency of such a cell calculated by AMPS in comparison with our modeling result.

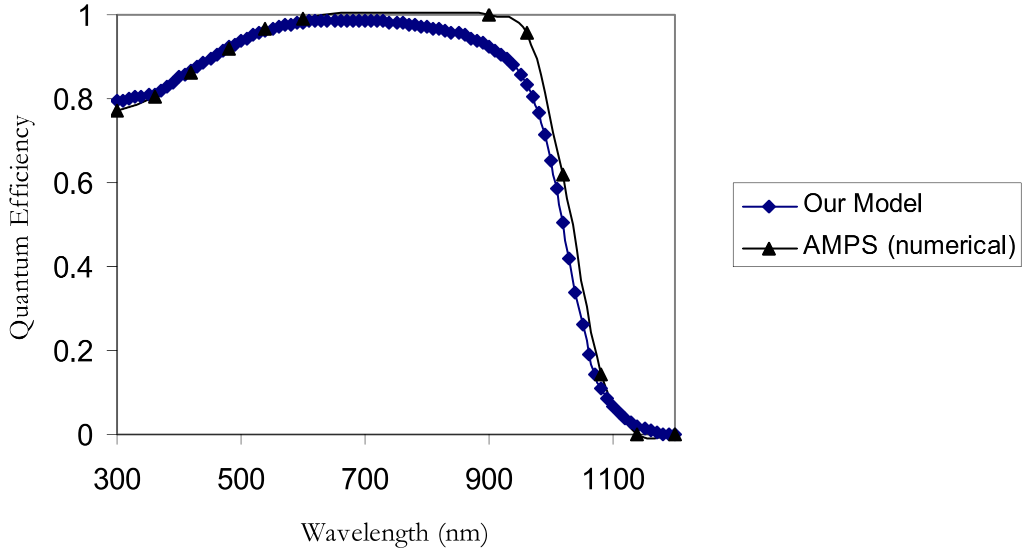

Fig 6.26 Total internal quantum efficiency of p^+in solar cell (AMPS & our model)

As we see, the main difference is for the long wavelength photons (>780nm). As we discussed in previous section (6.3.1), by setting an appropriate diffusion length in bulk, we can obtain better matched curves. Figure 6.27 shows the results with diffusion length of 500μm used in our model

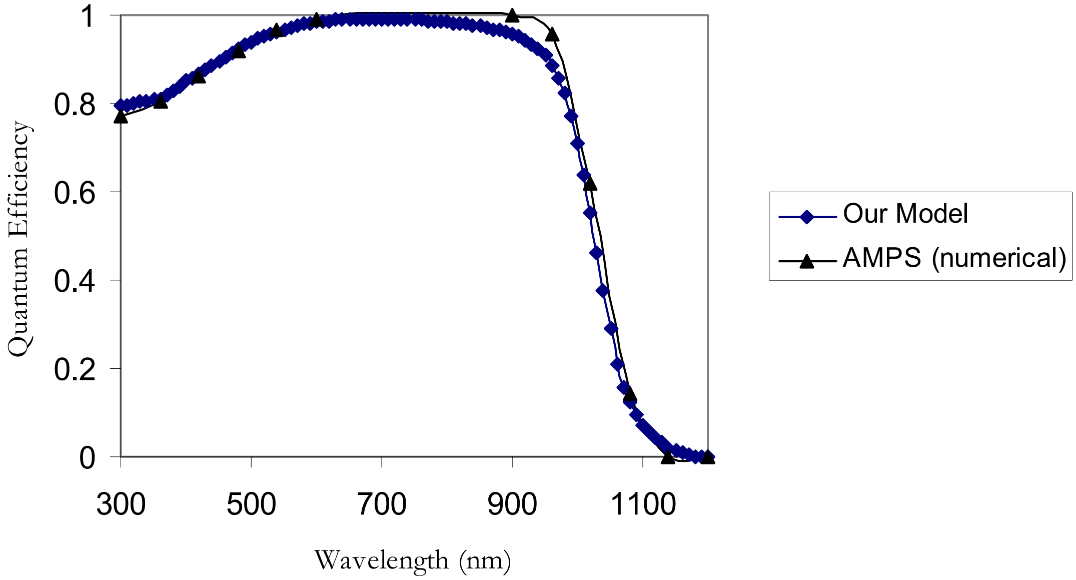

Fig 6.27 Total internal quantum efficiency of $p^{+}in$ solar cell (AMPS & our model with higher diffusion length in bulk ($L_p = 500\mu m$))

As we saw from our modeling result (Figure 6.19), the lowering factors effect on I-V curve of $p^{+}in$ heterojunction is significant and as discussed earlier, this is because of large discontinuity in valence band which limits the effective velocity of the carriers and makes the limited velocities be dominant in SCR and n-region interface. We see the same result using the AMPS program, showing that ΔE_V has main role in suppressing the current. Figure 6.28 shows that even for very thin intrinsic layer (5nm) the current is suppressed strongly. By increasing the width of the intrinsic layer, as our model explains, the drift-diffusion velocity of the carriers will be limited, resulting in lower current.

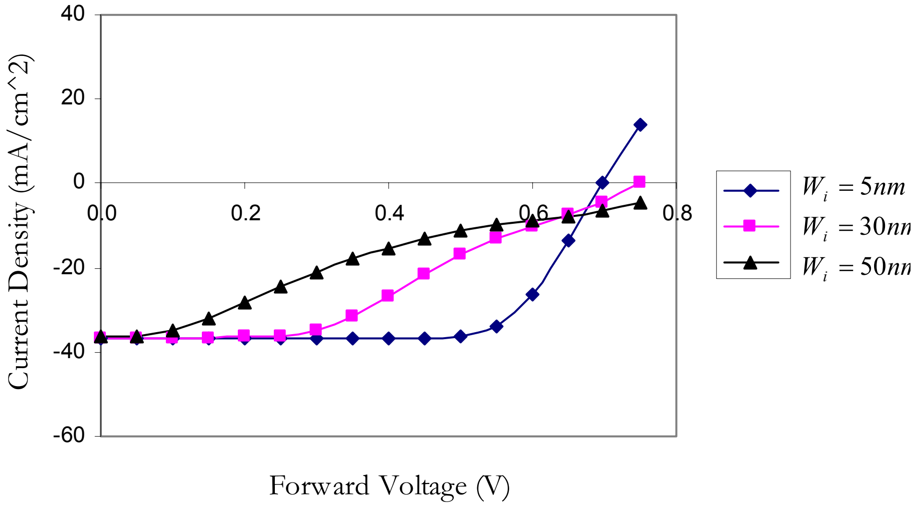

Fig 6.28 I-V graph of p^+in solar cell for different intrinsic layer widths (AMPS)

We have compared the AMPS result with our modeling result of I-V curve for p^+in solar cell with the intrinsic layer width of 5nm (Figure 6.29). The slight difference between two results can be because of the different methods that our model and AMPS have used for modeling purpose.

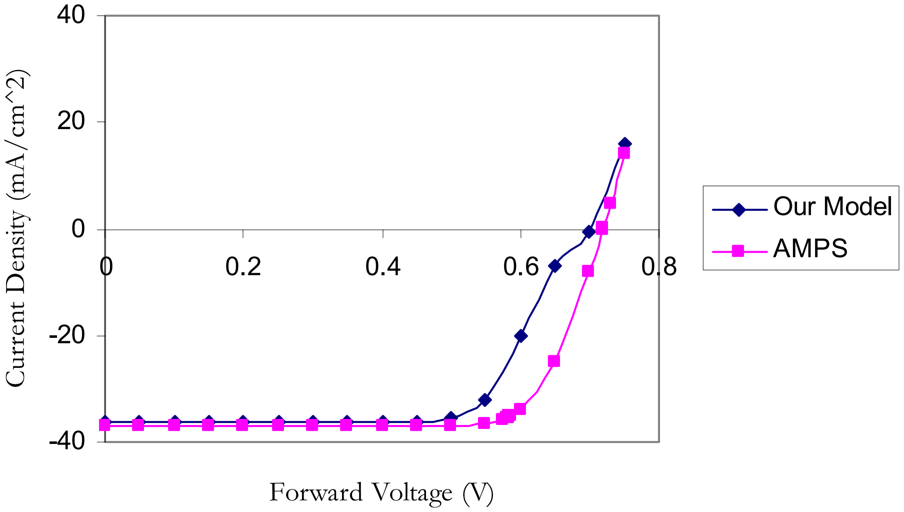

Fig 6.29 Comparison between AMPS and our model I–V result of p^+in solar cell for $W_i = 5nm$

We have considered the effects of depletion region and potential barrier on the carriers flow which limit the velocity of the carriers. Because we have taken into account the same considerations in photocurrent, it is expected that the photocurrent will be suppressed as well. The forward voltage range within which the difference between results is considerable (0.6 to 0.65) is the range in which the drift-diffusion and thermionic emission mechanisms are absolutely dominant. Therefore, the effects of limiting factors that come from these mechanisms are significant. The AMPS program, on the other hand, uses a built-in model for "density of defects" to model the device. However, by increasing the minority hole diffusion length (L_p), our analytical model curve can be brought closer to the numerically solved AMPS simulation.

Chapter 7

The n^+ *ip* Heterojunction Solar Cell Fabrication and Characterization

We have used the heterojunction cells fabricated in our laboratory to analyze and compare with our model. In this chapter, we discuss the solar cell fabrication sequence, characterization of fabricated cells and comparison with the analytical model.

In section 7.1, we have reviewed the fabrication sequence of solar cell, in section 7.2, its characterization has been covered and finally in section 7.3 we have discussed the experimental results for quantum efficiency.

7.1 The n^+ *ip* Solar Cell Fabrication

n^+ip amorphous silicon/crystalline silicon heterojunction solar cells were fabricated based on the structure shown in Figure 7.1. The cells were prepared by silicon wafer cleaning as a starting point of the process. The p-type c-Si was 380µm thick and with the resistivity of 8-12 ohm-cm. After cleaning the wafer, by RCA I and RCA II, dilute hydrofluoric acid (HF) was used to remove native silicon dioxide from wafers. Since it acts quickly, one needs to only expose the wafer for a short time (less than 30s) ("dip"). After the HF-dip was done, a 10nm thick intrinsic layer followed by a heavily doped, 20nm thick, n^+ a-Si layer was deposited by Plasma Enhanced Chemical Vapour Deposition (PECVD) at the substrate temperature of 260°C. The process was done under the pressure of 250mTorr with the Silane flow of 50sccm and RF power= 12W. The contact to n^+ a-Si was provided by a transparent conductive oxide (ITO) deposited by RF sputtering. In another sputtering system, Al films were deposited on the front-side and backside of the wafer and annealed at 200°C to improve contact resistance. Finally, the front metal contact was patterned by photolithography and metal etching.

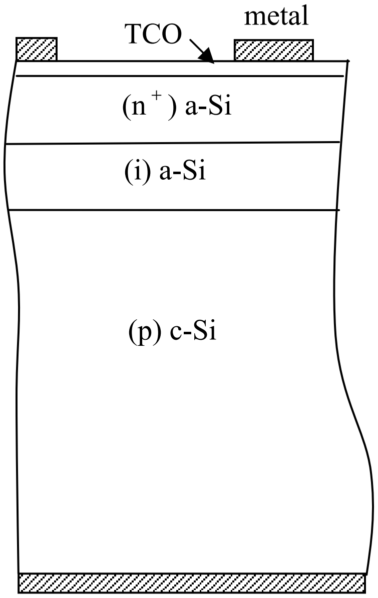

Fig. 7.1 The structure of n^+ip heterojunction solar cell

1	Wafer cleaning (RCA I and II)
2	HF- Dip (1% HF in DI water)
3	i-layer deposition (PECVD)
4	n-plus deposition (PECVD)
5	ITO deposition (RF Sputtering)
6	Al deposition on wafer front side (RF sputtering)
7	Al deposition on wafer back-side (RF sputtering)
8	Al contact annealing at 200°C
9	Lithography
10	Al etching
11	Dicing

Table 7.1 Process sequence

Table 7.1 shows the fabrication sequence that we have followed. The doping levels for n- and p-regions were estimated as 10^{19} (from the standard n^+ films deposited in the lab) and $10^{16} cm^{-3}$ (from wafer data) respectively. The solar cell layout, given in Figure 7.2, takes the advantage of a comb structure. In order to overcome probable sheet resistance problems of the non-optimized ITO layer, finger spacing is low. The main bus is designed wide to simplify the electrical characterization.

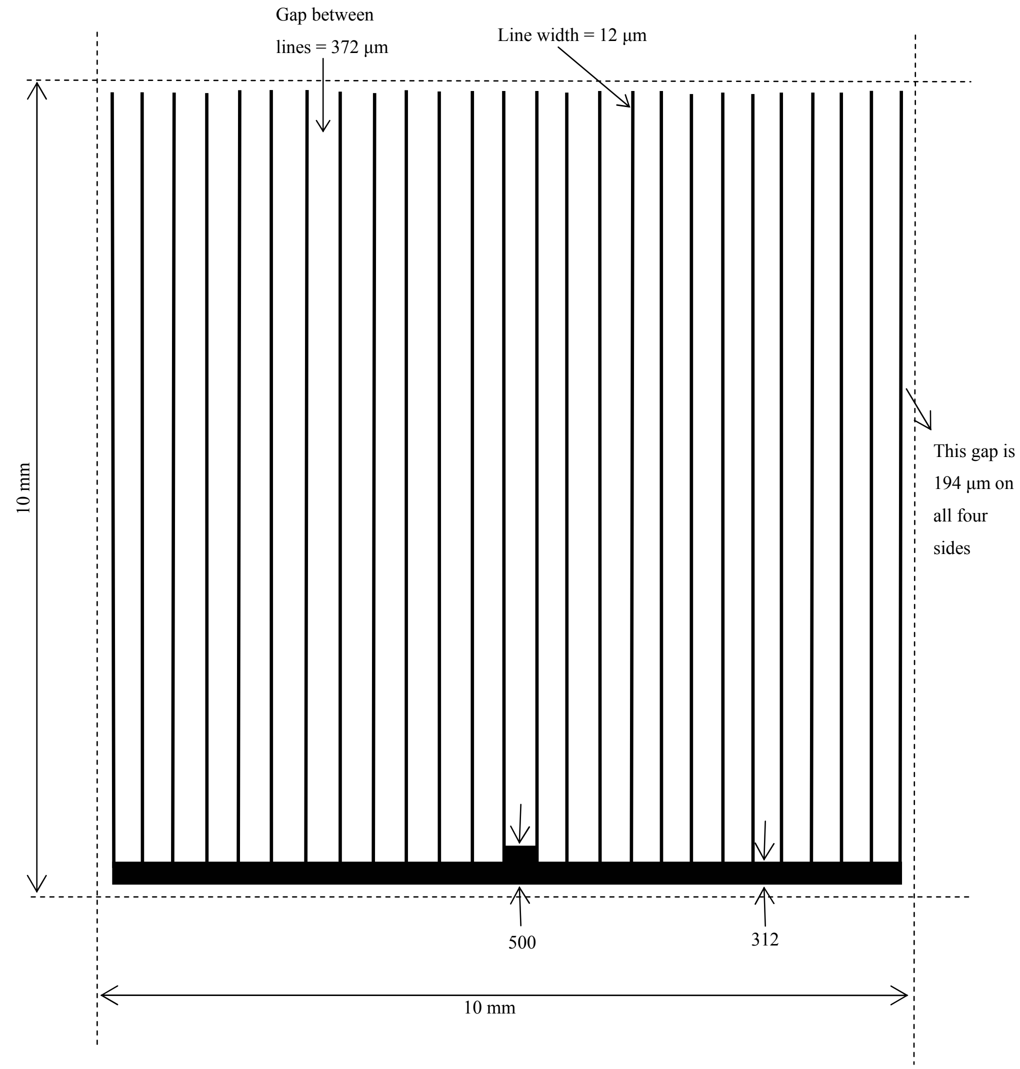

Fig. 7.2 The layout used in solar cell fabrication

7.2 The $n^+ ip$ Solar Cell Characterization

The data that we have measured as quantum efficiency of solar cell is external quantum efficiency. Figure 7.3 shows the block diagram of the measuring system (Oriel) that we have used to measure the quantum efficiency of the solar cell.

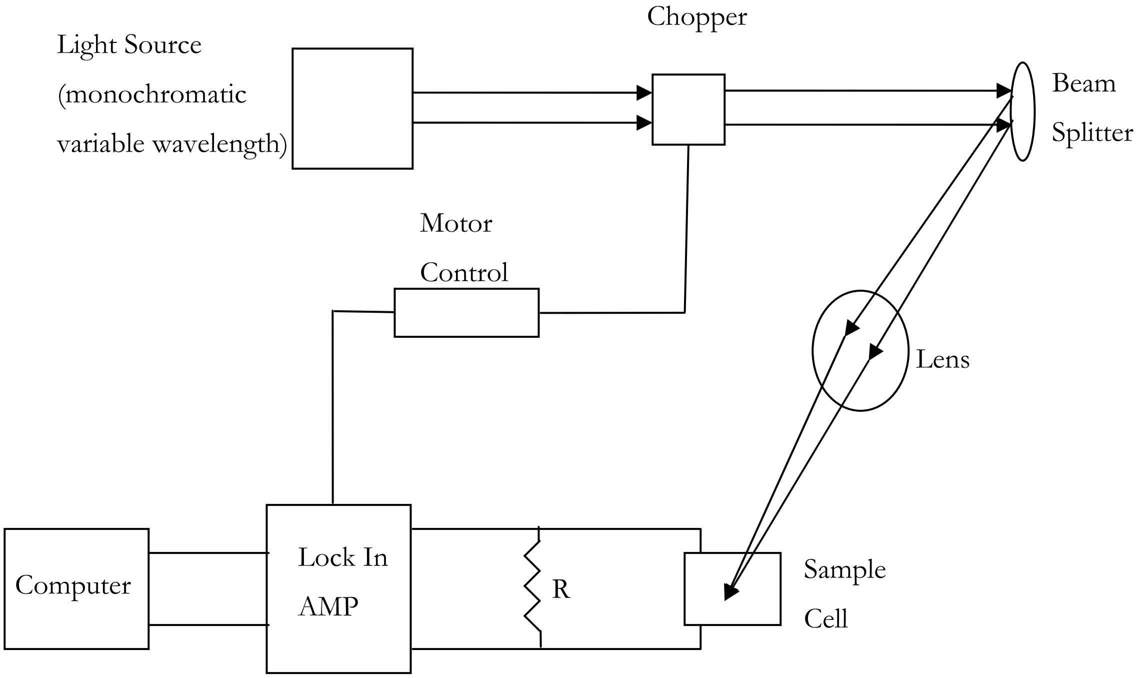

Fig 7.3 Block diagram of the measuring system for quantum efficiency

To measure the external quantum efficiency, the solar cell is illuminated by light with different wavelengths coming from light source with the step of 10nm. The light is first chopped and then after passing through a monochromator, is directed by a beam splitter onto the sample cell. The short circuit current of sample cell and reference cell is measured by the lock-in technique at each wavelength. Reference cell is a silicon photodetector with simple p-n junction structure with known quantum efficiency. The sample cell is replaced by the reference cell for short current measurement of the reference cell. We use the same characterization set up for both devices, i.e. reference cell and fabricated cell. Then we use the reference cell quantum efficiency to measure the calibration factor. By having the short circuit current of the sample cell, we can calculate its quantum efficiency. The responsivity is defined as the ratio of the photocurrent of cell to the consumed power:

$$R = \frac{I}{P} \tag{7.1}$$

Since both sample cell and reference cell has been given the same amount of power, we can write:

$$P_{ref} = P_{sample} \tag{7.2}$$

therefore:

$$\frac{I_{ref}}{R_{ref}} = \frac{I_{sample}}{R_{sample}} \tag{7.3}$$

We can replace the responsivity in equation 7.3 by the quantum efficiency since both define the ratio of energy conversion:

$$\frac{I_{ref}}{QE_{ref}} = \frac{I_{sample}}{QE_{sample}} \tag{7.4}$$

and consequently:

$$QE_{sample} = \frac{I_{sample}}{I_{ref}} QE_{ref} \tag{7.5}$$

Equation 7.5 shows that by measuring the short circuit current of sample cell and reference cell and using the quantum efficiency of the reference cell we can calculate the (external) quantum efficiency of the sample solar cell.

7.3 The Experimental Results

The external quantum efficiency that we have obtained using equation 7.5 includes reflection of light. Since in our modeling we have not included the reflection of light, (the calculated quantum efficiency is internal QE) a difference between the two curves is expectable. Therefore, the measured quantum efficiency is lower than the calculated one. The relationship is expressed as follows:

$$QE_{\text{int}} = \frac{QE_{ext}}{1-R} \tag{7.6}$$

Figure 7.4 shows the experimental data of the external quantum efficiency in comparison with our model result for internal quantum efficiency of n^+ip heterojunction solar cell. As we can see from the figure, the difference between experimental data and our model result is because of light reflection.

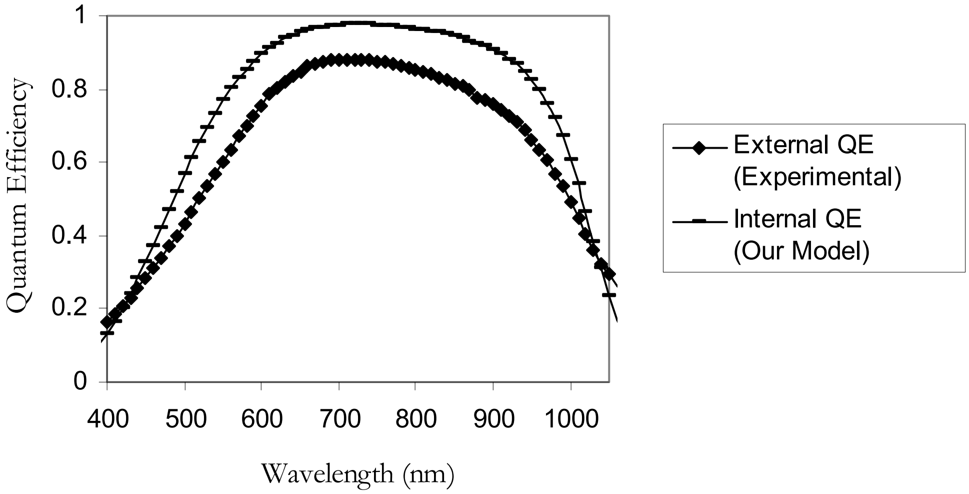

Fig 7.4 Experimental data for external QE and our model result for internal QE of n^+ip solar cell

To obtain the internal quantum efficiency of the measured solar cell, we should consider the reflection that different layers impose on the incident light. Each layer has different index of refraction.

Figure 7.5 shows the refractive index of c-Si, a-Si and ITO. We have extracted refractive index data from [37] and [38]. By having the refractive index of different layers, we can use the Fresnel's formula to find out the percentage of the incident light that has been reflected.

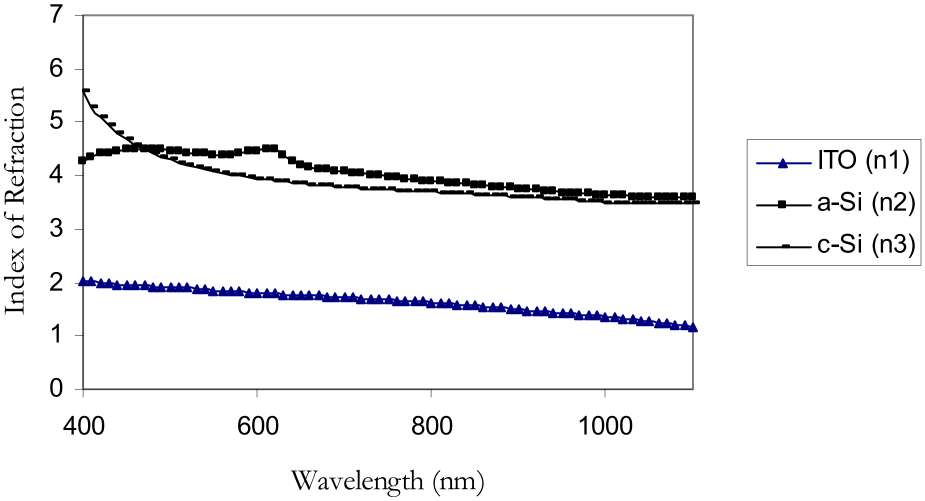

Fig 7.5 Refractive index of c-*Si, a-Si* and *ITO*

Fresnel's formula for the total reflectance of a cell with three different layers is [7,39]:

$$R = \frac{r_1^2 + r_2^2 + r_3^2 + r_1^2 r_2^2 r_3^2 + 2r_1 r_2 (1 + r_3^2)\cos 2\theta_1 + 2r_2 r_3 (1 + r_1^2)\cos 2\theta_2 + 2r_1 r_3 \cos 2(\theta_1 + \theta_2) + 2r_1 r_2^2 r_3 \cos 2(\theta_1 - \theta_2)}{1 + r_1^2 r_2^2 + r_1^2 r_3^2 + r_2^2 r_3^2 + 2r_1 r_2 (1 + r_3^2)\cos 2\theta_1 + 2r_2 r_3 (1 + r_1^2)\cos 2\theta_2 + 2r_1 r_3 \cos 2(\theta_1 + \theta_2) + 2r_1 r_2^2 r_3 \cos 2(\theta_1 - \theta_2)} \tag{7.7}$$

where:

$$r_1 = \frac{n_0 - n_1}{n_0 + n_1} \tag{7.8}$$

$$r_2 = \frac{n_1 - n_2}{n_1 + n_2} \tag{7.9}$$

$$r_3 = \frac{n_2 - n_3}{n_2 + n_3} \tag{7.10}$$

$$\theta_1 = \frac{2\pi n_1 d_1}{\lambda} \tag{7.11}$$

$$\theta_2 = \frac{2\pi n_2 d_2}{\lambda} \tag{7.12}$$

n_0, n_1, n_2 and n_3 are the refractive index of air, ITO, a-Si and c-Si, respectively, and d_1 and d_2 are the width of ITO and a-Si layers, respectively. Since the index of refraction of air is 1, we can substitute n_0 by 1.

Using equation 7.7, we have calculated the total reflection of the device as shown in Figure 7.6.

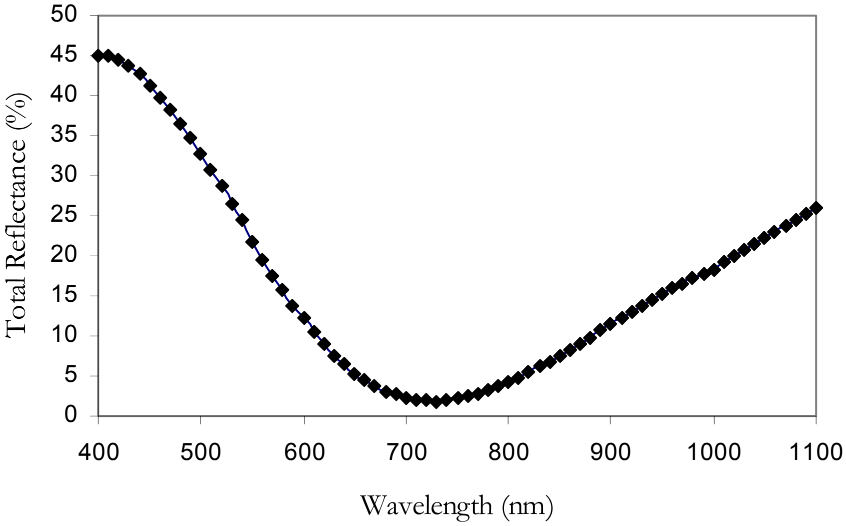

Fig 7.6 Calculated total reflectance of three layers in $n^+ ip$ solar cell

Figure 7.6 shows that the minimum reflection takes place at wavelength of 730 nm. By using the total reflectance of device, we can calculate the internal quantum efficiency of it using the equation 7.6 ($QE_{\text{int}} = \frac{QE_{ext}}{1-R}$), where R is the total reflectance of the device. It is worth to mention that there is another possible source of error which is the very small percentage of metal pattern has a 100% reflection. From Figure 7.2, we can calculate the amount of reflection that the metal pattern causes:

total area=$10000\mu m \times 10000\mu m = 10^8\ \mu m^2$

metal pattern area=

$26 \times (12\mu m \times 10000\mu m) + 24 \times (372\mu m \times 312\mu m) + 500\mu m \times 372\mu m = 6.09 \times 10^6\ \mu m^2$

(metal pattern area)/(total area)=0.0609

This error which is 6% of total reflection of the device has not been included in total reflectance of the cell.

Figure 7.7 shows the external quantum efficiency of measured cell as well as the internal quantum efficiency that we have calculated using the equation 7.6.

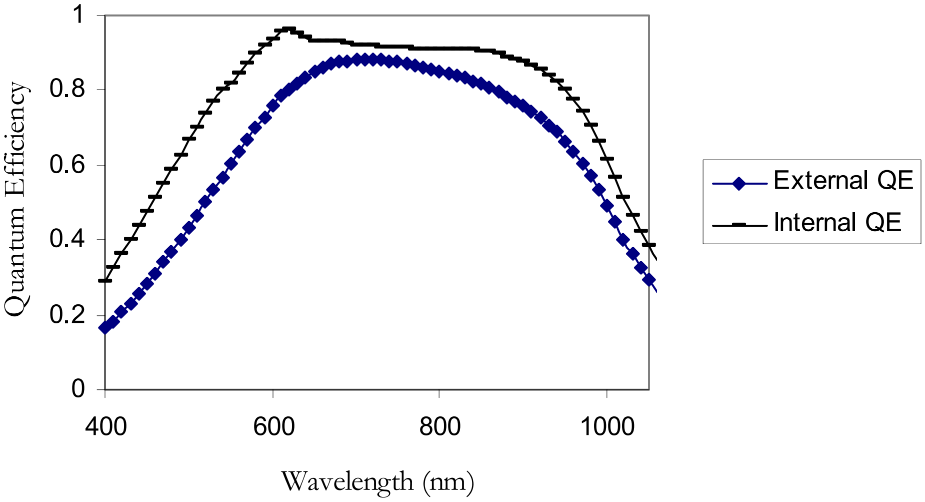

Fig 7.7 Internal and External quantum efficiency of the fabricated n^+ip solar cell

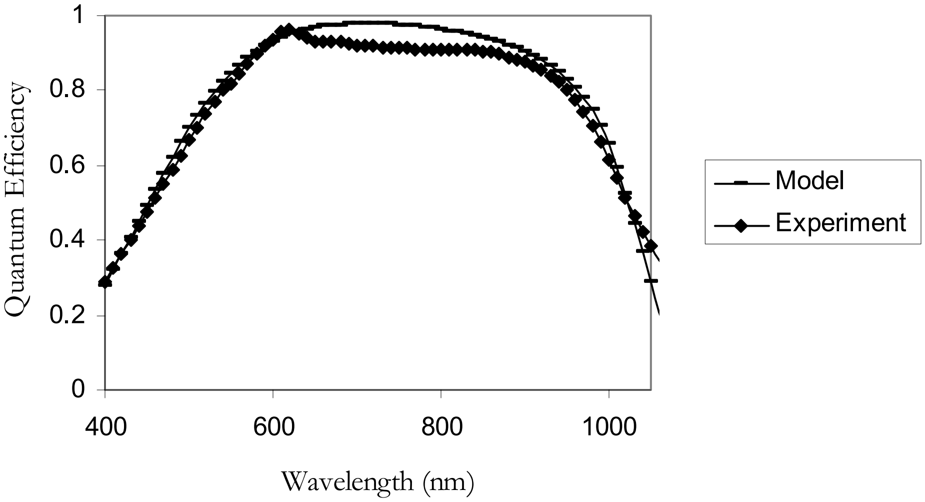

Fig 7.8 Internal quantum efficiencies of n^+ip : model and experiment

By having the internal quantum efficiency for experimental data, now we can compare the result of our model for n^+ip a-Si/c-Si heterojunction and the fabricated cell (Figure 7.8). We see that the major difference between the internal quantum efficiency of fabricated cell and our model result is at the wavelength of 730nm in which the total reflectance of the device is minimum (Figure 7.6). Since we have calculated the device reflectance using the standard values for different layers refractive indices [37,37], the difference between experimental data and our model result can be for this reason.

By setting following values for our modeling, we have drawn the Figure 7.8.

n^+ -layer width=20nm,
i -layer width =10nm,
p -layer width=380μm,
$N_a = 10^{16} cm^{-3}$,
$N_d = 10^{19} cm^{-3}$,
$L_n = 260 \mu m$,
$s_n = 200 cm/s$.

Conclusion

We have performed a complete study of the physics of heterojunctions and have developed analytical models for $n^{+}ip$ and $p^{+}in$ a-Si/c-Si heterojunction solar cells. These models have been used for device simulation. The complete static analysis of a-Si/c-Si heterojunction devices have been fully studied and the equations derived including the expressions for built in voltage, depletion region width, and the amount of voltage dropped across each part of SCR. The carrier transport and recombination mechanisms in illuminated a-Si/c-Si heterojunction devices have been fully studied and understood, and equations have been derived. The analyses were very distinct for $n^{+}ip$ and $p^{+}in$ structures. The $n^{+}ip$ and $p^{+}in$ a-Si/c-Si device structures were simulated for several design features and the internal quantum efficiency and illumination I-V behavior were analyzed. The specific nature of the heterojunctions and their effects on both $n^{+}ip$ and $p^{+}in$ devices I-V characteristics have been modeled through a number of factors. We have calculated these factors in terms of effective velocities and have modeled the I-V characteristics of the cells. Substrates with various surface and bulk passivation levels have been considered in our simulations. It has been found that thin silicon substrates (<100 μm) in combination with low-T bulk and surface passivation schemes can lead to a cost effective device fabrication process with competitive conversion efficiency.

We have also compared our analytical simulations with a numerical simulator (AMPS) that is widely used for optoelectronic devices. When heterojunction solar cell structures (with similar parameters) are simulated by AMPS and our model, the results agree very well.

Finally, we have compared our analytical simulation results to experimental results obtained from $n^{+}ip$ a-Si/c-Si heterojunction solar cells fabricated in our laboratory. The optical reflection of the device has been accounted for by considering the thin-films (a-Si, ITO) used in the device fabrication process. By comparing the simulated spectral response of the device to the experimental curves we were able to extract a number of device parameters such as doping levels, bulk & surface recombination parameters.

Bibliography

[1] A. Goetzberger, C. Hebling, H. Schock, Photovoltaic materials, history, status and outlook, Material Science and Engineering, 40, pp 1-46 (2003)

[2] P. Bhattacharya, Semiconductor Optoelectronic Devices, Prentice Hall, New Jersey (1997)

[3] S. M. Sze, Physics of Semiconductor Devices, John Wiley & Sons, New Jersey (1984)

[4] American Society for Testing and Materials (http://rredc.nrel.gov/solar/standards/am1.5) (Last accessed on July 29th, 2003)

[5] Key center for photovoltaic engineering UNSW (http://www.pv.unsw.edu.au) (Last accessed on July 29th, 2003)

[6] S. O. Kasap, Optoelectronics and Photonics, Principles and Practices. Prentice Hall. (2002)

[7] A. Goetzberger, J. Knobloch, B. Voss, Crystalline Silicon Solar Cells, John Willey & Sons, Essex, England (1998)

[8] M. A. Green, Solar cells: operating principles, technology, and system applications, Prentice Hall, New Jersey, (1982)

[9] H. Matsuura, T. Okuno, H. Hideyo, K. Tanaka, Electrical properties of n-amorphous/p-crystalline silicon heterojunctions. Journal of Applied Physics, 55, 4 (1984)

[10] J. S. Harris, Course notes EE328: Physics of Advanced Semiconductor Devices, Stanford University, Stanford (2002)

[11] M. Taguchi, K. Kawamoto, S. Tsuge, H. Baba, H, Sakata, M. Mrizane, K. Uchihashi, N. Nakamura, S, Kiyama, O. Oota, HIT Cells-High efficiency crystalline Si cells with novel structure, Progress in Photovoltaics: Research and Application, 8, pp503-5013 (2000)

[12] M. S. Lundstorm, An Ebers-Moll model for the heterostructure bipolar Transistor, Solid-State Electronics, 29, 11, pp.1173-1179 (1986)

[13] M. S. Lundstorm, Boundary conditions for pn heterojunctions, Solid-State Electronics, 27, 5, pp. 491-796 (1984)

[14] J. Furlan, F. Smole, P. Popovic, M. Topic, M. Kamin, Charge carrier transport in n-i-p and p-i-n a-Si/c-Si heterojunctions solar cell, Solar Energy Material & Solar Cells 53, pp. 15-21 (1998)

[15] J. Furlan, P. Popovic, F. Smole, M. Topic, Analytical model of a-Si/c-Si HIT solar cell, Material Society Symposium,4201(1996)

[16] V. Smid, J. J. Mares, L. Stouac, T. Kristofik, edited by D.Adler , H. Frizche, Tetrahedrally-bonded amorphous semiconductors, Plenum New York, p.483 (1985)

[17] M. F. Baroughi, Physical models, electrical properties, electrical characterization techniques and applications of a-Si/c-Si heterojunctions, E&CE 730 course project, University of Waterloo, Waterloo (2003)

[18] L. F. Marsal, J. Pallares, X. Correig, J. Calderer and R Alcubilla, Electrical model for amorphous/crystalline heterojunction silicon diodes (n a-Si:H/c-Si), Semiconductor Society Technology,11, pp. 1209-1213 (1996)

[19] M. W. M van Cleef, M. W. H. Philippens, F. A. Rubinelli, M. Kolter and R. E. I. Schropp, Electrical transport mechanism in p^+ a-SiC:H/n c-Si heterojunctions: Dark J-V-T characteristics, Material Society Symposium, 420, pp. 239-244 (1996)

[20] A.V. D. Zeil, Solid State Physical Electronic, Prentice Hall, New Jersey (1976)

[21] A. A. Grinberg, An investigation of the effect of graded layers and tunneling on the performance of AlGaAs/GaAs heterojunction bipolar transistors, IEEE Transactions on Electron Devices, ED.31, 12 (1984)

[22] S. Datta, K. P. Roenker, M. M. Cahay, A thermionic-emission-diffusion model for graded base Pnp heterojunction bipolar transistors. Journal of Applied Physics, 83, 12 (1998)

[23] Y. J. Song, M. R. Park, E. Guliants, W. A. Anderson, Influence of defects and band offsets on carrier transport mechanisms in amorphous silicon/crystalline silicon heterojunctions solar cells. Solar Energy Material & Solar Cells, 64, pp. 225-240 (2000)

[24] J. Hamel, Course notes E&CE 730: Physics and Modeling of Semiconductor Devices, University of Waterloo, Waterloo (2002)

[25] M. W. M van Cleef, R. E. I. Schropp, Significance of tunneling in p+ amorphous silicon carbide n crystalline silicon heterojunction solar cells, Applied Physics Letters, 73,18 (1998)

[26] M. A. Steller, M. S. Lundstorm, A detailed investigation of heterojunctions transport using a rigorous solution to the boltzman equation, IEEE Transactions on Electron Devices, 41, 4 (1994)

[27] E. H. Rhoderick, R. H. Williams, Metal-Semiconductor Contacts, Oxford Press, Oxford (1988)

[28] Math World (http://mathworld.wolfram.com/DawsonsIntegral.html) (Last accessed on July 29th, 2003)

[29] M. Hack, M. Shur, Physics of amorphous silicon alloy p-i-n solar cells, Journal of applied physics, 58 (2) (1985)

[30] M. Hack, M. Shur, Theoretical modeling of amorphous silicon-based alloy p-i-n solar cells. Journal of applied physics, 54(10) (1983)

[31] A .Froizheim, K. Bendel, L. Elstner, W. Fuhs, K. Kliefoth, M. Schmidt, Interface recombination in heterojunction of amorphous and crystalline silicon, Journal of Non-Crystalline Solids 299-302, pp. 663-667 (2002)

[32] N. Jensen, U. Rau, R. M. Hausber, S. Uppal, L. Oberbeck, R. B. Bergmann. Recombination mechanisms in amorphous silicon/crystalline silicon heterojunction solar cells. Journal of applied physics, 87, 5 (2000)

[33] F. Khalvati, S.Sivoththaman, Quantum efficiency modeling of amorphous/crystalline silicon Heterojunction photovoltaic devices, Material Society Symposium, 744, pp. M5.14.1-6 (2003)

[34] AMPS (Analysis of microelectronic and photonic structures) (www.psu.edu/dept/AMPS) (Last accessed on July 29th, 2003)

[35] M. W. M van Cleef, F. A. Rubinelli, J. K. Rath, R. E. I. Schropp, W. F. van der Weg, R. Rizzoli, C. Summonte, R. Pinghini, E. Centurioni, R. Galloni, Photocarrier collection in a-SiC:H/c-Si heterojunction solar cells, Journal of Non-Crystalline Solids, 227-230, pp. 1291-1294 (1998)

[36] M. W. M van Cleef, F. A. Rubinelli, R. Rizzoli, R. Pinghini, R. E. I. Schropp, W. F. van der Weg, Amorphous silicon carbide/crystalline silicon heterojunction solar cells: A comprehensive study of the photocarrier collection, Journal of Applied Physics, 37, pp. 3926-3932 (1998)

[37] R. A. Synowicki, Spectroscopic ellipsometry characterization of indium tin oxide film microstructure and optical constants, Elsevier Thin Solid Films, 313-314, pp 394-397 (1998)

[38] P. D. Edward, Handbook of Optical Constants of Solids, Academic Press, INC. (1985)

[39] H. J. Hovel, Semiconductors and Semimetals, Academic Press, INC. (1975)